**Synthesis of (Phosphino)silyl-Ligated Nickel Complexes for the Catalytic Hydroboration of Alkenes**

by

Sydney B. Shepard

Submitted in partial fulfilment of the requirements
for the degree of Master of Science

at

Dalhousie University
Halifax, Nova Scotia
August 2022

# Table of Contents

# List of Tables

<h1 style="text-align: center">List of Figures</h1>

**Abstract**

Bis(phosphino)silyl (PSiP) pincer ligands have been studied extensively. While there are several examples of late transition metal complexes, in recent years there has been a shift to study these ligands on first-row transition metals (i.e., Fe, Co, Ni).

These complexes have shown to be active in catalytic hydrofunctionalization; however, the turn-over for larger substrates has proved challenging. Therefore, the question of reducing the size of the phosphino(silyl) ancillary ligand is investigated in this document. While varying the substitution at phosphorus is common, access to smaller substituents is not straightforward. A different approach is to eliminate a phosphine donor.

A new bidentate PSi ligand has been synthesized and studied with respect to Ni complexes. In this regard, studying the catalytic hydroboration with a substrate scope involving terminal, di-, and tri-substituted alkenes and three $Ni^{II}$ precatalysts has been explored, where selectivity for chain-walking of internal alkenes to the terminal position was observed.

# List of Abbreviations and Symbols Used

$\text{Å}$ = angstrom
$\eta$ = *hapticity (contiguous donor)*
$\kappa$ = denticity (non-contiguous donor)
**DFT** = density functional theory
**h** = hour
**Hz** = hertz
**NMR** = Nuclear Magnetic Resonance
**COSY** = Homonuclear Shift Correlation Spectroscopy
**HMBC** = Heteronuclear Multiple Bond Correlation
**HSQC** = Heteronuclear Single Quantum Correlation
**HMQC** = Heteronuclear Multiple Quantum Correlation
$^{n}\boldsymbol{J}_{xx'}$ = n bond coupling constant between atoms X and X'
**L** = two electron donor (neutral electron counting formalism)
**X** = single electron donor (anionic electron counting formalism)
**s** = singlet
**d** = doublet
**t** = triplet
**q** = quartet
**m** = multiplet
$\boldsymbol{\delta}$ = chemical shift (ppm)
**ppm** = parts per million
**py** = pyridine
**NHC** = *N*-heterocyclic carbene
**SISHA** = secondary interaction between silicon and hydrogen atom
**TOF** = turnover frequency
**TON** = turnover number
**equiv.** = equivalents
**HBPin** = 4,4,5,5-tetramethyl-1,3,2-dioxaboralane
**ORTEP** = Oak Ridge thermal ellipsoid plot
**COD** = 1,5-cyclooctadiene
**DME** = 1,2-dimethoxyethane
**acac** = acetylacetonate

## Acknowledgements

# Chapter 1: Introduction

## 1.1 Overview

The utility of homogeneous transition metal catalysts to facilitate chemical transformations has become well established,[1, 2, 3] such that in recent years the development of improved metal catalysts has become one of the fundamental goals of organometallic chemistry. Modern day drug discovery, alternative energy schemes, and materials synthesis would not be achievable at the scale that they are without the use of organometallic compounds and their contributions to polymerization, metathesis, hydroformylation, hydrosilylation, cross-coupling reactions, hydrogenation, and many more.[4] While the use of platinum group metals (PGM; *i.e.*, Ru, Rh, Ir, Pd, Pt) in this regard has proven widely successful, there has been a recent push to develop catalysts based on significantly more abundant first-row transition metals (*i.e.*, Mn, Fe, Co, Ni) in an effort to develop increasingly sustainable chemical syntheses. By comparison with their $4d$- and $5d$-metal congeners, $3d$-transition metals have increased abundance in the Earth's crust, and as a result the energy costs for the mining and extraction of such metals are greatly reduced, leading to increased affordability and a reduced carbon footprint.[5] In addition, new reactivity manifolds may be accessible with $3d$-metal catalysts, leading to the discovery of new synthetic methodologies. However, developing $3d$-metal catalysts that are competitive with existing PGM catalysts is not trivial, as first-row transition metals tend to have lower activity as catalysts, and can often exhibit unpredictable single electron chemistry.

Ancillary ligand design has proven key to tempering undesirable side-reactions involving $3d$-metal complexes in order to achieve reactivity comparable to that of PGM-based catalysts. It is already well established that by modification of the ancillary ligand scaffold, one can control the steric and electronic features at the metal centre. In the case of ligand design for first row metal reactivity, strategies that have proven among the most effective include the use of multidentate

ligands, such as tridentate pincer ligands (Figure 1.1.1), that help prevent the formation of metal nanoparticles, as well as the incorporation of metal-ligand cooperativity that allows 3*d*-metals to undergo bond-making/-breaking transformations while maintaining a preferred low oxidation state.
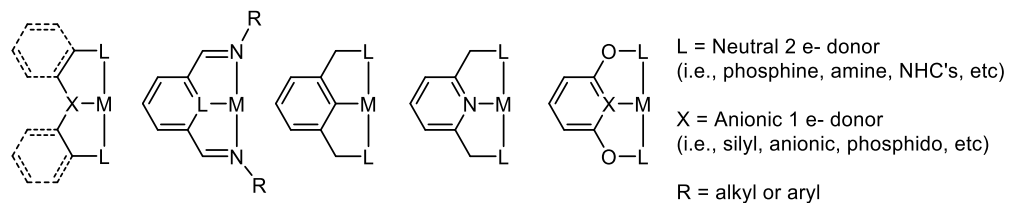


**Figure 1.1.1.** Common tridentate pincer ligand motifs.

The research outlined in this thesis builds on pervious work done in the Turculet group exploring the utility of tridentate bis(phosphino)silyl (PSiP) pincer ligation in 3*d*-metal coordination chemistry and hydrofunctionalization catalysis (Figure 1.1.2 **A**). In an effort to access increasingly reactive complexes by decreasing steric crowding and increasing coordinative unsaturation at the metal center, bidentate phosphino(silyl) (PSi) ligation has been pursued (Figure 1.1.2 **B**). Chapter 2 describes the synthesis and characterization of such phosphino(silyl)-ligated nickel complexes, as well as their utility as pre-catalysts for the hydroboration of alkenes.
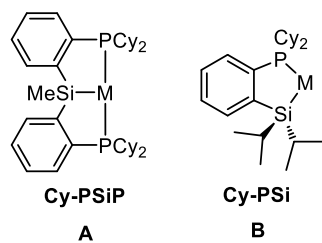


**Figure 1.1.2.** Parent bis(phosphino)silyl Cy-PSiP (**A**) employed in the Turculet group and bidentate (phosphino)silyl Cy-PSi (**B**). Chemsitry of Cy-PSi with M = Ni is described in Chapter 2 of this thesis.

## 1.2 Base Metals in Catalysis

Due to the rarity and high cost of precious metals typically utilized in catalysis (*i.e.*, Ru, Rh, Ir, Pd, Pt) and with the inspiration of metalloenzymes that are prevalent in nature, researchers have recently focused significant interest in developing the catalytic utility of Earth-abundant first row transition metal (*i.e.*, Fe, Co, Ni) complexes. However, this has not come without its challenges as first row transition metals tend to favour one electron chemistry which leads to lower stability and unpredictable reactivity.

One application where Earth-abundant catalysts have made in-roads is C-E (E = C, N) cross-coupling catalysis. Traditionally such reactions have utilized Pd-based catalysts that readily undergo key C-X (X = halide) oxidative addition and C-E reductive elimination steps required for C-E bond formation. However, in recent years Fe, Co, and Ni complexes have been reported to perform this catalytic transformation competitively with Pd metal catalysts.[6] Nickel, in particular, is the most widely reported 3$d$-metal replacement for palladium.[7] The use of Ni for the Suzuki–Miyaura (organoboron reagents) and Negishi (organozinc reagents) C-C cross-coupling reactions has been extensively studied,[8] and recently it has been shown that Ni is capable of performing increasingly challenging cross-coupling reactions of this type to afford products beyond the typical biaryl species that are commonly reported.

In this context, Jarvo and co-workers[9] have demonstrated the Suzuki–Miyaura cross-coupling of benzylic esters, carbonates and carbamates with arylboronic esters, by using 10 mol% Ni(COD)$_2$ as the pre-catalyst. Notably, the stereochemistry of the substrate can either be retained or inverted depending on the ligand (PCy$_3$ *vs.* *N*-heterocyclic carbene) used during the catalytic reaction (Scheme 1.2.1a). In another remarkable example of Ni-catalyzed C-C cross-coupling, Weix and co-workers demonstrated reductive cross-coupling reactivity, where rather than a

traditional coupling reaction involving nucleophile and electrophile partners, they were able to demonstrate electrophile-electrophile coupling.[10a] The coupling of an aryl iodide with an alkyl iodide electrophile was achieved in the presence of $NiI_2 \cdot H_2O$ and both a bipyridyl and a phosphine ligand, as well as a stoichiometric manganese reducing agent. The proposed mechanism for this unusual electrophile-electrophile coupling reactivity involves both polar and radical steps to form the new C−C bond (Scheme 1.2.1 b).[10b]
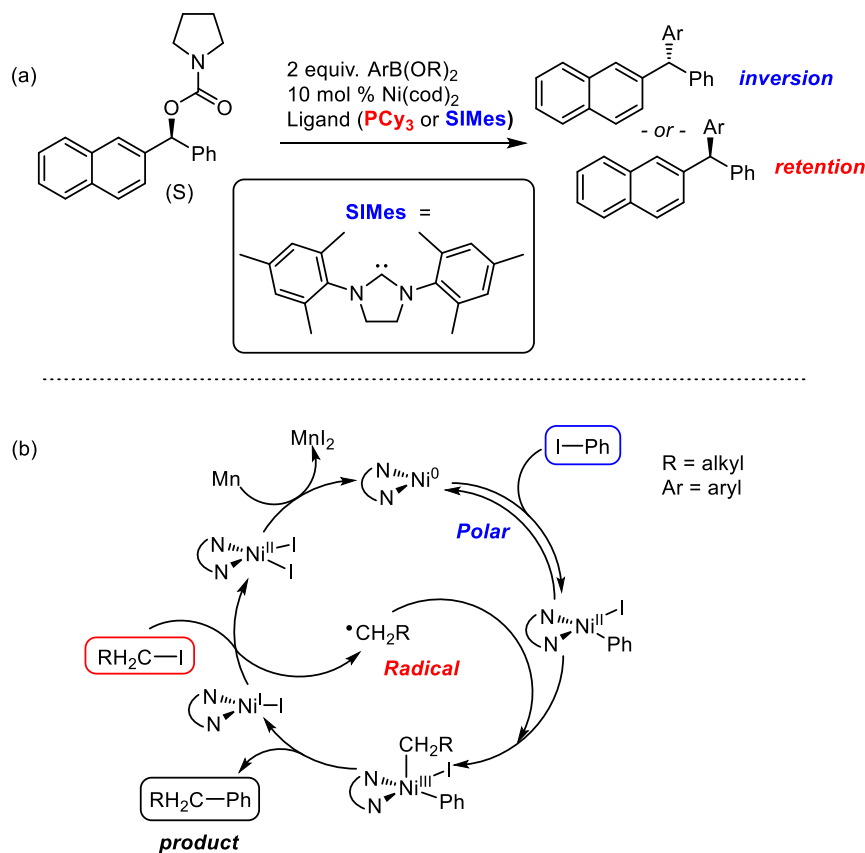


**Scheme 1.2.1** (a) Suzuki–Miyaura cross-coupling where stereochemistry of the substrate is either preserved or inverted depending on the ligand used. (b) Mechanism of unusual reductive cross-coupling reactivity.

Hydrofunctionalization involving the addition of an E-H (E = H, B, Si) bond to an unsaturated substrate (e.g., alkene or alkyne) is an atom-economical catalytic transformation that is widely applicable for both commodity and fine chemical synthesis. Although such reactivity

is well-precedented for platinum group metals,[11] efficient first-row transition metal catalysts are highly sought after. In this context, the catalytic hydrogenation of alkenes has been broadly demonstrated for Fe and Co pre-catalysts, with catalytic conditions that are competitive with precious metals.[12] The work of Chirik and co-workers is prominent in this area. The Chirik group has made extensive use of tridentate pyridine diimine (PDI) ligation in this regard,[13] and more recently they have utilized related tridentate *N*-heterocyclic carbene derivatives ($^{Me}$CNC)Fe(N$_2$)$_2$ (**1-1** Figure 1.2.1; $^{Me}$CNC = 2,6-(2,6-Me$_2$-C$_6$H$_3$-imidazol-2-ylidene)$_2$-C$_5$H$_3$N)[14] and ($^{iPr}$CNC)CoH, (**1-2**; Figure 1.2.1; $^{iPr}$CNC = 2,6-(2,6-$^i$Pr$_2$-C$_6$H$_3$-imidazol-2-ylidene)$_2$-C$_5$H$_3$N)[15] to achieve the challenging hydrogenation of tri- and tetra-substituted alkenes under mild conditions (4 atm H$_2$, 5 mol% catalyst). Remarkably, the latter CNC-supported complexes are competitive with Crabtree's catalyst.[16d]
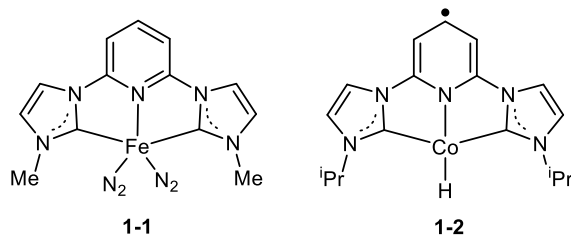


**Figure 1.2.1** ($^{Me}$CNC)Fe(N$_2$)$_2$ and ($^{iPr}$CNC)CoH base metal pre-catalysts used in the catalytic hydrogenation of tri- and tetra-substituted alkenes.

While achieving high catalytic activity is an important goal, tuning selectivity in base-metal catalyzed hydrofunctionalization is also a key area of investigation. The asymmetric hydrogenation of carbonyl containing compounds, imines, and alkenes using 3*d*-metal catalysts has increasingly been developed over the last two decades.[16] In this regard, Morris and co-workers have reported extensively on the asymmetric hydrogenation of various ketones to form chiral alcohols using Fe-based catalysts. The complex (*S*,*S*)-[Fe(P−CH=N−P′)(CO)$_2$(Br)][BF$_4$] (**1-3**; Figure 1.2.2) afforded up to >80% e.e. for the S enantiomer for most ketones in the study

under mild reaction conditions (5 atm $H_2$, 0.1 mol% catalyst, 1 mol% base, 50 °C).[17] Catalytic

asymmetric alkene hydrogenation has also been demonstrated by Chirik and co-workers by use

of enantiopure $C_1$-symmetric PDI cobalt pre-catalysts (**1-4**; Figure 1.2.2).[18] To make the $C_1$-

symmetric chiral PDI ligand the authors utilized a single enantiomer of a chiral alkyl amine to

functionalize one imine arm. They observed an enantiomeric excess (ee) of >90% for the

hydrogenation of substituted styrene derivatives under mild conditions (4 atm $H_2$, 5 mol%

catalyst, 22 °C, 24 h), where the incorporation of electron-donating or -withdrawing groups on

the substrate had no effect on either selectivity or conversion to product. At the time of

publication, this study represented the highest reported ee for a base-metal catalyzed alkene

hydrogenation using $H_2$ as the reductant.



**1-3**
*Morris*

**1-4**
*Chirik*
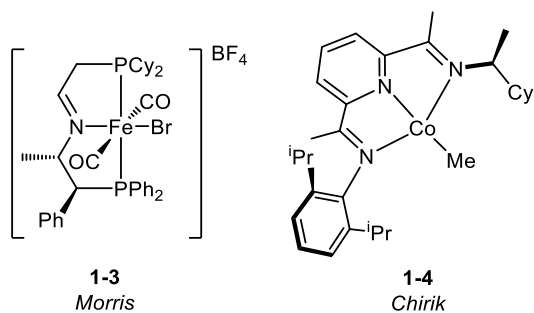
**Figure 1.2.2** Morris's Fe-based chiral pincer complex used in the catalytic asymmetric hydrogenation of ketones, and Chirik's Co-based chiral pincer complex used in the catalytic asymmetric hydrogenation of alkenes.

Hydrosilylation is another sought after catalytic hydrofunctionalization reaction for base

metal catalysis. Selectivity is important in such reactivity, as the anti-Markovnikov product is

preferred product for industrial applications.[19] Most of the hydrosilylation catalysts used in

industry are Pt-based, which makes Ni a logical, sustainable $3d$-metal alternative.[7, 19] Chirik and

co-workers have utilized an α-diimine nickel catalyst to achieve high activity and anti-

Markovnikov selectivity for the addition of tertiary silanes to terminal alkenes.[19b] In their

catalytic study, they reported 99% selectivity for the anti-Markovnikov $^n$octylSi(OEt) product in the hydrosilylation of 1-octene with $(EtO)_3SiH$. The proposed mechanism involves the formation of a Ni$^{II}$ hydride intermediate supported by a one-electron reduced α-diimine. Although chain walking of the substrate was observed, the terminally silylated product $^n$octylSi(OEt) was selectively produced with >98 % conversion and 92% isolated yield. The combination of a 3$d$-metal and a redox active diimine ligand enable a mechanistic pathway that is distinct from the typical Chalk-Harrod hydrosilylation mechanism usually invoked for Pt-based catalysts.
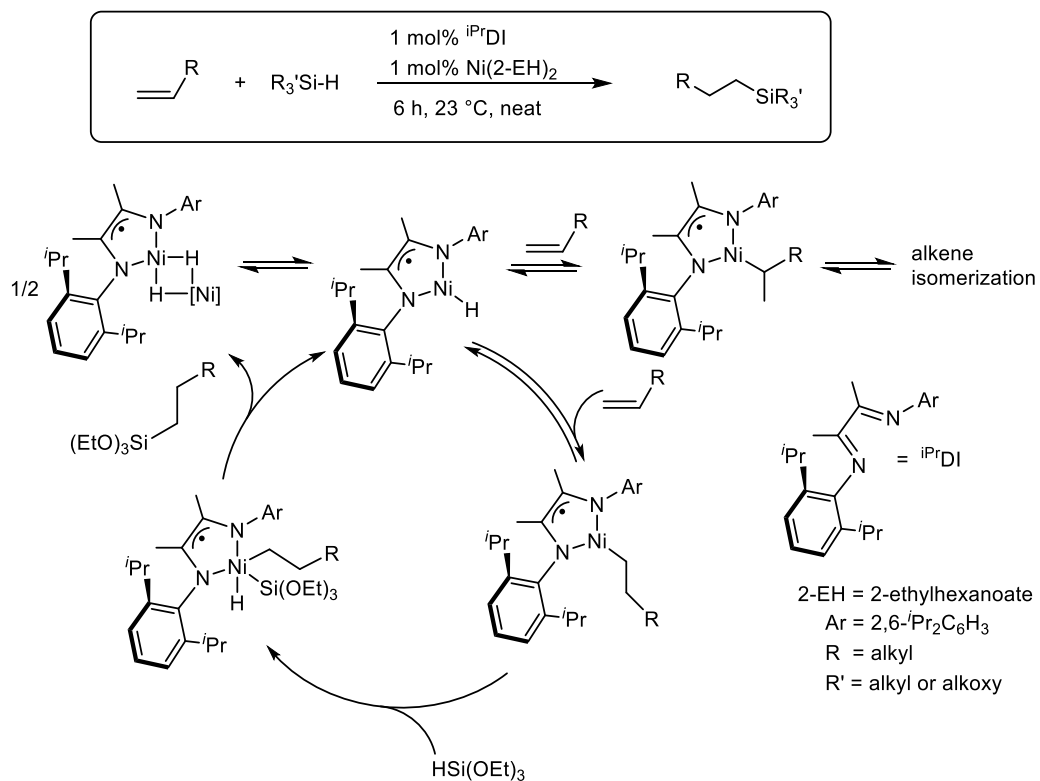


**Scheme 1.2.2** Proposed mechanism for the for the hydrosilylation of 1-octene with $(EtO)_3SiH$ using a diimine Ni catalyst.

Another prominent atom economical hydrofunctionalization reaction is the hydroboration reaction, whereby the B-H bond of $R_2BH$ (R = alkyl, aryl, ester…) is added across an unsaturated bond (e.g., alkene or alkyne). This reaction offers an attractive route to boronate ester derivatives that can be employed in subsequent organic transformations, including Suzuki−Miyaura cross-

couplings. Traditionally, metal-catalyzed hydroboration reactions have been performed using Rh and Ir catalysts,[20] but research has shifted to the use of base-metal catalysts (*i.e.*, Fe, Co, and Ni).[19a, 21] While hydroboration reactions can be uncatalyzed, transition metal catalyzed hydroboration reactions enable the use of otherwise unreactive B−H reagents that can generate air-stable boronate ester products and/or afford complementary chemoselectivity, regioselectivity and enantioselectivity compared with uncatalyzed transformations.[19a]

Both Chirik and co-workers, and Turculet and co-workers have reported on the Co-catalyzed isomerization and regioselective hydroboration of internal alkenes, where the terminally hydroborated product is preferrentially formed.[21a-d,g] In the Chirik example,[21a] the group showed that bis(imino)pyridine cobalt methyl complexes (**1-5**, Figure 1.2.3) are active for the catalytic anti-Markovnikov hydroboration of terminal, geminal, disubstituted internal, tri-, and tetrasubstituted alkenes using pinacolborane (HBPin) under mild conditions to afford terminal hydroboration products. Substrates that are challenging even for precious metal catalysts, such as 1-methylcyclohexene and *α*-pinene, were isomerize and hydroborated with >98% conversion at 50 °C with 1 mol% Co. Shortly thereafter, Turculet and co-workers[21b-d] demonstrated the use of *N*-phosphinoamidinate Co and Fe complexes for related catalytic alkene isomerization/hydroboration reactions (Figure 1.2.3). High conversions (>98%) were observed for a series of challenging substrates in the case of *N*-phosphinoamidinate supported Fe(II) (**1-6**) and Co(II) (**1-7**) pre-catalysts using mild conditions. By comparison, structurally analogous Mn(II) and Ni(II) complexes proves essentially inactive in this reactivity. Chain-walking in branched alkene substrates to the terminal product was reported when using both pinacolborane and 1,3,2-diazaborolanes as the borylating reagents in the catalytic reactions.[21c]
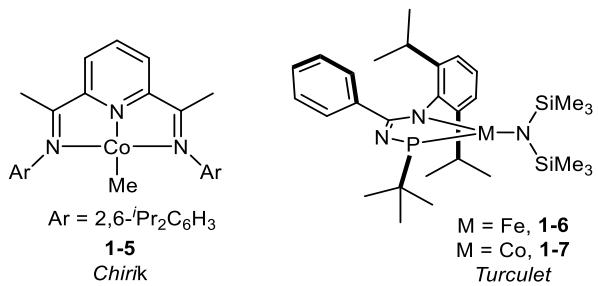
**Figure 1.2.3** Base-metal pre-catalysts used by Chirik and Turculet to perform catalytic alkene isomerization/hydroboration.

More recently, Ge and co-workers demonstrated Co-catalyzed regioselective chain-walking double hydroboration of 1,n-dienes to access gem-bis(boryl)alkanes, which has only been demonstrated once previously by precious metal catalysts (Scheme 1.2.3).[22] Using of $Co(acac)_2$ in the presence of (dicyclohexylphosphino)ethane (dcpe), they achieved 58-88% yields with up to 99% regioselectivity for the terminal gem-bis(boryl)alkane products under mild reaction conditions (1 mol % Co and 1 mol% dcpe). The catalyst also proved tolerant of a range of functional groups.
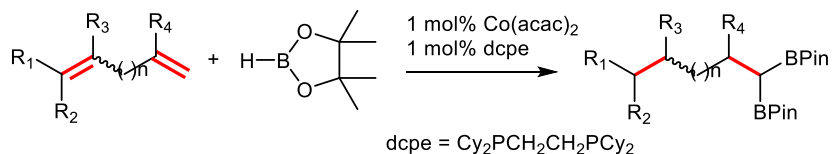


**Scheme 1.2.3** Co-catalyzed diene isomerization/double hydroboration to afford terminal gem-bis(boryl)alkane products.

The catalytic hydroboration of $CO_2$ using a Ni pre-catalyst was also demonstrated by Turculet and co-workers.[23a] Using a Ni hydride pre-catalyst supported by a tridentate bis(indolylphosphino)silyl pincer ligand (**1-8**) they reported the double reduction of $CO_2$ with HBPin to the bis(boryl)acetal product with 97% selectivity under mild conditions (1 atm $CO_2$, 0.2 mol% Ni, 2 equiv. HBPin, 4 h, room temperature; Scheme 1.2.4). Such selectivity for

reduction of $CO_2$ to the formaldehyde level is rare, with single reduction to formic acid or overreduction to methanol are typically observed.
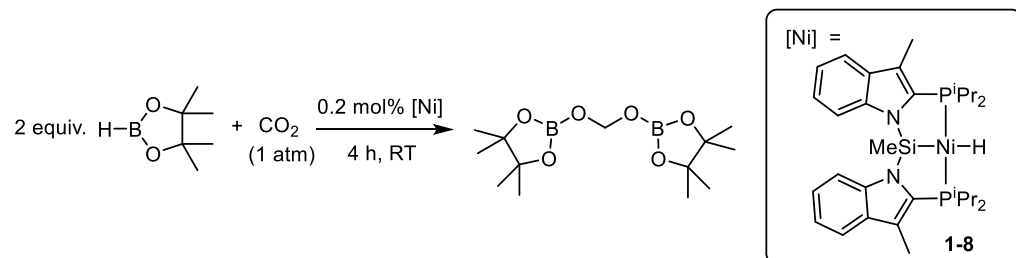


**Scheme 1.2.4** Hydroboration of $CO_2$ to form the bis(boryl)acetal product mediated by a Ni hydride pre-catalyst.

Related reactivity involving the hydroboration of $CO_2$ was also reported by Guan and co-workers,[23b] who demonstrated that a bis(phosphinite)-supported (PCP)Ni pincer pre-catalyst (**1-8**) enabled $CO_2$ reduction to the methanol level (Scheme 1.2.5). Using either catecholborane (HBCat) or 9-9-borabicycle[3.3,1]nonane (9-BBN) afforded the corresponding (methoxy)borane under mild catalytic conditions (1 atm $CO_2$, 1 mol% catalyst, room temperature). The proposed mechanism for this transformation involves successive steps of hydride insertion and hydride regeneration, with the exception of the step converting [Ni]OCH$_2$OBcat to [Ni]OBcat and HCHO, for which a β-alkoxy elimination process is invoked.
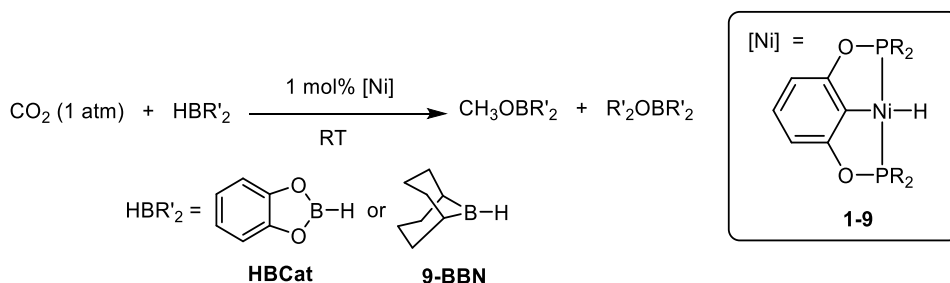


**Scheme 1.2.5** (POCOP)NiH catalyzed $CO_2$ hydroboration to methanol derivative product with HBCat and 9-BBN

The utility of Ni in alkene hydroboration has not been widely demonstrated to date,[24a] and

examples are limited to the hydroboration of styrene derivatives. In a report by Schomaker and

co-workers,[24b] a number of Ni pre-catalysts were screened for this transformation, including

$Ni(COD)_2$, bis(phosphine) Ni complexes supported by bidentate ligands such as dppp (dppp =

1,3-bis(diphenylphosphino)propane) and dcpe (dcpe = 1,2-bis(dicyclohexylphosphino)ethane),

and Ni NHC complexes. It was determined that mixed phosphine/NHC ligated Ni complexes

afforded high selectivity for the branched (Markovnikov) hydroboration product *vs*. the terminal

isomer. A broad range of styrene substrates were screened using the NHC derivative

$(IMes)(Cy_3P)NiCl_2$ (**1-10**) as a pre-catalyst with $KO^tBu$ as an activator. Both electron-donating

and -withdrawing groups in either the *para* or *ortho* positions were well tolerated, with the

branched (Markovnikov) product preferred. However, halide substitution in the substrates

produced poor yields. It is proposed that the strong *trans*-effect of the NHC ligand promotes

dissociation off the $PCy_3$ ligand, thereby opening a coordination site at the Ni center for alkene

coordination (Scheme 1.2.6). The selectivity for the Markovnikov product is postulated to result

from preferential 2,1-insertion facilitated by the formation of an $\eta^3$-benzyl intermediate.
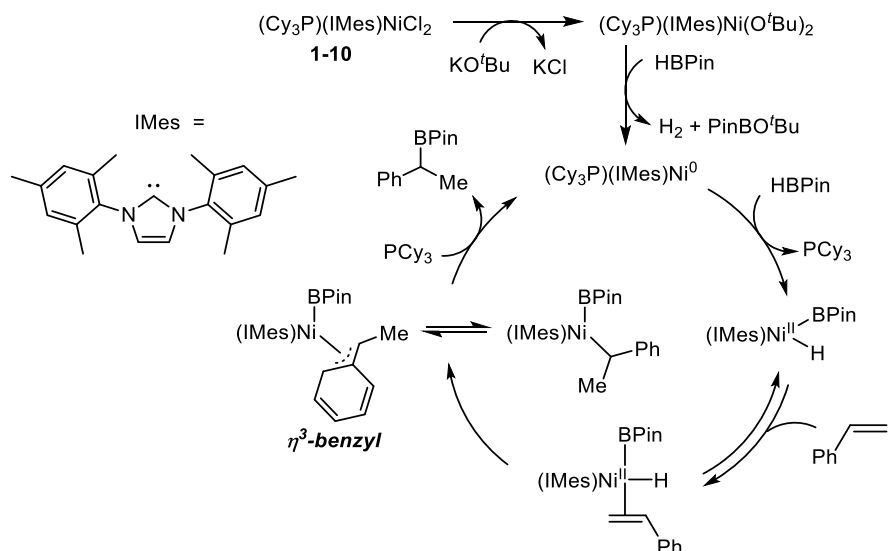


**Scheme 1.2.6 (**IMes)(Cy₃P)Ni-catalyzed hydroboration of styrenes with Markovnikov selectivity.

## 1.3 Ligand Design for Base Metal Reactivity

The development of catalytic reactivity involving Earth-abundant $3d$-metals is largely hindered by the unpredictable reactivity resulting from readily accessible one-electron processes. Such one-electron chemistry is rarely observed for platinum group metals that preferentially undergo predictable two-electron reactions such as oxidative addition and reductive elimination. Ancillary ligand design has emerged as the primary means by which the reactivity of $3d$-metals can be tempered to achieve efficient catalytic transformations. Strategies that have emerged as the most successful in this regard include the use of multidentate ligands to promote metal-ligand binding via the chelate effect, the incorporation of strong-field donors (e.g., alkyl, silyl, phosphino, NHC) to promote electron pairing, and the use of metal-ligand cooperativity[25] to facilitate bond making/breaking without needing to access high oxidation states that are not favored for first row metals.

The use of tridentate ligands that incorporate strong-field NHC donors to promote electron-pairing by supporting low-spin configurations has been utilized by the groups of Chirik[14] and Fout,[26] respectively. The Chirik group has used bis(arylimidazol-2-ylidene)pyridine ligation (**1-1**, Figure 1.2.1) in this regard to facilitate Fe-catalyzed hydrogenation of sterically hindered, unfunctionalized alkenes with high conversion rates and low catalyst loading (4 atm $H_2$, 23 °C, 5 mol % catalyst). Fout and co-workers utilized bis(mesityl-benzimidazol-2-ylidene)phenyl ligation (**1-11**, Figure 1.3.1) to support a $Co^I$ hydride complex that catalyzed the hydrogenation of sterically hindered alkenes under mild conditions (4 atm $H_2$, room temperature, 2 mol% catalyst). On the basis of extensive NMR studies, the mechanism of this reactivity was proposed to involve a $Co^I/Co^{III}$ redox cycle.

1-11

*Fout*
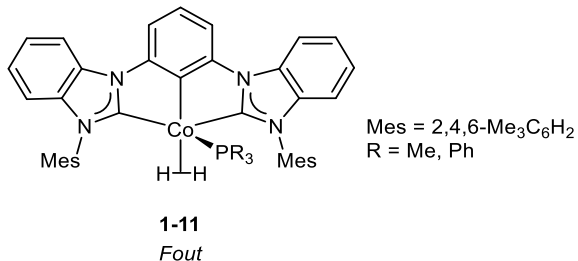
**Figure 1.3.1.** (CCC)Co complex featuring strong-field NHC donors facilitates alkene hydrogenation catalysis *via* a two-electron Co(I)/Co(III) cycle.

With respect to metal-ligand cooperativity, the primary approaches that have been developed are redox non-innocence,[27,28] whereby the ligand can undergo reversible redox processes and effectively functions as an electron reservoir, and the incorporation of Brønstead basic groups in the ligand architecture that can shuttle proton equivalents reversibly to the metal center.[25] The latter effect has also been achieved via a ligand aromatization/dearomatization process pioneered by the Milstein group. [29]

A state-of-the-art example of redox-active ligands that have been utilized effectively to facilitate 3$d$-metal catalysis is that of pyridine(diimine) (PDI)[13] ligands that have been studied extensively by the Chirik group (Scheme 1.3.1a). The occurrence of cooperative redox-events between the PDI ligand and 3$d$-metal center allows the base metal to mimic the behaviour of a platinum group metal and participate in redox reactivity, such as oxidative addition and reductive elimination, while storing electron density at the ligand to prevent the metal from experiencing unfavorable oxidation states during the catalytic cycle (Scheme 1.3.1b). This has allowed the Chirik group to develop highly active Fe and Co pre-catalysts for catalytic [2+2] cycloaddition,[30] hydroboration,[31] alkene hydrogenation,[32] and C-H activation reactions.[33]
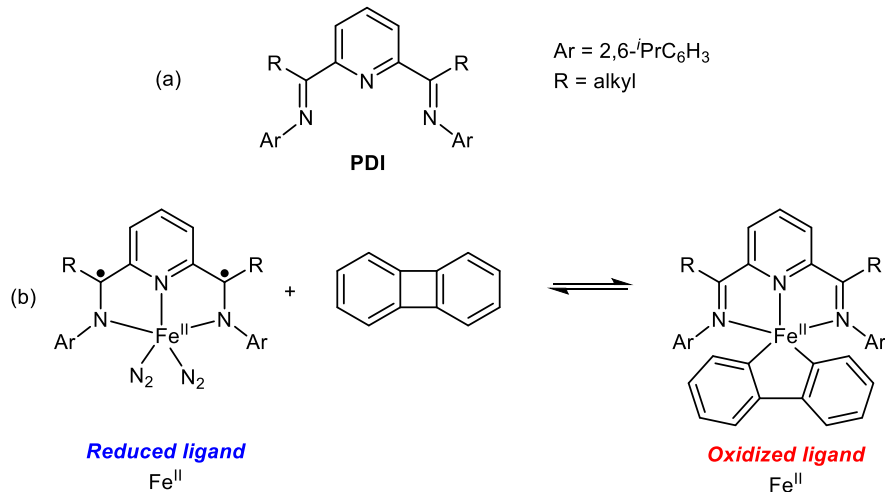
**Scheme 1.3.1.** (a) Example of redox-active pyridine(diimine) (PDI) ligand. (b) Example of a (PDI) supported Fe complex reacting in an oxidative addition reaction with biphenylene to produce an Fe metallocycle where the ligand acts as an 'electron reservoir' and the Fe(II) oxidation state is maintained.

A unique mode of metal ligand cooperativity involving the transfer of proton equivalents has been demonstrated by Milstein and co-workers,[34] whereby the ability to dearomatize/aromatize a pyridine-based pincer ligand provides the driving force for this reactivity. Deprotonation of a pyridinylmethylenic carbon in the tridentate ligand framework leads to dearomatization of the pyridine moiety (Scheme 1.3.2a). The ligand can then participate in E-H (E = main group element) bond activation in cooperation with the metal without a change in the formal oxidation state of the metal center (Scheme 1.2.3 A). The E-H bond adds such that an $H^+$ equiv. protonates the ligand arm, re-aromatizing the pyridine ring, while an $E^-$ equiv. binds to the metal for subsequent functionalization reactions. By utilizing this strategy for cooperative bond activation the Milstein group has been able to successfully develop 3$d$-metal catalyzed hydrogenation of ketones[35] and $CO_2$[36] using a 2,6-bis(diisopropyl-phosphinomethyl)pyridine)Fe pre-catalyst (**1-12a**, Scheme 1.3.2b). Treatment of complex **1-12a** with a catalytic amount of base in alcoholic solvent at ambient temperatures led to generation of the catalytically active dearomatized

complex **1-12b**. In the case of ketone reduction, racemic hydrogenated alcohol products were generated with up to 94% conversion. The proposed mechanism for this transformation (Scheme 1.3.2b) involves deprotonation of the acidic methylene linker (pKa in THF of approximately 35) to dearomatize the ligand backbone, ketone coordination and insertion into the remaining Fe-H to form an alkoxide species, followed by cooperative splitting of $H_2$ into $H^+$ and $H^-$ to restore the aromaticity of the PNP ligand. The catalytic cycle can then turn over by forming the alcohol product via reductive elimination/ligand dearomatization to regenerate **1-12b** and repeat the catalytic process.
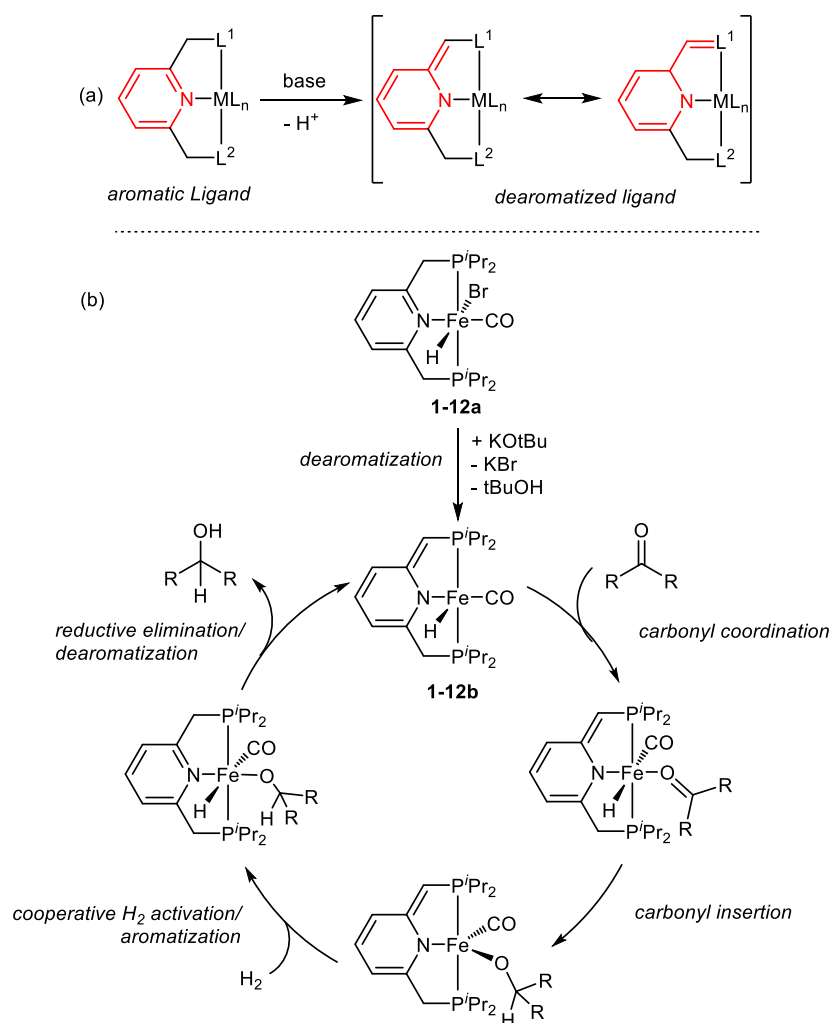


**Scheme 1.3.2** (a) Example of deprotonation of the acidic methylene proton in a PNP pincer ligand backbone, forming the reactive dearomatized complex. (b) Mechanism of

15

dearomatization/aromatization metal-ligand cooperativity for Fe-catalyzed ketone hydrogenation. (C) Example of $H_2$ splitting into a $H^+$ and $H^-$ across the amido group in the ligand back-bone and the Fe metal respectively.

Metal-ligand cooperativity involving a more general transfer of proton equivalents to Brønstead acidic groups (e.g., $R_2N^-$) in the ligand donor framework is well precedented in platinum group metal catalysis,[37] and has also successfully been applied to 3$d$-metal reactivity. In this regard, the Hazari group has demonstrated the catalytic hydrogenation of $CO_2$ utilizing a (PNP)Fe amido pre-catalyst (**1-13a**, Scheme 1.3.3a).[37] Under catalytic conditions, the amido group in the pincer ligand backbone reacts in cooperation with the Fe center to split $H_2$ into $H^+$ and $H^-$ to generate N-H and Fe-H linkages, respectively (**1-13b**). Intermediate **1-13b** subsequently reacts with $CO_2$ to deliver the $H^+$ and $H^-$ equivalents, resulting in catalytic reduction of $CO_2$ with high turnover numbers and low catalyst loadings. Morris and co-workers,[38] have utilized a similar approach to achieve the asymmetric transfer hydrogenation of ketones using Fe pre-catalysts that incorporate amido donors in the ligand backbone (Scheme 1.3.3b).
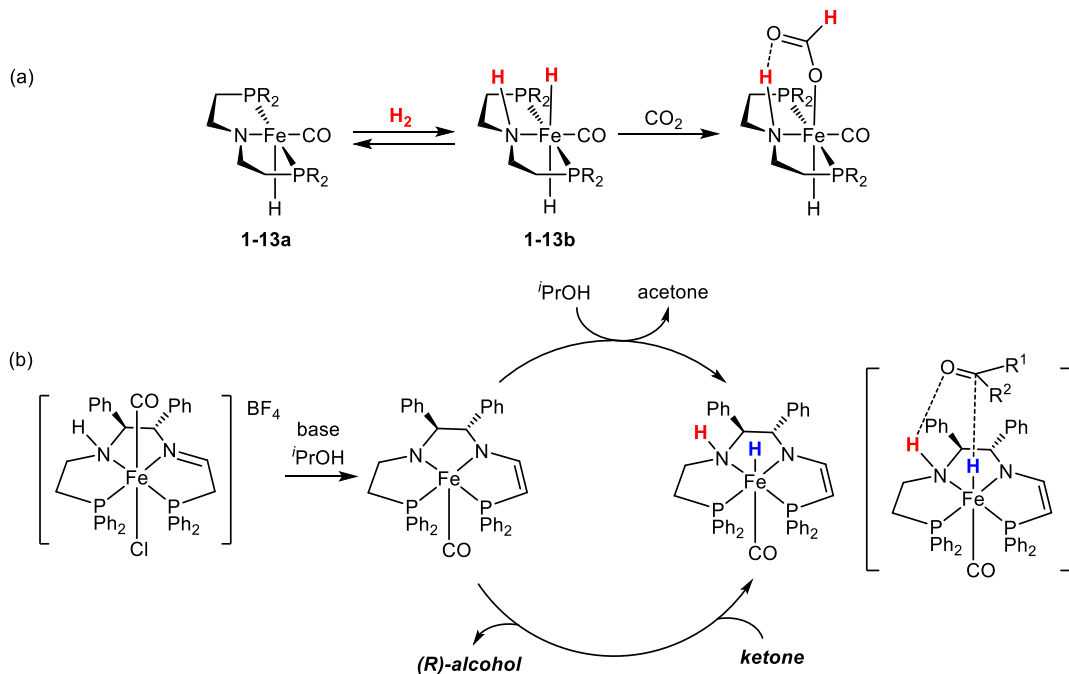
**Scheme 1.3.2** (a) Example of cooperative $H_2$ splitting into $H^+$ and $H^-$ across an Fe- amido linkage followed by $CO_2$ reduction. (b) Asymmetric transfer hydrogenation of ketones using Fe amido species that engage in metal-ligand cooperativity.

While the transfer of $H^+$ equivalents is well-precedented in metal-ligand coooperativity, the utility of related hydride transfer between the metal and an electropositive donor in the ligand framework has not been widely demonstrated. The Peters group has reported on (bis-phosphinoboryl) cobalt (**1-14**) and nickel (**1-15**) complexes for the hydrogenation of alkenes under mild conditions (1 atm $H_2$, room temperature, 2 mol % catalyst; Figure 1.3.2a).[39] In both examples, they were able to demonstrate boryl-mediated cooperative reactivity involving the transfer of hydride from the metal to the boron center. In this regard, under 1 atm of $H_2$ complex **1-16** undergoes reversible formation of the σ-borate complex (**1-17**). This process can be reversed by introducing 1 atm $N_2$ (Figure 1.3.2b).
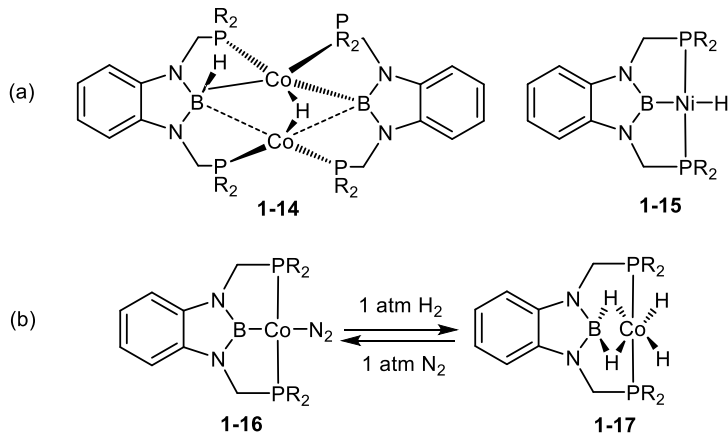


**Figure 1.3.2** (a) Boryl pincer (PBP)Co and (PBP)Ni catalysts for the catalytic hydrogenation of alkenes. (b) Metal-boryl cooperative cleavage of $H_2$ to afford a borohydride and a metal hydride species.

Examples of metal-boryl cooperativity suggest that such reactivity should be accessible with other types of electropositive donor groups, such as silyl donors. Indeed, Nagashima and co-workers have recently reported Fe-silyl cooperativity in alkene hydrogenation catalysis

involving1Q a disilyl bidentate ligand (Scheme 1.3.3).[40] Cleavage of $H_2$ across the Fe-Si bond leads to the formation of σ-SiH coordinated species that can transfer H equivalents to a coordinated alkene.
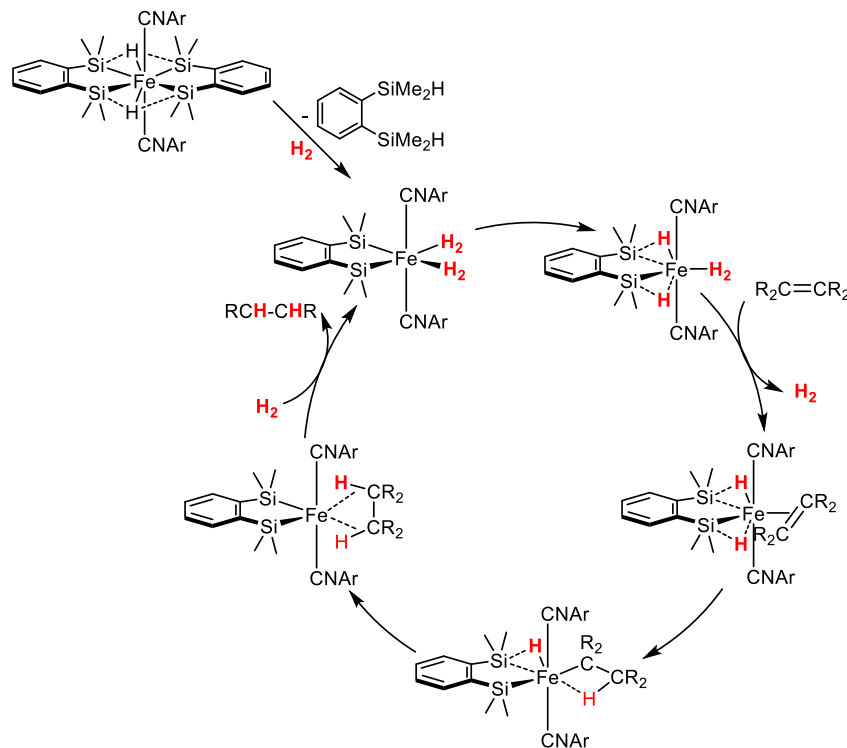


**Scheme 1.3.3** Example of metal-silyl cooperativity in Fe-catalyzed alkene hydrogenation reactivity.

Although metal-silicon chemistry is well-precedented across the transition series, mainly in the context of hydrosilylation reactions,[19c] the use of silyl fragments in multidentate ancillary ligands is much less developed. In this regard, the incorporation of silyl donors in ancillary ligands resulting in metal-silyl cooperativity via σ-SiH coordination may open-up new avenues of reactivity for first-row transition metals, leading potentially to increased catalytic ability in hydrofunctionalization reactions. The formation of σ-SiH complexes is well established across the transition series.[40, 41] Such σ-complexes are preferentially formed in the case first-row transition metals as 3*d*-orbital overlap with the Si-H σ* antibonding orbital of a coordinated silane

is relatively poor, leading to minimal backdonation of electron density necessary for Si-H complete cleavage.[41] The Turculet group has been actively pursuing this strategy of metal-silyl cooperativity in their pursuit of new hydrofunctionalization catalysis mediated by first row metal bis(phosphino)silyl (PSiP) complexes.

## 1.4 (Phosphino)silyl Ligand Design for Base Metal Reactivity and Catalysis

The utilization of silyl fragments in multidentate ancillary ligands was first established in the 1990's by Stobart and co-workers.[42] Bi- and tridentate phosphinosilyl ligands featuring aliphatic linkers were synthesized, and their coordination chemistry with platinum group metals was investigated (Scheme 1.4.1a). In an effort to reduce the conformational flexibility of these ligands Stobart and co-workers also synthesized phosphinosilyl variants that featured a benzyl linker connecting silicon to phosphorus (Scheme 1.4.1b).[42] Rigid tridentate and tetradentate phosphinosilyl ligands featuring a *o*-phenylene backbone were later introduced by the Turculet[43-45] and Peters[46] groups, respectively (Figure 1.4.1). Phenylene linkers remove the ability for the ensuing complexes to undergo decomposition via β-hydride elimination. Peters and co-workers utilized such tetradentate $P_3Si$ ligands to synthesize multiple first-row metal complexes, including Fe, Co and Ni derivatives, and reported a seminal example of $N_2$ reduction by a trisphosphinosilyl iron complex.
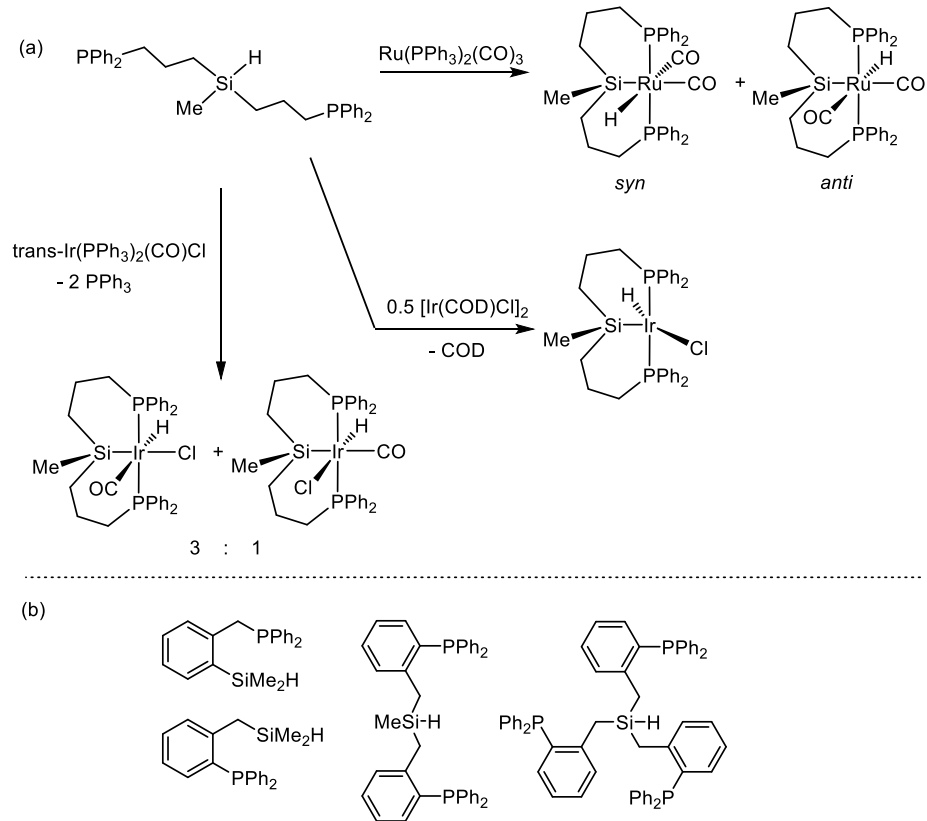
**Scheme 1.4.1** (a) Examples of Ru and Ir coordination chemistry with tridentate PSiP ligands featuring aliphatic linkers. (b) Structures of mono, bis, and tris(phosphino)silyl ligand precursors featuring benzylic linkers.
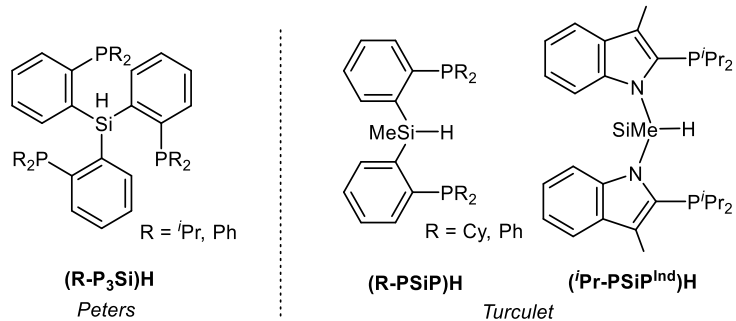


**Figure 1.4.1** Tri- and tetradentate (phosphino)silyl ligands featuring rigid aromatic linkers.

The Turculet group initially pursued predominantly platinum group metal chemistry supported by bis(phosphino)silyl ligation, as the electron donating ability of Si was anticipated to produce highly electron rich complexes that would undergo facile oxidative addition chemistry. The strongly σ-donating silyl group was also anticipated to promote coordinative

unsaturation. Such features should result in highly reactive platinum group metal complexes. Indeed, Cy-PSiP ligated (Cy-PSiP = (2- Cy$_2$PC$_6$H$_4$)$_2$SiMe) Ir complexes were shown to readily undergo challenging N–H and $sp^2$C–H bond oxidative addition to form (Cy-PSiP)Ir(H)(NHR) (**1-18**, R = H, alkyl, aryl) and (Cy-PSiP)Ir(H)(aryl) (**1-19**) species, respectively (Scheme 1.4.2a).[44] As well, Turculet and co-workers also reported on the synthesis and characterization of exceptionally rare, four-coordinate, 14-electron (Cy-PSiP)Ru$^{II}$ complexes (**1-20**, Scheme 1.4.2b).[45] These complexes feature an unusual trigonal pyramidal coordination geometry, and DFT studies showed arises due to the strongly trans-directing silyl donor of the Cy-PSiP ligand.
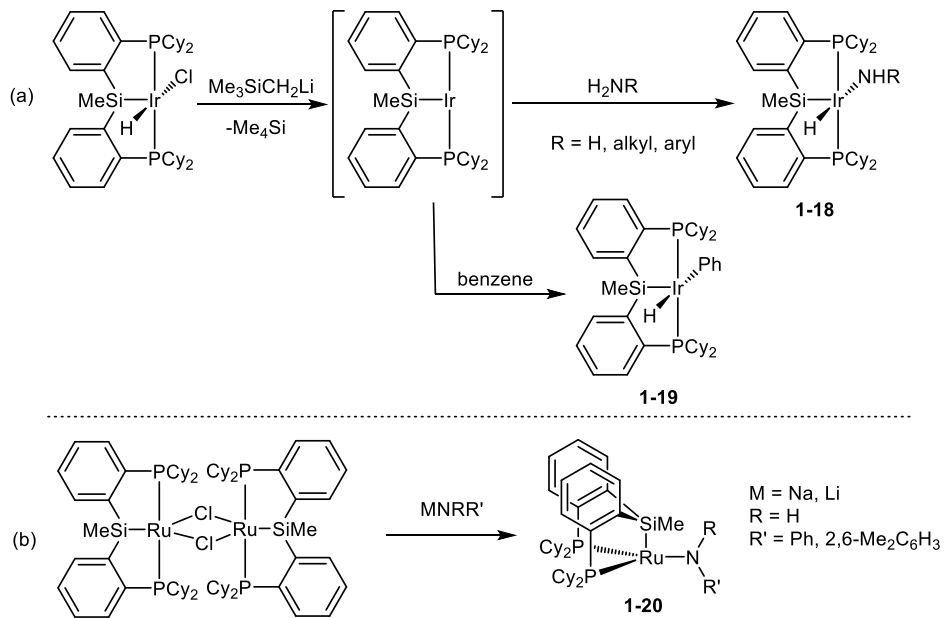


**Scheme 1.4.2** (a) Oxidative addition of amine N-H and benzene C-H bonds by Cy-PSiP supported Ir$^I$. (b) Unusual 4- coordinate Ru(II) complexes featuring trigonal pyramidal geometry enforced by Cy-PSiP ligation.

The Turculet group, among others,[47,48] have more recently transitioned to studying the synthesis and catalytic utility of 3$d$-metal complexes supported by PSiP ligation. Turculet and co-workers have reported examples of PSiP ligated Fe, Co, and Ni species, as well as their utility in alkene, alkyne, and CO$_2$ reduction chemistry[47a,d, 23a]. Examples of σ-SiH coordination were

documented in each of the latter three systems, and the role of Si in the activation of E-H bonds and the transfer of H- equivalents to facilitate catalytic turnover is currently being investigated in the group.

In the case of Fe,[47a] a variety of Cy-PSiP supported Fe hydride complexes stabilized by $PMe_3$ coordination could be isolated (Scheme 1.4.3a). The crystallographically characterized, diamagnetic polyhydride complex **1-21** features two terminal Fe hydrides and a third apparent σ-(Si-H) interaction. NMR studies including NOESY, $^1H$-$^{29}Si$ HMBC, and variable temperature experiments facilitated the unambiguous characterization of **1-21** in solution. Unfortunately, such $PMe_3$ stabilized complexes proved unreactive in alkene hydrogenation catalysis. As such, complexes without stabilization from additional phosphine ligands were targeted. In this regard, the diamagnetic complex (Cy-PSiP)FeH(N2)2 (**1-22**) was prepared and characterized (Scheme 1.4.3b). X-ray crystallographic analysis of **1-22** revealed an acute Si-Fe-H angle of 78.8(7)° and relatively short Si-H distance of 2.44 Å (less than the sum of the van der Waals radii of 3.4 Å for H and Si). Furthermore, a $^2J_{SiH}$ coupling constant of 70 Hz was measured for **1-22** in solution. These data are indicative of a σ-SiH interaction in this complex.
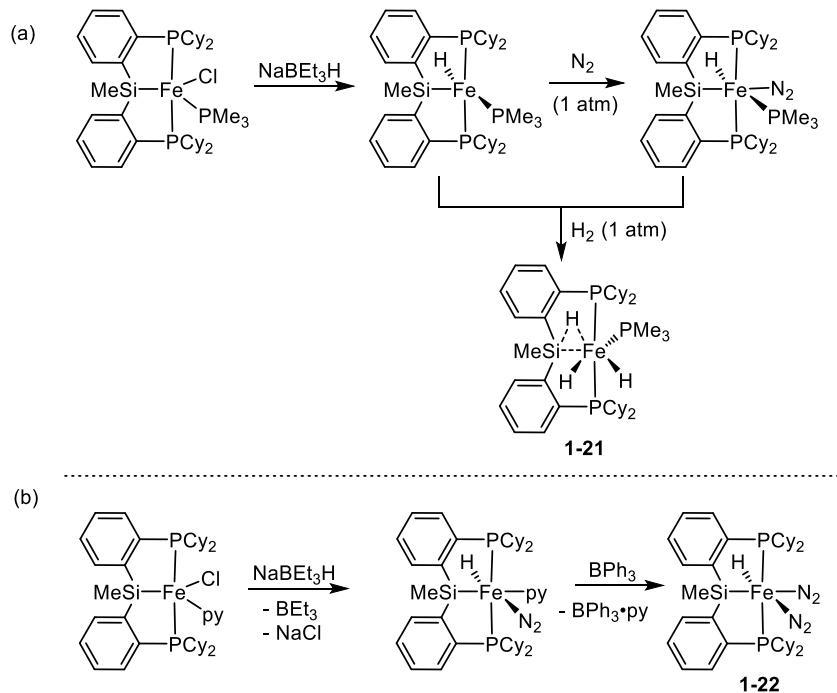
**Scheme 1.4.3** (a) Synthesis of (Cy-PSiP)Fe hydride complexes stabilized by $PMe_3$ coordination. (b) Synthesis of (Cy-PSiP)FeH($N_2$)$_2$ (**1-22**).

Complex **1-22** is an active pre-catalyst for the hydrogenation of alkenes under relatively mild conditions (10 atm $H_2$, 5 mol % Fe, 65 °C, 4 h). Terminal alkenes, *cis/trans* internal alkenes, 1,1-disubstituted alkenes, and an example of a trisubstituted alkene were all hydrogenated with near quantitative conversions. Substrates featuring ether and ester functional groups were also well-tolerated. These results compare favorably to the PDI and bis(arylimidazol-2-ylidene)pyridine supported Fe systems previously reported by Chirik and co-workers for alkene hydrogenation (*vide supra*).

Cobalt hydride species supported by Cy-PSiP ligation were generated by treatment of (Cy-PSiP)Co($N_2$)($PMe_3$) with 1 atm of $H_2$.[47b] This reaction afforded a diamagnetic Co hydride product (**1-23**) featuring broad $^{31}P\{^1H\}$ and $^1H$ NMR resonances. Complex **1-23** proved stable under an atmosphere of $H_2$ but was not isolable, as it reverted back to the starting Co complex upon exposure to an atmosphere of $N_2$. Variable temperature NMR study of **1-23** under an $H_2$

atmosphere revealed complex coalescence/decoalescence phenomena over the range of +80 - -80 °C, highlighting the dynamic nature of this Co hydride species. As such, it appears plausible that multiple hydride/dihydrogen species may be rapidly equilibrating in solution (Figure 1.4.2). The utility of **1-23** as a pre-catalyst for alkene hydrogenation was evaluated. Although complex **1-23** was capable of hydrogenating terminal alkenes under relatively mild conditions (10 atm H$_2$, 5 mol % Co, 60 °C, 4 h), internal alkenes and substrates featuring carbonyl functionality were not readily hydrogenated.
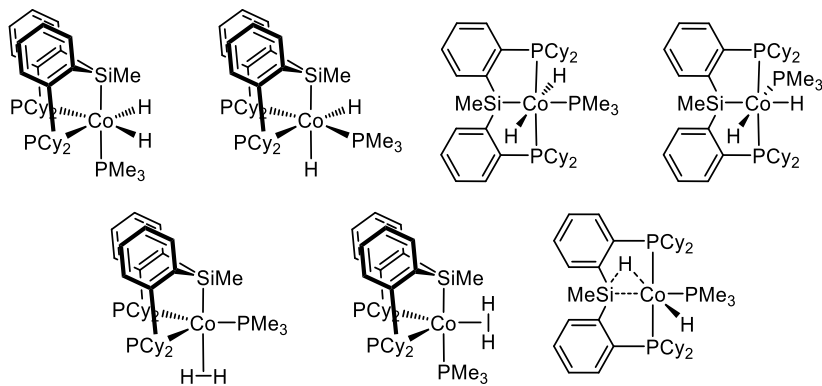


**Figure 1.4.2.** Possible Co(I) and Co(III) structures for the Co hydride species (**1-23**) arising from exposure of (Cy-PSiP)Co(PMe$_3$)(N$_2$) to an atmosphere of H$_2$.

The majority of studies involving PSiP coordination chemistry and catalysis have focused on the chemistry of Ni. In 2009 Turculet and co-workers[47c] described an unusual example of Ni mediated Si-C cleavage involving Cy-PSiP ligation (Scheme 1.4.4). This reactivity was proposed to involve a Ni(0) intermediate species **1-24** that can undergo either *sp*$^2$-SiC cleavage in the ligand backbone to afford complex **1-25a** or *sp*$^3$-SiC bond cleavage of the Si-Me to form a (Cy-PSiP)Ni(Me) complex **1-25b**. Complexes **1-25a** and **b** undergo chemical exchange in solution. Such facile, reversible Si-C cleavage was unprecedented, especially for *sp*$^3$-SiC bonds.
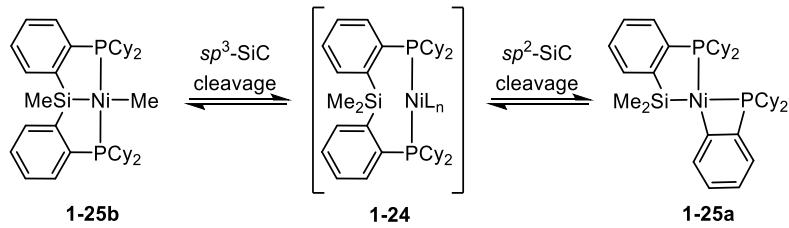
**Scheme 1.4.4** Ni mediated $sp^2$- and $sp^3$-SiC cleavage involving Cy-PSiP ligation.

Subsequently, the Turculet group developed the bis(indolyl)phosphino silyl ligand $^i$PrPSiP$^{Ind}$ and reported its coordination chemistry with Ni.[23a, 47d] The complex ($^i$PrPSiP$^{Ind}$)NiH (**1-26**) was found to undergo reversible Si-H reductive elimination upon coordination of $N_2$ to afford a Ni(0) σ-SiH complex **1-27a** (Scheme 1.4.5a). An analogue of **1-27a** featuring DMAP coordination rather than $N_2$ (**1-27b**) was crystallographically characterized, confirming this formulation. Related coordination chemistry was also reported by Hazari and co-workers for (Cy-PSiP)NiH.[48a-e,] Interestingly, in the case of the Pd(II) and Pt(II) hydride analogues (with either Cy-PSiP or $^i$PrPSiP$^{Ind}$) no such σ-SiH coordination was observed. The Ni hydride complex **1-26** was found to be highly reactive and selective in the catalytic hydroboration of $CO_2$ with HBPin to afford the bis(boryl)acetal product (*vide infra*). Interestingly, the analogous Pd and Pt hydride species afforded low conversions in this reactivity, as well as poor selectivity. Complex **1-26** is also an effective pre-catalyst for the selective semihydrogenation of alkynes to afford the *E*-alkene isomers under exceptionally mild conditions (1 atm $H_2$, 1 mol% Ni, room temperature; Scheme 1.4.5b).[47d] Attempts to carry out other types of hydrofunctionalization reactions (e.g., alkene hydroboration) using **1-26** as a pre-catalyst proved largely unsuccessful.
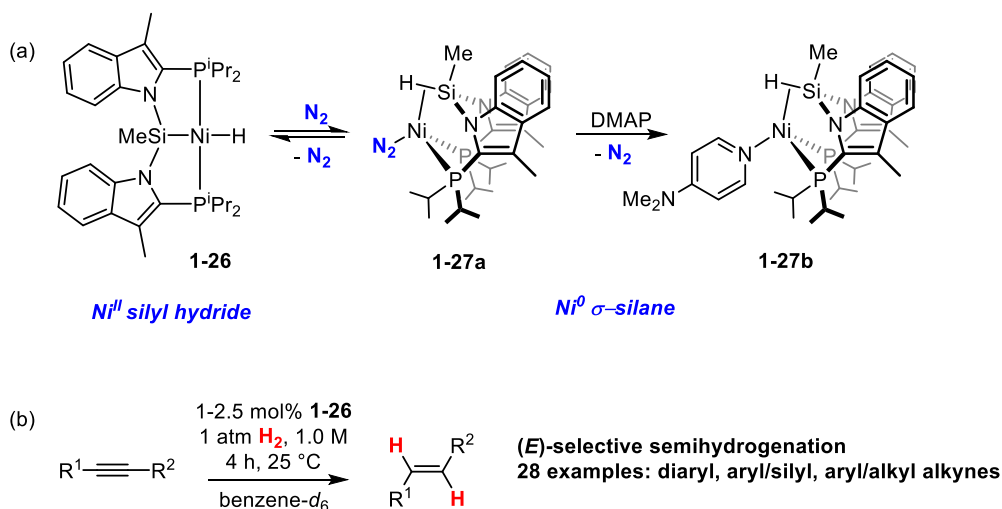
**Scheme 1.4.5** (a) Reversible Si-H reductive elimination in ($^i$PrPSiP$^{Ind}$)NiH (**1-26**) affords Ni(0) σ-SiH complexes. (b) The Ni hydride complex **1-26** catalyzes the selective semihydrogenation of alkynes to afford *E*-alkene products.

One factor that can be implicated to justify the hydrofunctionalization performance of **1-26** is a sterically congested metal coordination sphere that is only accessible to relatively small substrates and reducing agents (i.e., $H_2$, $CO_2$). In this regard, the question of reducing the size of the phosphino(silyl) ancillary ligand is currently being investigated extensively in the Turculet group. In an effort to achieve this goal, an approach that is explored in this thesis is to transition from tridentate PSiP ligation to bidentate PSi by eliminating a phosphino donor from the ancillary ligand architecture (Figure 1.1.2). While such bidentate phosphino(silyl) ligands with aliphatic and benzylic linkers were initially explored by Stobart and co-workers in the context of platinum group metal chemistry[49] (*vide infra*), their reactivity with 3*d*-metals has not been explored.

Such formally anionic PSi ligands are conceptually related to the ubiquitous neutral bis(phosphine) ligands that have been featured prominently in the organometallic literature for many decades.[50] Strong-field bis(phosphine) ligands readily bind to electron rich platinum group metal centers and can be systematically tuned by modifying either the substitution at phosphorus or the nature of the linker connecting the two phosphorus donors. Varying the ligand backbone

in this manner can significantly change the reactivity properties of the resulting metal complex by changing the ligand bite angle, as can be seen in the series of bis(phosphine) ligands depicted in Figure 1.4.3.
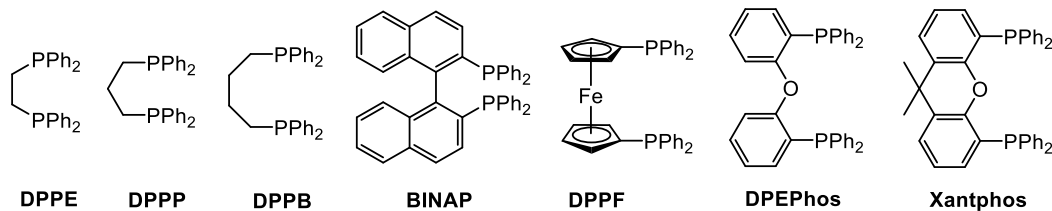


**Figure 1.4.3** Common bidentate bis(phosphine) ligands.

Bidentate, monoanionic ligands that feature strong-field donors are scarce in the literature. While examples of monoanionic P,N bidentate ligands have been reported,[51] many monoanionic bidentate ligands are solely N-based, such as the well-known β-diketiminates (colloquially known as NacNac).[52] In this regard, the development of coordination chemistry with strong-field bidentate (phosphino)silyl ligands represents a new direction in the coordination chemistry of 3*d*-transition metals. Progress towards the synthesis, characterization, and catalytic application of (PSi)Ni(II) species is detailed herein.

## Chapter 2: Synthesis and Charaterization of (PSi)Ni Complexes for Alkene Hydroboration Catalysis

**2.1 Introduction**

Tridentate bis(phosphino)silyl (PSiP) ligands featuring an aliphatic or a benzylic ligand backbone were first reported by Stobart and co-workers in the 1980s.[42, 49] More recently, the Turculet group has introduced related PSiP ligands that feature a phenylene backbone to access more rigid chelate formation upon complexation to a transition metal center and to eliminate the possibility of β-hydride elimination as an undesired side reaction.[43] The organometallic chemistry of closely related PCP "pincer" derivatives has been studied extensively,[53] but replacing the electronegative central carbon donor, with an electropositive silicon donor is anticipated to introduce important reactivity differences. The electropositive nature of Si means that more electron density should be localized on the metal in a M-Si linkage versus a M-C bond. Furthermore, a silyl donor is strongly *trans*-labilizing, which can better promote the generation of coordinatively unsaturated complexes. Lastly, the ability to readily form σ-(Si-H) complexes, especially in the case of 3$d$-metal complexes, introduces an avenue for metal-ligand cooperative reactivity that may prove beneficial in the course of a catalytic transformation by facilitating the transfer of hydride equivalents between Si and the metal center.[53]

The Turculet group has previously developed and utilized three different PSiP ligands: (Cy-PSiP)H, (Ph-PSiP)H, and (iPr-PSiP$^{Ind}$)H (Figure 2.1.1).[43-45, 47] Both Cy-PSiP and iPr-PSiP$^{Ind}$ ligation have been successfully utilized in first-row transition metal (Fe, Co, and Ni) coordination chemistry and catalytic hydrofunctionalization reactions, including alkene hydrogenation, alkyne semihydrogenation, and $CO_2$ hydroboration.[23a, 47d] Hydride species featuring Si···H···M interactions have been observed and/or isolated in all such reactivity studies.
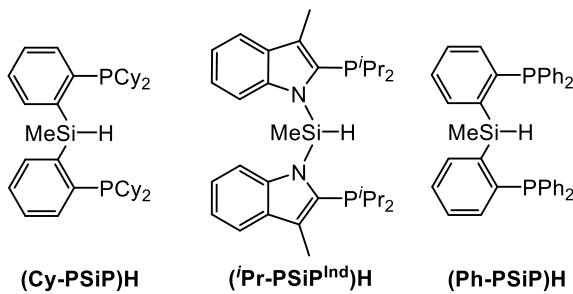
**Figure 2.1.1** Examples of PSiP ligands used in the Turculet group for transition metal reactivity and catalytic transformations.

In the case of Ni, Hazari and co-workers have reported that attempts to prepare a hydride complex by treatment of (Ph-PSiP)NiCl with $LiEt_3BH$ led to $H_2$ elimination and the formation of a dinuclear complex featuring two hypervalent five-coordinate Si atoms bridging two Ni centers (Scheme 2.1.1a).[54] By comparison, under an $N_2$ atmosphere both (Cy-PSiP)NiH and ($^i$Pr-PSiP$^{Ind}$)NiH are found in equilibrium with Ni(0) $N_2$ adducts featuring σ-(Si-H) coordination (Scheme 2.1.1b, c).[23a, 48] While the former complex is thermally sensitive and therefore challenging to work with, ($^i$Pr-PSiP$^{Ind}$)NiH can be readily generated and has been used as a pre-catalyst for $CO_2$ hydroboration and alkyne semihydrogenation reactivity. Both of these reactions exhibited somewhat unusual selectivity. In the case of $CO_2$ reduction with HBPin, exclusive selectivity for hydroboration to the formaldehyde level was obtained to provide the bis(boryl)acetal PinBOCH$_2$OBPin in high yield. [23a] The high selectivity obtained for alkyne semihydrogenation with no evidence for over-reduction to the corresponding alkane was also surprising, and reactivity studies indicated that the Ni hydride complex isomerizes *Z*-alkenes to the *E*-isomer, but does not show appreciable activity for alkene reduction.[47d] These results suggest that steric factors may be at play in this reactivity. Attempts to carry out other types of hydrofunctionalization reactions (e.g., alkene hydroboration) using ($^i$Pr-PSiP$^{Ind}$)NiH were largely unsuccessful.
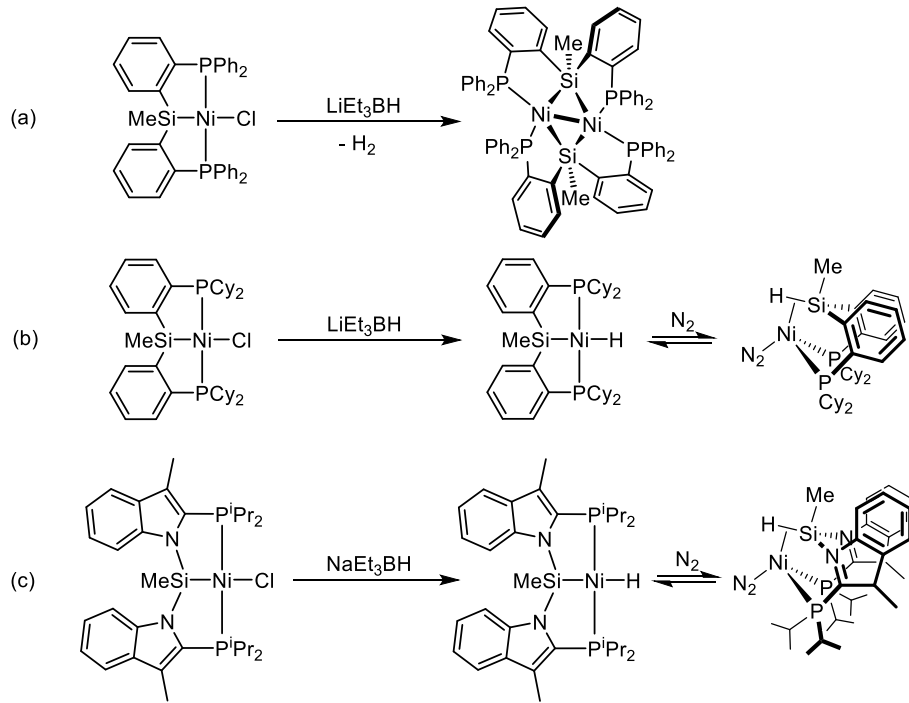
**Scheme 2.1.1** Attempted syntheses of Ni hydride complexes supported by PSiP ligation.

In this regard, the question of reducing the size of the phosphino(silyl) ancillary ligand is currently being investigated in the Turculet group. While varying the substitution at phosphorus is a common approach to modifying the steric features of phosphine ligands, access to substituents smaller than Ph and $^i$Pr is not straightforward.[55] A different approach that is synthetically more accessible is to entirely eliminate a phosphine donor from the ligand architecture resulting in a bidentate PSi chelate (Figure 2.1.2). This strategy is explored in this thesis. The synthesis and characterization of Ni complexes, including a Ni hydride derivative, supported by such Cy-PSi ligation is described, and their utility in alkene hydroboration catalysis is evaluated.
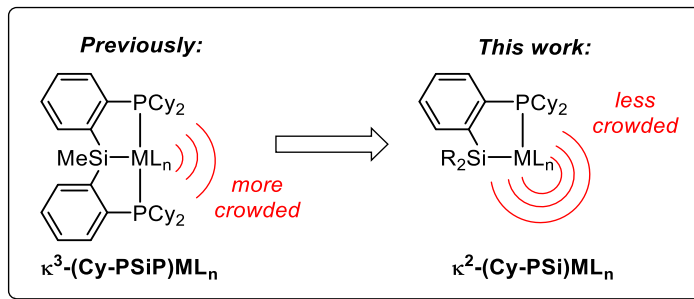
**Figure 2.1.2** Bidentate PSi ligation targeted in this thesis.

## 2.2 Results and Discussion

### 2.2.1 Synthesis and Characterization of (Cy-PSi)H and Corresponding (Cy-PSi)Ni Complexes

The tertiary silane (Cy-PSi)H was readily prepared starting from commercially available 2-bromoiodobenzene via a two-step process (Scheme 2.2.1). Treatment of 2-bromoiodobenzene with one equiv. each of $Cy_2PH$ and $Cs_2CO_3$ in the presence of catalytic $Pd(OAc)_2$/DiPPF afforded the product of P-C cross-coupling at the aryl iodide position.[56] Subsequent treatment of the resulting phosphino(bromoarene) with one equiv. of $^n$Buli followed by quenching with $^iPr_2SiHCl$ afforded the desired tertiary silane **(Cy-PSi)H** as a white solid in 94% yield. The nature of the chlorosilane used in the latter step can be varied readily. The isopropyl silane derivative used herein was chosen as it was available in the lab and affords reasonable steric protection at the metal centre.
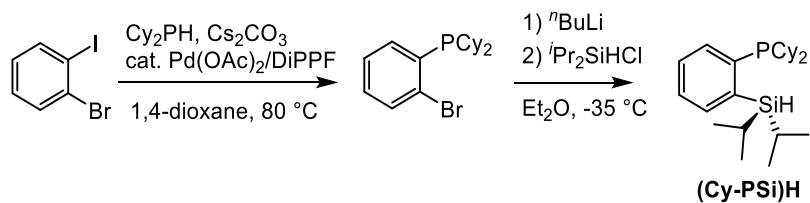


**Scheme 2.2.1** Synthetic route for the preparation of **(Cy-PSi)H**.

The solution (benzene-$d_6$) NMR data for **(Cy-PSi)H** is in full agreement with the expected structure, as indicated by a characteristic resonance in the $^1$H NMR spectrum at 4.81 ppm (dt, $^4J_{PH}$ = 7 Hz, $^3J_{HH}$ = 4 Hz, $^1J_{SiH}$ = 188 Hz) corresponding to the Si-*H*. This resonance correlates to a cross-peak at 5.04 ppm in a $^1$H-$^{29}$Si HMQC experiment. The $^{31}$P{$^1$H} NMR spectrum of **(Cy-PSi)H** features a single peak at -6.5 ppm.

The first target complex for this work was a simple Ni halide complex of the type (Cy-PSi)NiX. Such a halide complex is a good starting point for the preparation of other (Cy-PSi)Ni derivatives (*e.g.* hydrides, alkyls) that can function as potential pre-catalysts for hydrofunctionalization catalysis. In this regard, treatment of (Cy-PSi)H with one equiv. of NiCl$_2$(DME) (DME = dimethoxyethane) and excess triethylamine led to the formation of the diamagnetic complex [(Cy-PSi)NiCl]$_2$ (**2-NiCl**, Scheme 2.2.2), which was isolated as a yellow solid in 30% yield. The solid-state structure of **2-NiCl** was determined by use of X-ray crystallographic techniques, revealing a dinuclear complex featuring two Ni atoms bridged by two Cl atoms to form a dimer in a square planar geometry (Scheme 2.2.2). The coordination geometry at each Ni(II) center is approximately square planar. The solution (benzene-$d_6$) NMR spectroscopic data obtained for **2-NiCl** is in agreement with the structure observed in the solid state, as indicated by the absence of a $^1$H NMR resonance that can be attributed to an Si-*H* and a shift in the $^{31}$P{$^1$H} NMR resonance observed from -6.5 ppm in **(Cy-PSi)H** to 70.8 ppm in **2-NiCl**.
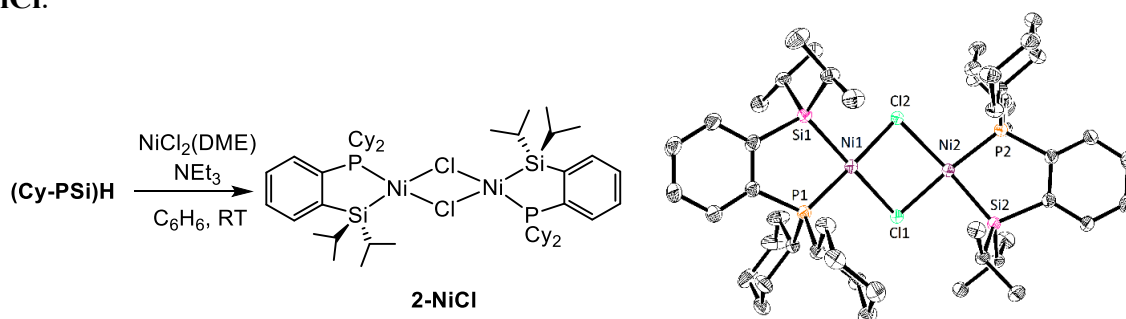
**Scheme 2.2.2** Synthesis (left) and crystallographically determined structure (right) of **2-NiCl** with thermal ellipsoids shown at the 30% probability level. Hydrogen atoms have been omitted for clarity. Selected interatomic distances (Å) and angles (°): Ni(1)-P(1) 2.1315(6), Ni(1)-Cl(2) 2.2248(6), Ni(1)-Si(1) 2.2522(6), Ni(1)-Cl(1) 2.3375(5), Ni(2)-P(2) 2.1286(6), Ni(2)-Cl(1) 2.2099(5), Ni(2)-Si(2) 2.2410(6), Ni(2)-Cl(2) 2.3375(5), P(1)-Ni(1)-Cl(2) 177.82(2), P(1)-Ni(1)-Si(1) 86.83(2), Cl(2)-Ni(1)-Si(1) 91.22(2), P(1)-Ni(1)-Cl(1) 94.52(2), Cl(2)-Ni(1)-Cl(1) 87.366(19), Si(1)-Ni(1)-Cl(1) 176.11(2), P(2)-Ni(2)-Cl(1) 175.12(2), P(2)-Ni(2)-Si(2) 87.00(2), Cl(1)-Ni(2)-Si(2) 88.83(2), P(2)-Ni(2)-Cl(2) 96.81(2), Cl(1)-Ni(2)-Cl(2) 87.714(19), Si(2)-Ni(2)-Cl(2) 169.93(2), Ni(2)-Cl(1)-Ni(1) 88.983(19), Ni(1)-Cl(2)-Ni(2) 88.625(19).

Having prepared the targeted Ni(II) chloride complex, a series of salt metathesis reactions were carried out to derivatize **2-NiCl**. Treatment of **2-NiCl** with 2 equiv. of BnMgCl led to clean formation (by $^{31}$P NMR) of the corresponding benzyl complex (Cy-PSi)NiBn (**2-NiBn**, Scheme 2.2.3), which was isolated as a yellow solid in 73% yield. The $^1$H NMR spectrum (benzene-$d_6$) of **2-NiBn** features a diagnostic peak at 2.25 ppm (d, 2 H, $^3J_{PH}$ = 4 Hz) that corresponds to the benzylic protons. The benzylic carbon gives rise to a doublet resonance at 29.7 ppm ($^2J_{PC}$ = 25 Hz) in the $^{13}$C{$^1$H} NMR spectrum of **2-NiBn**, consistent with *trans*-coordination relative to the phosphino donor. The solid-state structure of **2-NiBn** was determined by use of X-ray crystallographic techniques and indicates $\eta^3$-coordination of the benzyl ligand to the Ni center (Scheme 2.2.3).
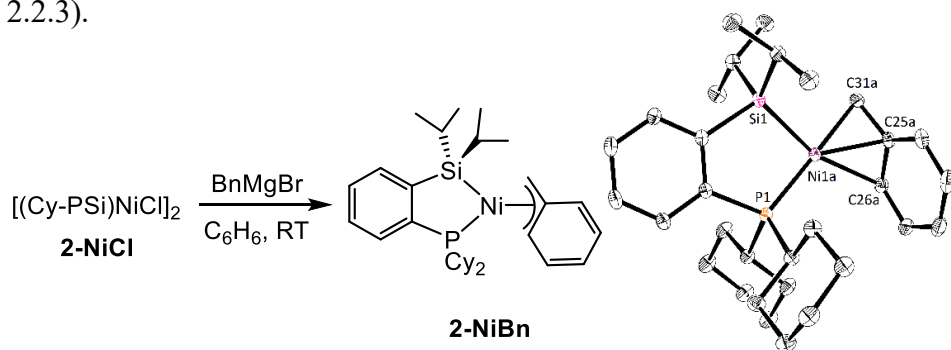


**Scheme 2.2.3** Synthesis (left) and crystallographically determined structure (right) of **2-NiBn** with thermal ellipsoids shown at the 30% probability level. Hydrogen atoms have been omitted for clarity. Selected interatomic distances (Å) and angles (°): P(1)-Ni(1A) 2.1584(6), Si(1)-Ni(1A) 2.1964(7), Ni(1A)-C(31a) 1.9709(18), Ni(1A)-C(25A) 2.0720(17), Ni(1A)-C(26A) 2.2003(18), C(31A)-Ni(1A)-C(25A) 41.71(8), C(31A)-Ni(1A)-P(1) 178.57(7), C(25A)-Ni(1A)-P(1) 139.63(6), C(31A)-Ni(1A)-Si(1) 88.18(6), C(25A)-Ni(1A)-Si(1) 124.29(6), P(1)-Ni(1A)-

Si(1) 90.87(3), C(31A)-Ni(1A)-C(26A) 72.23(8), C(25A)-Ni(1A)-C(26A) 38.64(7), P(1)-Ni(1A)-C(26A) 108.70(5), Si(1)-Ni(1A)-C(26A) 160.37(6)

In a preliminary study preformed by Dylan Hale (Turculet group) attempts to synthesize a Ni(II) hydride complex, **2-NiCl** was reacted with two equiv. of NaEt$_3$BH. NMR analysis of the crude reaction product indicated the presence of (Cy-PSi)H, unreacted **2-NiCl**, as well as several minor products giving rise to $^{31}$P{$^1$H} NMR resonances at 67.4, 53.6, and 32.6 ppm respectively. In an effort to trap a potential Ni hydride species in situ, this reaction was repeated in the presence of two equiv. of PPh$_3$ (Scheme 2.2.4a). Treatment of a benzene solution of **2-NiCl** with PPh$_3$ resulted in a color change from yellow to dark orange. A subsequent color change to dark red was observed upon the addition of two equiv. of NaEt$_3$BH. The $^1$H NMR (benzene-$d_6$) spectrum of the isolated material featured a doublet of doublets resonance centered at -3.06 ppm (1 H, $^2J_{\text{HPcis}}$ = 18 Hz, $^2J_{\text{HPtrans}}$ = 80 Hz), with $^{29}$Si satellites visible in the baseline ($^1J_{\text{HSi}}$ = 23 Hz). The upfield chemical shift associated with this resonance is consistent with a Ni-H species in a complex formulated as (Cy-P*Si*)*Ni*($\mu$-H)(PPh$_3$) (**2-NiHPPh$_3$**). The observation of $^{29}$Si satellites for the Ni-*H* resonance indicates that there is significant $\sigma$-SiH character present in **2-NiHPPh$_3$**, reminiscent of previously reported N$_2$ adducts of (Cy-PSiP)NiH and ($^i$Pr-PSiP$^{\text{Ind}}$)NiH (*vide supra*). The solid-state structure of **2-NiHPPh$_3$** was determined by use of X-ray crystallographic techniques and is consistent with the proposed formulation (Scheme 2.2.4a). The Ni center features distorted square planar coordination geometry, with the PPh$_3$ ligand coordinated *trans* to Si (P2-Ni1-Si1 152.08(2)°). The hydride ligand was located in the difference Fourier map and refined. The acute Si1-Ni1-H1 angle of 56.9(9)° and short Si1-H1 distance of 1.89(2) Å (cf., the sum of the van der Waals radii for these atoms of 3.4 Å) are consistent with $\sigma$-SiH coordination.[49]

34
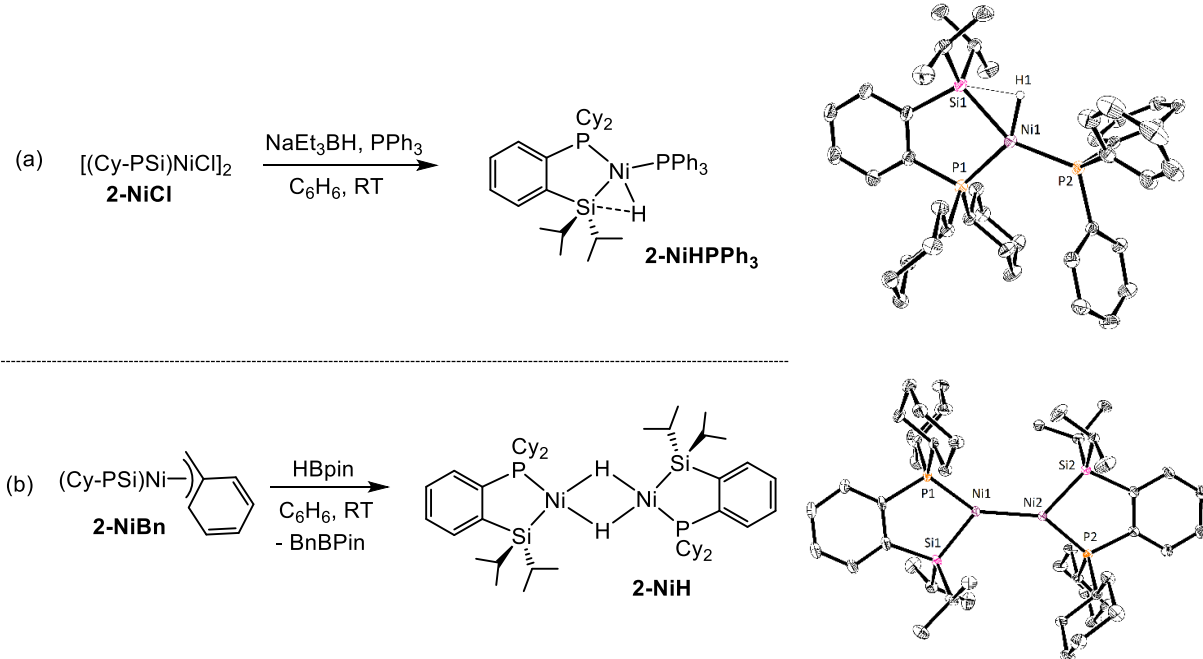
**Scheme 2.2.4** (a) Synthesis (left) and crystallographically determined structure (right) of (Cy-PSi$^H$)Ni(PPh$_3$) with thermal ellipsoids shown at the 30% probability level. Most hydrogen atoms have been omitted for clarity. Selected interatomic distances (Å) and angles (°): Ni1-P1 2.1503(5), Ni1-P2 2.1849(5), Ni1-Si1 2.2381(5), Ni1-H1 1.45(2), Si1-H1 1.89(2), P1-Ni1-P2 117.909(18), P1-Ni1-Si1 90.014(18), P2-Ni1-Si1 152.08(2), P1-Ni1-H1 146.7(9), P2-Ni1-H1 95.3(9), Si1-Ni1-H1 56.9(9). (b) Synthesis (left) and crystallographically determined structure (right) of **2-NiH** with thermal ellipsoids shown at the 30% probability level. Hydrogen atoms have been omitted for clarity. Selected interatomic distances (Å) and angles (°): Ni(1)-P(1) 2.1345(16), Ni(1)-Si(1) 2.2185(17), Ni(1)-Ni(2) 2.3469(9), Ni(2)-P(2) 2.1277(15), Ni(2)-Si(2) 2.2204(17), P(1)-Ni(1)-Si(1) 87.90(6), P(1)-Ni(1)-Ni(2) 146.18(5), Si(1)-Ni(1)-Ni(2) 124.72(6), P(2)-Ni(2)-Si(2) 86.99(6), P(2)-Ni(2)-Ni(1) 143.57(5), Si(2)-Ni(2)-Ni(1) 129.30(6).

Work completed in this thesis includes further efforts to access a Ni(II) hydride complex, **2-NiBn** was treated with one equiv. of HBpin in benzene solution, which resulted in an immediate color change from yellow to dark red. The $^1$H NMR spectrum (benzene-$d_6$) of the isolated material (**2-NiH**) features an apparent doublet of doublets resonance centered at δ -10.16 ppm ($^2J_{PH}$ = 32 Hz) that is assigned as a Ni-$H$. This resonance collapses to a singlet in the $^1$H{$^{31}$P} NMR spectrum of **2-NiH**, consistent with hydride coupling to magnetically nonequivalent phosphorus nuclei (Figure 2.2.1). No $^{29}$Si satellites for this resonance could be observed, and no

correlation was observed in $^1$H-$^{29}$Si HMBC or $^1$H-$^{29}$Si HMQC experiments between this resonance and the $^{29}$Si NMR resonance for **2-NiH** at 58.0 ppm. The $^{31}$P{$^1$H} NMR spectrum of **2-NiH** contains a singlet resonance at 71.7 ppm. These data suggest that **2-NiH** likely adopts a dimeric structure featuring μ-H ligands, with no Si-H interaction (Scheme 2.2.4b).
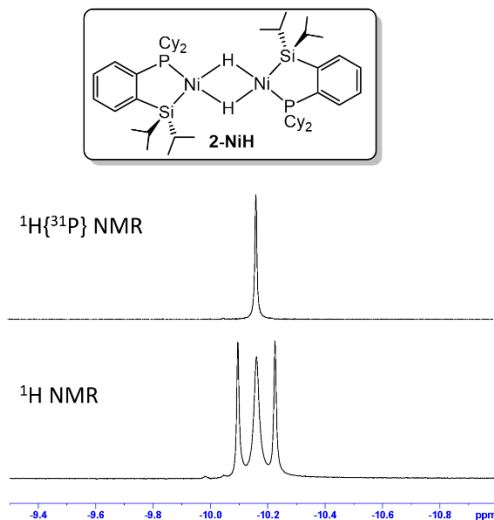


**Figure 2.2.1** Hydride region of the $^1$H and $^1$H{$^{31}$P} NMR spectra of **2-NiH** illustrating magnetic nonequivalence of the phosphino groups.

The solid-state structure of **2-NiH** was determined by use of X-ray crystallographic techniques (Scheme 2.2.4b). The structure reveals a dinuclear [κ$^2$-(Cy-PSi)Ni]$_2$ core with a Ni-Ni distance of 2.3469(9) Å. Unfortunately, the hydride positions could not be located in the difference Fourier map. The Ni-Ni distance observed in **2-NiH** is significantly shorter than the analogous distance in **2-NiCl**, which measures 3.188 Å. The short Ni-Ni distance in **2-NiH** may be attributed to a Ni-Ni bond. However, dinuclear Ni complexes with a Ni(II)-Ni(II) bond are relatively rare,[57, 58] with reported Ni-Ni distances ranging from 2.2911(8) Å for [Ni$_2$(μ-NMes)(μ-Cl)(I$^i$Pr$_2$)$_2$]$^+$ to 2.569(1) Å in (μ-η$^3$,η$^3$-C$_8$Me$_6$)Ni$_2$.[58] Furthermore, in some cases theoretical analysis shows no appreciable 3$d$ covalent interaction in such complexes, with the short Ni-Ni distance attributed to other factors, such as stereoelectronic effects from the ligands. A related

complex to **2-NiH** featuring a relatively short Ni-Ni distance of 2.4069(5) Å has been previously reported by the Turculet group (Figure 2.2.2).[21d] Alternatively, it is possible that the solid-state structure obtained corresponds to a minor Ni(I) impurity resulting from $H_2$ loss in **2-NiH**. However, the solution NMR data is not consistent with this proposal. DFT geometry optimization of **2-NiH** is currently in progress in collaboration with Dylan Hale (Turculet group).
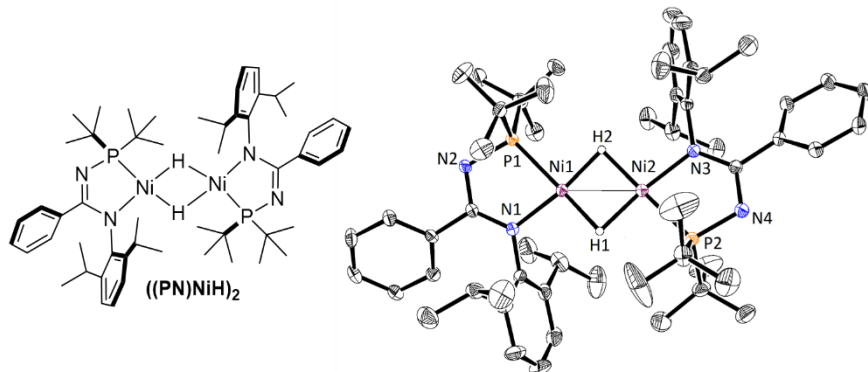


**Figure 2.2.2** Dinuclear $[(P,N)Ni(\mu-H)]_2$ complex (Ni(1)-Ni(2) 2.4069(5) Å) structurally related to **2-NiH**.[23d]

Lastly, in an attempt to synthesize another potential Ni(II) pre-catalyst for the hydroboration of alkenes, **(Cy-PSi)H** was reacted with $Ni(COD)_2$. NMR spectroscopic data for the material isolated from this reaction is consistent with a formulation of $(Cy-PSi)Ni(\eta^3-C_8H_{13})$ (**2-NiCOD**, Scheme 2.2.5). This complex can be envisioned to arise from the intermediate formation of (Cy-PSi)NiH, which subsequently inserts an equiv. of 1,5-COD and undergoes rearrangement via successive β-hydride elimination/hydride insertion steps to ultimately afford the $\eta^3$-cyclooctenyl species observed. The $^1H$ NMR spectrum solution (benzene-$d_6$) for **2-NiCOD** features diagnostic resonances at 4.76 (m, 1 H), 4.52 (m, 1 H), and 4.36 (m, 1 H) ppm corresponding to the allylic cyclooctenyl protons, and a single peak in the $^{31}P\{^1H\}$NMR spectrum at 73.7 ppm. The solid-state structure of **2-NiCOD** was determined by use of X-ray crystallographic techniques and is consistent with the formulation from solution NMR data (Scheme 2.2.5).
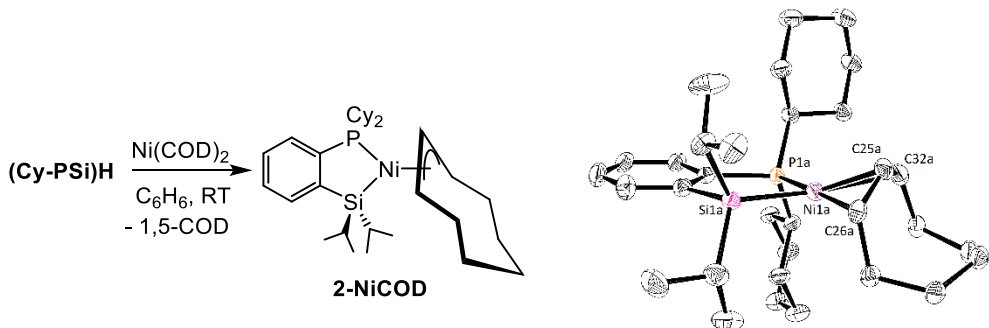
**Scheme 2.2.5** Synthesis (left) and crystallographically determined structure (right) of **2-NiCOD** with thermal ellipsoids shown at the 30% probability level. Hydrogen atoms have been omitted for clarity. Selected interatomic distances (Å) and angles (°): Ni(1A)-C(25A) 1.988(9), Ni(1A)-C(26A) 2.041(9), Ni(1A)-C(32A) 2.135(9), Ni(1A)-P(1A) 2.189(6), Ni(1A)-Si(1A) 2.220(6), C(25A)-Ni(1A)-C(26A) 40.4(4), C(25A)-Ni(1A)-C(32A) 39.4(4), C(26A)-Ni(1A)-C(32A) 72.9(4), C(25A)-Ni(1A)-P(1A) 139.9(5), C(26A)-Ni(1A)-P(1A) 177.3(5), C(32A)-Ni(1A)-P(1A) 106.3(4), C(25A)-Ni(1A)-Si(1A) 123.5(5), C(26A)-Ni(1A)-Si(1A) 93.0(4), C(32A)-Ni(1A)-Si(1A) 162.7(5), P(1A)-Ni(1A)-Si(1A) 88.3(2)

## 2.3 Catalytic Hydroboration of Alkenes

Transition metal-catalyzed alkene hydroboration is a widely used, atom-economical transformation for chemical synthesis. Although uncatalyzed hydroboration reactions are well-established,[59] transition metal catalysts offer opportunities for unique selectivity (i.e., chemoselectivity, regioselectivity, and enantioselectivity) that are not otherwise accessible in uncatalyzed reactions. In this regard, while platinum-group metal catalysts for alkene hydroboration have been studied for over 30 years,[20] catalysts based on Earth-abundant 3*d* metals are only recently emerging,[21] and at this time there are few examples of catalytic hydroboration of alkenes using Ni.[24] As such, the development of effective Ni-based catalysts for selective alkene hydroboration is an area of interest.

It is envisioned that the catalytically active species in such a hydroboration reaction would be a Ni-H complex that could undergo 1,2-insertion of an alkene (Scheme 2.3.1a). In this regard, complexes **2-NiCl**, **2-NiBn**, **2-NiH**, and **2-NiCOD** are all suitable pre-catalysts that can be

envisioned to generate a potential catalytically active (Cy-PSi)NiH species in situ upon appropriate activation (Scheme 2.3.1b).
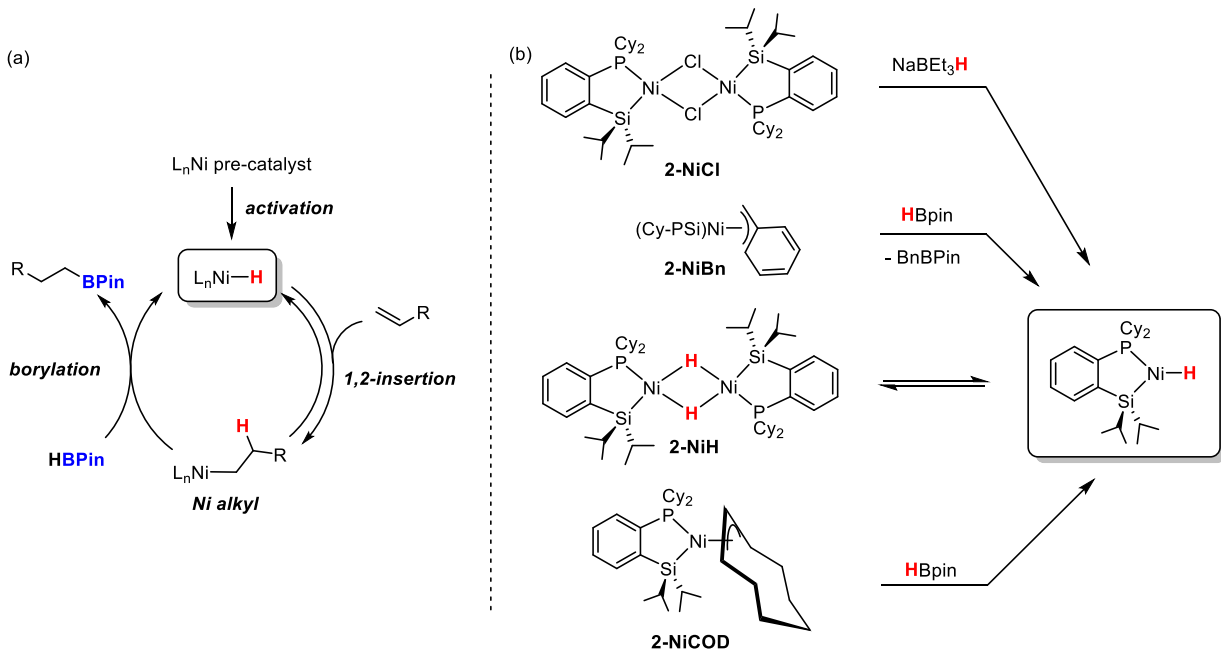


**Scheme 2.3.1** (a) Proposed catalytic cycle for Ni-mediated alkene hydroboration via a Ni-H intermediate, and (b) proposed pre-catalyst activation pathways.

## 2.3.1 Initial Hydroboration Studies

During initial studies a 5 mol% pre-catalyst loading of either **2-NiCl**, **2-NiBn**, and **2-NiCOD** were evaluated for 1-octene hydroboration with one equiv. HBPin (Table 2.3.1). The initial screening conditions involved a 4 h reaction time at room temperature. Based on the $^1$H NMR all three catalysts hydroborate at the terminal position with alkene remaining in cases of low conversion; however due to simplicity integrations as the product peaks overlapped with remaining alkene, clear remaining alkene peaks were used relative to an internal standard of 1,3,5-trimethoxybenzene and the conversion was determined to be highest when using **2-NiBn** as the pre-catalyst (96%), far outperforming both **2-NiCl** (49% conversion with NaEt$_3$BH as an activator) and **2-NiCOD** (42% conversion). Based on these results, **2-NiBn** was used for a subsequent substrate scope evaluation. Decreasing the loading of **2-NiBn** to 2.5 mol% afforded

60% conversion after 18 h at room temperature (entry 3), indicating that a 5 mol% loading is optimal.

**Table 2.3.1** Catalytic hydroboration of 1-octene using **2-NiCl**, **2-NiBn** and **2-NiCOD**.[a]



| Entry | Pre-catalyst | Activator | mol% [Ni] | Time (h) | % Conversion[a] |
|-------|--------------|-----------|-----------|----------|-----------------|
| 1 | **2-NiCl** | 15 mol% NaEt₃BH | 5 | 4 | 49 |
| 2 | **2-NiBn** | - | 5 | 4 | 96 |
| 3 | **2-NiBn** | - | 2.5 | 18 | 60 |
| 4 | **2-NiCOD** | - | 5 | 4 | 42 |

[a]Conversion determined on the basis of $^1$H NMR integration relative to 1,3,5-trimethoxybenzene as the internal standard (0.4 mmol, average of two runs).

In the case of internal alkene substrates, the possibility for alkene isomerization subsequent to 1,2-insertion exists (Scheme 2.3.2). This is postulated to occur via β-hydride elimination in the Ni alkyl intermediate, followed by re-insertion of the resulting alkene. In an effort to assess the selectivity of **2-NiBn** in such internal alkene hydroboration reactivity, the hydroboration of *trans*-4-octene was also evaluated (Table 2.3.2). Using the same screening conditions as before (5 mol% [Ni], room temperature, 4 h), it was determined that **2-NiBn** catalytically isomerizes *trans*-4-octene to selectively afford the terminally hydroborated product with 71% conversion ($^1$H NMR relative to 1,3,5-trimethoxybenzene; the selectivity of the borylation step was determined on the basis of $^{13}$C{$^1$H} DEPT-135 NMR analysis). Increasing the reaction duration to 18 h afforded 94% conversion to the terminal hydroboration product (entry 2).
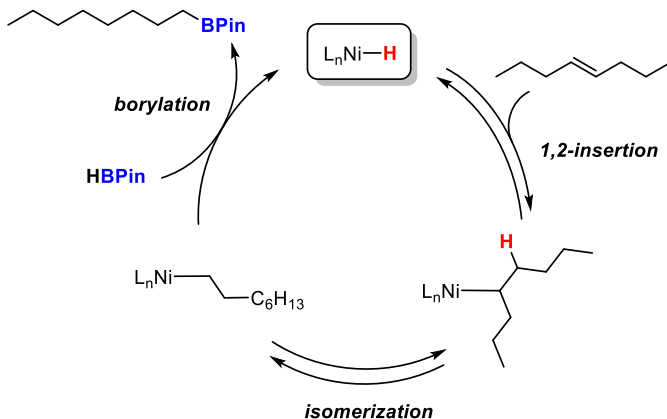
**Scheme 2.3.2** Catalytic hydroboration of *trans*-4-octene with isomerization to selectively afford the terminal borylated product.

The effect of varying temperature and catalyst loading on the isomerization/hydroboration of *trans*-4-octene was also evaluated (Table 2.3.2). Decreasing the pre-catalyst loading to 2.5 mol% afforded 43% conversion to the terminal hydroboration product after 18 h at room temperature (entry 3). Decreasing the pre-catalyst loading to 2.5 mol% and increasing the temperature to 65 °C while keeping all other conditions the same decreased the conversion to 50 % after 4 h (Table 2.3.2 entry 4) with a mixture of terminal hydroborated product and remaining substrate. Increasing the temperature to 80 °C and running the catalysis at either 5 or 2.5 mol% [Ni] afforded further decreased conversions of 38 and 32%, respectively (Table 2.3.2 entries 5 and 6) with a mixture of terminal hydroborated product, remaining substrate and what appeared to be decomposition of the catalyst causing broadness of the peaks observed in the $^1$H NMR data. Due to this observation, it was proposed that the increase of temperature may hinder catalysis due to potential thermal instability of **2-NiBn**. Based on this hypothesis, a series of reactions were performed to assess the thermal stability of **2-NiBn**. Heating **2-NiBn** in benzene-$d_6$ solution at 40 °C for 4 h resulted in the appearance of a trace amount of (Cy-PSi)H, on the basis of $^{31}$P{$^1$H} NMR analysis. Heating a 1:1 mixture of **2-NiBn** and HBpin at 65 °C for 4 h in benzene-$d_6$

solution resulted in the formation of **2-NiH** (by $^{31}P\{^1H\}$ NMR), as well as trace amounts of (Cy-PSi)H and an unknown impurity giving rise to a $^{31}P\{^1H\}$ NMR resonance at 76 ppm. Subsequent heating of this mixture at 65 °C for a total of 6 h led to the formation of a trace amount of another impurity giving rise to a $^{31}P\{^1H\}$ NMR resonance at 51 ppm. Additional heating of this mixture at 80 °C for 4 h led to further conversion to the latter impurity, and the formation of yet another impurity giving rise to a $^{31}P\{^1H\}$ NMR resonance at -14 ppm. Based on these results it appears that some decomposition of **2-NiBn** does occur at higher temperatures, and thus hydroboration catalysis should be evaluated at room temperature with a longer reaction time of 18 h and a 5 mol% [Ni] loading.

**Table 2.3.2** Catalytic isomerization/hydroboration of *trans*-4-octene varying time, temperature, and catalyst loading.[a]



| Entry | Pre-catalyst | mol% [Ni] | Temperature (°C) | Time (h) | % Conversion[a] |
|-------|--------------|-----------|------------------|----------|-----------------|
| 1 | **2-NiBn** | 5 | RT | 4 | 71 |
| 2 | **2-NiBn** | 5 | RT | 18 | 94 |
| 3 | **2-NiBn** | 2.5 | RT | 18 | 43 |
| 4 | **2-NiBn** | 2.5 | 65 | 4 | 50 |
| 5 | **2-NiBn** | 5 | 80 | 4 | 38 |
| 6 | **2-NiBn** | 2.5 | 80 | 4 | 32 |

[a]Conversion was determined on the basis of $^1H$ NMR integration relative to 1,3,5-trimethoxybenzene as the internal standard (0.4 mmol, average of two runs).

## 2.3.2 Hydroboration Substrate Scope

Having optimized the reaction conditions for isomerization/hydroboration catalysis, the substrate scope was expanded to include additional substrates with the potential to chain walk (Table 2.3.3, entries 1-8), as well as substrates featuring alternative substitution/functional groups (entries 9-12). As in the case of *trans*-4-octene, *cis*-4-octene also underwent isomerization to

afford the terminal hydroboration product with 86% conversion (entry 3). Both *trans*-4-methyl-1-pentene and *trans*-4-methyl-2-pentene afford the terminal hydroboration product on the basis of $^{13}C\{^1H\}$ DEPT-135 NMR analysis, with 66 and 63% conversion, respectively (entries 4 and 5). The terminal hydroboration product was also obtained in the case of 4-vinylcyclohexane (entry 6) and ethylidene cyclohexane (entry 7) with 84% and 62% conversion, respectively. The latter result was obtained after 72 h at room temperature. By comparison, 1-methylcyclohexene proved unreactive under these conditions, with no hydroboration product obtained after 72 h at room temperature (entry 8).

**Table 2.3.3** Substrate scope for the catalytic hydroboration of alkenes with **2-NiBn**.[a]



| Entry | Substrate | Product | Time | Conversion[b] |
|-------|-----------|---------|------|---------------|
| 1 | | Bpin | 18 | 64 |
| 2 | | Bpin | 18 | 71 |
| 3 | | Bpin | 18 | 86 |
| 4 | | Bpin | 18 | 63 |
| 5 | | Bpin | 18 | 66 |
| 6 | | Bpin | 18 | 84 |
| 7 | | Bpin | 72 | 62 |
| 8 | | Bpin | 72 | <1 |
| 9 | Br | Br Bpin | 18 | 5 |

| 10 | styrene |  | 18 | 25 (linear) 47 (branched) 31 (unreacted) |
|----|---------|---------|----|----------|
| 11 | allylbenzene | PhCH2CH2CH2Bpin | 18 | 94 |
| 12 | Me2N—allyl | Me2N~~~Bpin | 18 | 18 (terminal) 41 (unreacted) |

[a]Reaction conditions: substrate (0.4 mmol), HBpin (0.4 mmol), **2-NiBn** (5 mol%, 0.1 M stock solution), neat at room temperature. [b]Reaction conversion determined on the basis of $^1$H NMR integration relative to 1,3,5-trimethoxybenzene as an internal standard (0.4 mmol) *vs*. product.

Functionalized substrates such as bromobutene (entry 9) and allyldimethylamine (entry 12) have much lower conversions of 5 and 18 % respectively. By comparison, allylbenzene afforded 94% conversion to the terminal hydroboration product (entry 11). Interestingly, in the case of styrene 47% conversion to the branched product was obtained, with 25% conversion to the linear isomer (entry 10). Selectivity for the branched hydroboration product in (dppe)NiCl$_2$ catalyzed hydroboration has been reported recently by Yamaguchi and co-workers.[24e] The preference for the branched product may arise due to preferential 2,1-insertion, which can lead to formation of a stabilized $\eta^3$-benzyl intermediate.

## 2.4 Summary and Conclusions

In summary, the facile synthesis of Ni complexes supported by the versatile new strong-field, bidentate (phosphino)silyl ligand $\kappa^2$-(2-Ph*P*C$_6$H$_4$)*Si*Me ([PSi]) has been described. Chloride, benzyl, hydride, and cyclooctenyl Ni(II) complexes were isolated and structurally characterized. In the first application of these complexes in catalysis, alkene hydroboration was achieved. Moderate conversions were observed for a scope of terminal, di-, and tri-substituted alkenes, with moderate selectivity noted in the case of internal alkenes for chain-walking and hydroboration at the terminal alkene position. The benzyl derivative **2-NiBn** was shown to perform the most

favorably in such catalysis. Stoichiometric reactivity studies demonstrated that treatment of **2-NiBn** with HBPin leads to the formation of a dinuclear μ-hydride Ni complex, which supports the intermediacy of Ni hydride species in the hydroboration catalysis. This work represents a relatively rare example of the application of Ni(II) species in hydroboration catalysis. Notably, this study demonstrates that previously inaccessible catalytic turnover in alkene hydrofunctionalization could be achieved by removing a phosphino donor from the tridentate PSiP architecture typically employed in the Turculet group.

## 2.5 Experimental Section

### 2.5.1 General Considerations

All experiments were conducted under nitrogen in a glovebox under a $N_2$ atmosphere or using standard Schlenk techniques. Tetrahydrofuran and diethyl ether were distilled from Na/benzophenone ketyl and subsequently stored over 4 Å molecular sieves. Benzene, toluene, and pentane were first sparged with $N_2$ and subsequently dried by storage over 4 Å molecular sieves. Benzene-$d_6$ was degassed via three freeze-pump-thaw cycles and stored over 4 Å molecular sieves. The compound 1-bromo-2-dicyclohexylphosphinobenzene was prepared according to literature procedure.[56] All other reagents were purchased from commercial suppliers and used without further purification. Unless otherwise stated, $^1$H, $^{13}$C, $^{11}$B, $^{31}$P, and $^{29}$Si characterization data were collected at 300K, with chemical shifts reported in parts per million downfield of SiMe$_4$ (for $^1$H, $^{13}$C, and $^{29}$Si), BF$_3$·OEt$_2$ (for $^{11}$B), or 85% H$_3$PO$_4$ in D$_2$O (for $^{31}$P). $^1$H and $^{13}$C NMR chemical shift assignments are based on data obtained from $^{13}$C{$^1$H}, $^{13}$C-DEPTQ, $^1$H-$^1$H COSY, $^1$H-$^{13}$C HSQC, and $^1$H-$^{13}$C HMBC NMR experiments. $^{29}$Si NMR assignments are based on $^1$H-$^{29}$Si HMBC and $^1$H-$^{29}$Si HMQC experiments. X-ray data collection, solution, and refinement were carried out by Dr. Katherine Robertson at the Saint Mary's

University X-ray Crystallography Laboratory, Halifax, Nova Scotia, except for the structure of **2-NiHPPh₃**, for which data collection, solution and refinement were carried out by Dr. Michael Ferguson of the University of Alberta X-ray Crystallography Laboratory. Additional NMR characterization data, as well as X-ray crystallographic parameters and details of structure solution and refinement are provided in Appendices 1 and 2, respectively.

### 2.5.2 Synthetic Procedures and Characterization Data

**Synthesis of (2-CyPC₆H₄)SiMe)H [(Cy-PSi)H].** A pre-cooled (-35 °C) solution of 1-bromo-2-dicyclohexylphosphinobenzene (1.00 g, 2.72 mmol) in ca. 3 mL of diethyl ether was treated via drop-wise addition with a solution of $^n$BuLi (2.5 M in hexanes, 2.72 mmol, 1.09 mL) that had been diluted with 1 mL of diethyl ether. The reaction mixture was allowed to stir at room temperature for 10 minutes, over the course of which a precipitate was observed. The reaction mixture was cooled to -35 °C and was subsequently treated with $^i$Pr₂SiHCl (2.72 mmol, 0.47 mL). The mixture was allowed to stir at room temperature for 18 h. The solvent was removed in *vacuo* where the residue was then residue was then extracted with 3 mL of pentane. The pentane extract was filtered through Celite and the volatile components of the filtrate solution were removed in *vacuo*. The remaining residue was recrystalized from a concentrated pentane solution at -35 °C to afford **(Cy-PSi)H** (1.00 g, 94% yield) as an off-white solid. $^1$H NMR (500 MHz, benzene -$d_6$): δ 7.60 (m, 1 H, H$_{arom}$), 7.47 (m, 1 H, H$_{arom}$), 7.20-7.13 (overlapping resonances, 2 H, H$_{arom}$), 4.81 (dt with $^{29}$Si satellites, 1 H, $^4J_{PH}$ = 7 Hz, $^3J_{HH}$ = 4 Hz, $^1J_{SiH}$ = 188 Hz, Si*H*), 2.00 (m, 2 H, P*Cy*), 1.89 (m, 2 H, P*Cy*), 1.76-1.46 (overlapping resonances, 10 H, PCy + SiC*H*Me₂), 1.42-0.99 (overlapping resonances, 22 H, P*Cy* + SiCH*Me₂*; the resonances corresponding to the SiCH*Me₂* protons were identified as doublets centered at 1.26 and 1.13 ppm, $^3J_{HH}$ = 7 Hz). $^{13}$C NMR (125.8 MHz, benzene -$d_6$): δ 144.9 (d, $^1J_{CP}$ = 47 Hz, C$_{arom}$), 143.5 (d, $^2J_{CP}$ = 19 Hz, C$_{arom}$), 136.5 (d, $J_{CP}$

= 15 Hz, CH$_\text{arom}$), 132.2 (CH$_\text{arom}$), 128.3 (CH$_\text{arom}$), 127.9 (CH$_\text{arom}$), 35.5 (d, $^1J_\text{CP}$ = 15 Hz, P$Cy$),

30.6 (d, $J_\text{CP}$ = 16 Hz, $PCy$), 30.0 (d, $J_\text{CP}$ = 10 Hz, P$Cy$), 27.5-27.0 (overlapping resonances, P$Cy$),

26.4 (P$Cy_2$) 19.6 (SiCH$Me_2$), 19.2 (SiCH$Me_2$), 12.4 (SiC$H$Me$_2$), 12.3 (SiC$H$Me$_2$). $^{31}$P{$^1$H} NMR

(202 MHz, benzene -$d_6$): δ -6.5 (s). $^{29}$Si{$^1$H} NMR (99.4 MHz, benzene-$d_6$): δ 5.0.

**Synthesis of [(Cy-PSi)NiCl]$_2$ (2-NiCl).** NiCl$_2$DME (0.64 mmol, 0.14 g) was suspended in

ca. 2 mL of benzene. A solution of **(Cy-PSi)H** (0.25 g, 0.64 mmol) in ca; 1 mL of benzene was

added dropwise to the NiCl$_2$DME suspension with stirring at room temperature. Neat Et$_3$N (6.4

mmol, 0.89 mL) was added to the reaction mixture. The reaction mixture was allowed to stir at

room temperature for 16 h. The mixture was then filtered through Celite and the filtrate solution

was collected. The volatile components of the solution were removed in *vacuo* and the remaining

residue was triturated with 3 × 3 mL of pentane. The remaining yellow solid was extracted with

ca. 3 mL of benzene. The benzene extract was filtered through Celite, the filtrate solution was

collected, and the volatile components were removed in *vacuo*. The crude extract was washed

with 3 × 3 mL of pentane. The remaining residue was dried under vacuum to afford **2-NiCl** (0.094

g, 30% yield) as a yellow solid. $^1$H NMR (500 MHz, benzene -$d_6$): δ 7.57 (apparent d, 2 H, $J_\text{HH}$

= 8 Hz, H$_\text{arom}$), 7.26 (overlapping resonances, 2 H, H$_\text{arom}$), 7.11 (overlapping resonances, 4 H,

H$_\text{arom}$), 2.66 (m, 4 H, P$Cy$), 2.21 (m, 4 H, P$Cy$), 1.68 (overlapping resonances, 12 H, P$Cy$ +

SiC$H$Me$_2$), 1.16-1.54 (overlapping resonances, 11 H, P$Cy$), 1.41 (overlapping resonances, 13 H,

P$Cy$), 1.37-1.31 (overlapping resonances, 7 H, P$Cy$), 1.11-1.06 (overlapping resonances, 9 H,

P$Cy$). $^{13}$C NMR (125.8 MHz, benzene -$d_6$): δ 154.9 (d, $^1J_\text{CP}$ = 49 Hz, C$_\text{arom}$), 141.8 (d, $^2J_\text{CP}$ = 52

Hz, C$_\text{arom}$), 133.8 (d, $^2J_\text{CP}$ = 22 Hz, CH$_\text{arom}$), 129.9 (CH$_\text{arom}$), 129.6 (CH$_\text{arom}$), 36.1 (d, $^1J_\text{CP}$ = 22 Hz,

P$Cy$), 30.4 (P$Cy$), 29.7 (P$Cy$), 27.6 (d, $^2J_\text{CP}$ = 12 Hz, P$Cy$), 27.4 (d, $^2J_\text{CP}$ = 10 Hz, P$Cy$), 26.4

(P*Cy*), 21.8 (SiCH*Me₂*), 20.4 (SiCH*Me₂*), 17.9 (Si*C*HMe₂). ³¹P{¹H} NMR (202 MHz, benzene -

*d₆*): δ 70.8 ppm (s). ²⁹Si{¹H} NMR (99.4 MHz, benzene-*d₆*): δ 56.0.

**Synthesis of (Cy-PSi)NiBn (2-NiBn).** A solution of **2-NiCl** (0.21 mmol, 0.20 g) in ca, 2 mL

of benzene was treated via drop-wise addition with a solution of BnMgBr (1.4 M in THF, 0.42

mmol, 0.30 mL) diluted with 1 mL of benzene. The reaction mixture was allowed to stir at room

temperature for 16 h. The volatile components of the reaction mixture were then removed in

*vacuo* and the remaining residue was triturated with 3 × 3 mL of pentane. The remaining residue

was extracted with ca. 3 mL of pentane, and the extract solution was filtered through Celite. The

filtrate solution was collected, and the volatile components were removed in *vacuo*. The residue

was recrystalized from a concentrated pentane solution at -35 °C to afford **2-NiBn** (0.13 g, 73%

yield) as a yellow solid. ¹H NMR (500 MHz, benzene -*d₆*): δ 7.78 (apparent d, 1 H, $J_{HH}$ = 8 Hz,

H$_{arom}$), 7.34 (m, 1 H, H$_{arom}$), 7.26-7.19 (overlapping resonances, 3 H, H$_{arom}$), 7.14 (m, 1 H, H$_{arom}$)

6.68 (t, 1 H, $^3J_{HH}$ = 7 Hz, H$_{arom}$), 6.02 (d, 2 H, $^3J_{HH}$ = 7 Hz, H$_{arom}$), 2.25 (d, 2 H, $^3J_{PH}$ = 4 Hz,

NiC*H₂*Ph), 1.79 (m, 2 H, P*Cy*), 1.70-1.42 (overlapping resonances, 12 H, P*Cy* + SiC*H*Me₂), 1.26

(d, 6 H, $^3J_{HH}$ = 7 Hz, SiCH*Me₂*), 1.24 (d, 6 H, $^3J_{HH}$ = 7 Hz, SiCH*Me₂*), 1.18-0.84 (overlapping

resonances, 10 H, P*Cy*). ¹³C NMR (125.8 MHz, benzene -*d₆*): δ 158.9 (d, $^1J_{CP}$ = 51 Hz, C$_{arom}$),

142.6 (d, $^2J_{CP}$ = 49 Hz, C$_{arom}$), 134.1 (d, $^2J_{CP}$ = 20 Hz, CH$_{arom}$), 132.5 (CH$_{arom}$), 129.7 (br d, $J_{CP}$ =

3 Hz, CH$_{arom}$), 128.8 (CH$_{arom}$), 127.3 (d, $J_{CP}$ = 6 Hz, CH$_{arom}$), 121.0 (CH$_{arom}$), 117.8 (C$_{arom}$), 113.5

(CH$_{arom}$), 36.0 (d, $^1J_{CP}$ = 20 Hz, P*Cy*), 30.1 (d, $J_{CP}$ = 6 Hz, P*Cy*), 29.7 (d, $^2J_{CPtrans}$ = 26 Hz,

Ni*C*H₂Ph), 29.5 (P*Cy*), 27.3-26.8 (overlapping resonances, P*Cy*), 26.2 (P*Cy*), 20.8 (SiCH*Me₂*),

20.6 (SiCH*Me₂*), 18.8 (Si*C*HMe₂). ³¹P{¹H} NMR (202 MHz, benzene -*d₆*): δ 67.3 ppm (s).

²⁹Si{¹H} NMR (99.4 MHz, benzene-*d₆*): δ 52.3.

**Synthesis of (Cy-PSi$^H$)Ni(PPh$_3$) (2-NiHPPh$_3$).** A solution of **2-NiCl** (0.051 mmol, 0.049 g)

in 3 mL of benzene was treated with a solution of triphenylphosphine in 1 mL of benzene. A

solution1.0 M NaEt$_3$BH diluted in ca. 2 mL of benzene was added dropwise (0.102 mL of 1.0 M

solution in toluene, 0.102 mmol, 2 equiv. relative to **2-NiCl**). The reaction mixture was allowed

to stir at room temperature over the course of 15 minutes where a colour change from light orange

to dark read was observed. The volatile components of the reaction mixture were then removed

in *vacuo* and the remaining residue was triturated with 3 × 2 mL of pentane. The residue was then

extracted in ca. 12 mL of pentane and filtered though Celite to afford a clear red-orange filtrate.

The solvent was removed in *vacuo* and the remaining residue was triturated with 3 × 2 mL of

pentane to afford an orange powder. This crude extract was washed with 1 mL cold (-35 °C)

pentane to afford a yellow powder identified as **2-NiHPPh$_3$** (0.038 g, 53 % yield). $^1$H NMR (500

MHz, benzene -$d_6$): δ 7.86 (overlapping resonances, 7 H, H$_{arom}$), 7.56-7.17 (overlapping

resonances, 6 H, H$_{arom}$), 7.05-6.86 (overlapping resonances, 6 H, H$_{arom}$), 1.95 (overlapping

resonances, 3 H, P$Cy$), 1.71-1.51 (overlapping resonances, 10 H P$Cy$), 1.44 (apparent d, 12 H,

$^2J_{HH}$ = 6 Hz, SiC$H$Me$_2$), 1.26 (apparent d, 12 H, $^2J_{HH}$ = 7 Hz, SiC$H$Me$_2$), 1.17-0.78 (overlapping

resonances, 12 H, P$Cy$), -3.06 ppm (dd, 1 H, $^2J_{HPcis}$ = 18 Hz, $^2J_{HPtrans}$ = 80 Hz, $^1J_{HSi}$ = 23 Hz Ni$H$).

$^{31}$P{$^1$H} NMR (202 MHz, benzene -$d_6$): δ 68.3 (d, $^2J_{PP}$ = 38 Hz, P$Cy$) 27.8 (d, $^2J_{PP}$ = 38 Hz, P$Ph_3$).

**Synthesis of [(Cy-PSi)Ni(μ-H)]$_2$ (2-NiH).** A solution of **2-NiBn** (0.093 mmol, 0.050 g) in

1.5 mL of benzene was treated with a solution of HBPin (0.093mmol, 13.4 μL) in ca. 1 mL of

benzene. The reaction mixture was allowed to stir at room temperature over the course of 16 h.

The volatile components of the reaction mixture were then removed in *vacuo* and the remaining

residue was triturated with 3 × 2 mL of pentane. The residue was then suspended in ca. 3 mL of

pentane and filtered though Celite. The filtrate solution was discarded, and the filter was washed

with ca. 3 mL of benzene. The benzene filtrate solution was collected and the solvent was removed in *vacuo*. The residue obtained was triturated with $3 \times 2$ mL of pentane and dried under vacuum to afford **2-NiH** (0.030 g, 72% yield) as a red solid. ^{1}H NMR (500 MHz, benzene-$d_6$): δ 7.70 (apparent d, 2 H, $J_{HH}$ = 7 Hz, $H_{arom}$), 7.33 (m, 2 H, $H_{arom}$), 7.22 (m, 2 H, $H_{arom}$), 7.18 (m, 2 H, $H_{arom}$), 2.40 (m, 4 H, P$Cy$), 2.13 (m, 4 H, P$Cy$), 1.88-1.45 (overlapping resonances, 20 H, P$Cy$ + SiC$H$Me$_2$ + SiCH$Me_2$), 1.45-1.26 (overlapping resonances, 8 H, PCy + SiCH$Me_2$), 1.12 (4 H, P$Cy$), -10.16 (dd, 2 H, $^2J_{HP}$ = 32 Hz, Ni$H$). ^{13}C NMR (126 MHz, benzene -$d_6$): δ 156.4 (d, $^1J_{CP}$ = 56 Hz, $C_{arom}$), 142.3 (d, $^2J_{CP}$ = 48 Hz, $C_{arom}$), 133.6 (d, $J_{CP}$ = 24 Hz, $CH_{arom}$), 129.8 ($CH_{arom}$), 128.9 ($C_{arom}$), 127.8 ($CH_{arom}$), 36.2 (d, $^1J_{CP}$ = 21 Hz, P$Cy$), 30.5 (P$Cy$), 29.9 (P$Cy$), 27.4-26.8 (overlapping resonances, P$Cy$), 26.1 (P$Cy$), 21.5 (SiCH$Me_2$), 20.9 (SiCH$Me_2$), 18.6 (Si$C$HMe$_2$). ^{31}P{^{1}H} NMR (202 MHz, benzene -$d_6$): δ 71.7 (s). ^{29}Si{^{1}H} NMR (99.4 MHz, benzene-$d_6$): δ 57.8

**Synthesis of (Cy-PSi)Ni($\eta^3$-C$_8$H$_{13}$) (2-NiCOD).** A solution of Ni(COD)$_2$ (0.26 mmol, 0.071 g) in 2 mL of benzene was treated with a solution of **(Cy-PSi)H** (0.26 mmol, 0.10 g) in ca. 1 mL of benzene. The reaction mixture was allowed to stir at room temperature over the course of 16 h. The volatile components of the reaction mixture were then removed in *vacuo* and the remaining residue was triturated with $3 \times 3$ mL of pentane. The residue was recrystalized at -35 °C from a concentrated pentane solution to afford **2-NiCOD** (0.089 g, 62% yield) as a yellow solid. ^{1}H NMR (500 MHz, benzene-$d_6$): δ 7.89 (apparent d, 1 H, $J_{HH}$ = 7 Hz, $H_{arom}$), 7.48 (m, 1 H, $H_{arom}$), 7.28 (m, 1 H, $H_{arom}$), 7.21 ppm (m, 1 H, $H_{arom}$), 4.77 ppm (m, 1 H, $\eta^3$-C$_8H_{13}$), 4.52 ppm (m, 1 H, $\eta^3$-C$_8H_{13}$), 4.36 ppm (m, 1 H, $\eta^3$-C$_8H_{13}$), 2.50-0.77 (overlapping resonances, 46 H, P$Cy$ + $\eta^3$-C$_8H_{13}$ + SiCH$Me_2$ + SiC$H$Me$_2$; the resonances corresponding to the SiCH$Me_2$ protons were identified at 1.45, 1.24, and 0.96 ppm). ^{13}C NMR (125.8 MHz, benzene -$d_6$): δ 159.4 (d, $^1J_{CP}$ =

51 Hz, $C_{arom}$), 143.2 (d, $^2J_{CP}$ = 47 Hz, $C_{arom}$), 134.3 (d, $^2J_{CP}$ = 20 Hz, $CH_{arom}$), 129.5 (d, $J_{CP}$ = 3 Hz, $CH_{arom}$), 128.8 ($CH_{arom}$), 127.2 (d, $J_{CP}$ = 6 Hz, $CH_{arom}$), 107.7 ($\eta^3$-$C_8H_{13}$), 75.7 ($\eta^3$-$C_8H_{13}$), 59.1 ($\eta^3$-$C_8H_{13}$), 36.8 (d, $^1J_{CP}$ = 22 Hz, P$Cy$), 36.5 (d, $^1J_{CP}$ = 20 Hz, P$Cy$), 32.3 ($\eta^3$-$C_8H_{13}$), 31.7 ($\eta^3$-$C_8H_{13}$), 31.4 (d, $J_{CP}$ = 3 Hz, P$Cy$), 30.6 (d, $J_{CP}$ = 5 Hz, P$Cy$), 29.5 (P$Cy$), 29.0 (d, $J_{CP}$ = 3 Hz, P$Cy$), 28.6 ($\eta^3$-$C_8H_{13}$), 27.4-26.8 (overlapping resonances, P$Cy$ + $\eta^3$-$C_8H_{13}$), 26.2 (P$Cy$), 26.1 (P$Cy$), 23.7 ($\eta^3$-$C_8H_{13}$), 21.4 (SiCH$Me_2$), 20.9 (SiCH$Me_2$), 20.3 (SiCH$Me_2$), 20.1 (SiCH$Me_2$), 18.3 (Si$C$HMe_2), 17.3 (Si$C$HMe_2). $^{31}$P{$^1$H} NMR (121.5 MHz, benzene -$d_6$): δ 73.7 ppm (s). $^{29}$Si{$^1$H} NMR (99.4 MHz, benzene-$d_6$): δ 56.6.

**General Procedure for the Catalytic Hydroboration of Alkenes.** In the glovebox, a one dram vial was charged with **2-NiBn** (0.02 mmol, 10.75 mg) added as a 0.1 M solution in benzene. The solvent was removed in *vacuo*. HBpin (0.4 mmol) was added via a syringe to the pre-catalyst. After approximately five minutes, the substrate (0.4 mmol) was added to the vial. The vial was capped and the reaction mixture was allowed stir for 18 h at room temperature. Excess alkene and HBpin were removed in *vacuo*. The reactions were then exposed to air and diluted with 600 μL of a 0.66 M stock solution of 1,3,5-trimethoxybenzene in chloroform-$d$. This solution was then filtered through silica and a microfibre filter to remove the catalyst. An additional 3.0 mL of chloroform-$d$ was run through the filter to remove any excess borylalkane product from the silica. The chloroform solution was transferred to an NMR tube for data acquisition. For calculation of NMR yields, a chosen diagnostic product signal was integrated relative to that of the internal standard. A long (60 s) relaxation delay was used to ensure accurate integration.

## Chapter 3: Conclusions and Future Work

### 3.1 Summary and Conclusions

In Chapter 2 of this document, the facile synthesis of Ni complexes including chloride (**2-NiCl**), hydride (**2-NiH**), benzyl (**2-NiBn**) and cyclooctenyl (**2-NiCOD**), supported by the versatile new strong-field, bidentate (phosphino)silyl ligand $\kappa^2$-(2-Ph$PC_6H_4$)$Si$Me ([PSi]) has been described. The catalytic abilities of these complexes were tested and compared in catalytic alkene hydroboration reactions using 1-octene as the substrate. The benzyl derivative **2-NiBn** proved to be the most catalytically active for this transformation and was used in a substrate scope involving of terminal, di-, and tri-substituted alkenes, with moderate selectivity noted in the case of internal alkenes for chain-walking and hydroboration at the terminal alkene position. Interesting bonding was observed for the **2-NiH** complex which has been investigated by NMR spectroscopy and X-ray crystallographic data collection, and if further being investigated by DFT geometry optimization in collaboration with group member Dylan Hale. This work represents a relatively rare example of the application of Ni(II) species in hydroboration catalysis.

### 3.2 Future Work

### 3.2.1 Future Work Involving Bidentate (Phosphino)silyl Ligation

There is still plenty of chemistry left to be explored by (Cy-PSi) ligated Ni complexes. In preliminary studies not discussed in this document, reactions with bulky silanes and phosphines were explored. As there is evidence from the reaction of **2-NiBn** to reaction with borane HBpin to from a hydride species, the interest to react with similar species such as silanes and phosphines were targeted. The hopes of reacting (Cy-PSi)NiBn complexes with silanes would be to form a (Cy-PSi)Ni silylene complex (Scheme 3.1.1).[60] There are a few examples in the literature from West and co-workers[60a,b] and Cui and coworkers[66c] that Ni has the ability to react with silylenes

and form Ni$^{II}$ species; therefore, this type of transformation was pursued by use of (Cy-PSi) ligated Ni complexes. From the NMR data that was obtained, there was evidence that a new complex was formed; however further characterization methods would need to be taken to determine what this (Cy-PSi)Ni complex may be as the NMR results were inconclusive as to what species was formed. Similar with the studies performed with bulker silanes, the NMR data that was obtained from reacting **2-NiBn** with bulky phosphines such as cyclohexylphosphine (H$_2$PCy) and mesitylphosphine (H$_2$PMes), showed that there had been a new complex formed, however further characterization data would need to be obtained to further understand the data in the NMR obtained.
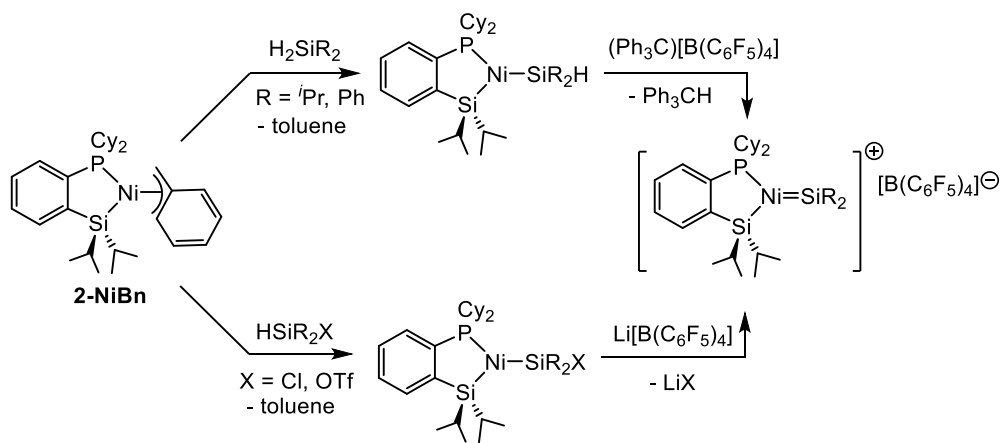


**Scheme 3.1.1** Proposed synthesis of a cationic Ni(II) silylene complex.

The complexes that have been characterized in this document, **2-NiCl**, **2-NiBn**, and **2-NiCOD** are great candidates to be used precatalysts in hydrofunctionalization reactions such as hydrogenation and hydrosilylation. Both catalyst hydrofunctionalization reactions have been performed in the Turculet group by PSiP and PN' ligated transition metal complexes; therefore, having this new monoanionic, strong-field, bidentate ligand in hand, it would be a great comparison study to perform reactions of this type with the fully characterized **2-NiCl**, **2-NiBn**, and **2-NiCOD** precatalysts already available. Such reactions as the hydrogenation catalytic

reaction have proven to be challenging when using tri- and tetra-substituted alkenes for PSiP ligated metal complexes. Current, unpublished, studies in the Turculet group have been targeting smaller PSiP, PSi and PSiN metal complexes to use in hopes of improving the turnover of these catalytic reactions; therefore, the use of (Cy-PSi)H ligated complexes would be an interesting study for these catalytic reactions as it is using half of the PSiP ligand that has already proven to be a viable ligand for metal complexes in these types of transformations, and it is much smaller than the full PSiP ligand.

While (Cy-PSi)H = (2-CyPC$_6$H$_4$)SiMe)H ligated nickel complexes were the target in this thesis, the utility and synthesis of this ligand on other first-row transition metals such as Fe and Co are still left to be explored. Nickel was chosen for this thesis to react with this ligand as it leads to Ni$^{II}$, d$^8$, square planar, diamagnetic complexes allowing ease of use when obtaining NMR data to characterize and study the reactivity of the synthesized complexes. The use of Co and Fe often lead to unpredictable one electron reactivity due to the complexes being paramagnetic and the use of NMR to determine the reactivity and characterization for complexes of this type are not as useful. In this regard, complexes such as metal alkyl and metal hydrides are of interest for future synthesis and studies for Co and Fe, to compare the reactivity and catalytic ability of these metal complexes with (Cy-PSi)NiLn complexes (Figure 3.1.1).



**(Cy-PSi)FeL$_n$**    **(Cy-PSi)CoL$_n$**    **(Cy-PSi)NiL$_n$**
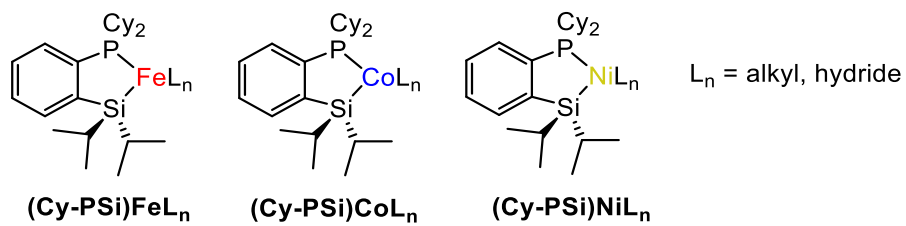
**Figure 3.1.1** Examples of (Cy-PSi)H ligated Fe and Co complexes to synthesize and compare to (Cy-PSi)Ni complexes characterized in this work

Both the phosphorous and silicon substituents offer tunable positions to change the steric and electronic effects that can change the reactivity of the metal complexes. The future tunability at the phosphine substituent includes phenyl groups, and ethyl groups, varying the size of the ligand and the ability of the phosphine to electron donate to the metal center in hopes of studying how changing these substituents changes the reactivity (i.e., catalytic ability) of the metal complex (Figure 3.1.2 (a)). In this regard, decreasing the size of the ligand would, in theory, open a larger coordination sphere around the metal, leading to the coordination of larger substrates such as tri- and tetra-substituted alkenes. The effect of changing the substituents on the phosphine to less electron donating substituents such as phenyl groups versus cyclohexyl groups used in this work would allow for the observation on whether this would either increase the coordination to the metal or decrease the coordination to the metal. Two arguments could be made in this regard: the less electron rich metal center may more readily coordinate the electron rich alkene to gain electron density and increase the reactivity, or it may readily coordinate to the alkene; however it may not readily insert into the alkene as the lower electron density around the metal may not be enough to break the C — C double bond via $\pi$ back donation, hindering the reactivity of the complex. This idea can also be extended to the silicon fragment as currently the work done in this thesis includes *iso*propyl substituents on silicon. Target complexes include mesityl, phenyl and methyl substituents to study the steric and electronic effects varying the substituent at silicon will have on the metal complex (Figure 3.1.2 (b)). In this case, increasing the size of the substituents to mesityl groups would decrease the size of the coordination sphere of the metal, in theory leading to a decrease in size of the substrates that are most likely to coordinate.
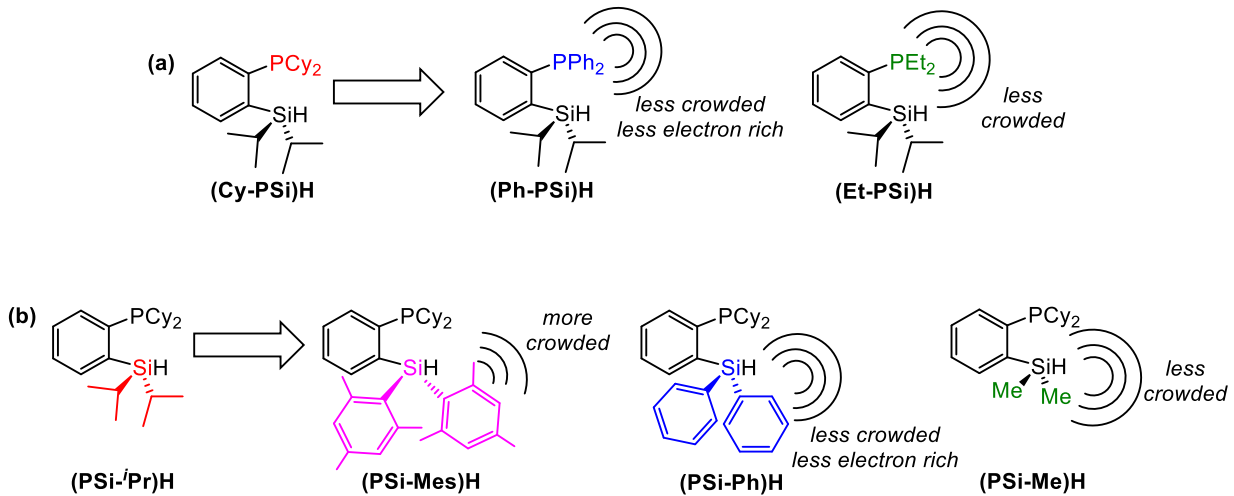
**Figure 3.1.2** (a) Variations of bidentate (phosphino)silyl ligands decreasing the steric profile and altering the electronics of the phosphorous substituents. (b) Variations of bidentate (phosphino)silyl ligands altering the steric profile and electronics of the silicon substituents

### 3.2.2 Future Work Involving Tridentate Bis(phosphino)silyl Ligation

In preliminary work not discussed in this document, along a similar theme of synthesizing smaller ligands, studies involving the change in phosphorus substituents for both (Cy-PSiP)H and ($^i$Pr-PSiP$^{Ind}$)H ligands were performed in hopes of forming smaller pincer ligands of this type. Work performed by previous student Marshall Hoey proved that one of the cyclohexyl substituents on one of the phosphines for the (Cy-PSiP)H ligand could be changed to a phenyl substituent, forming an asymmetrical PSiP ligand of the type (Cy-PSiP-Ph)H = [$\kappa^3$ -(2-CyPC$_6$H$_4$)( 2- CyPC$_6$H$_4$)SiMe]$^-$) (Scheme 3.1.2). In this work, (Cy-PSiP-Ph) ligated Ni complexes were targeted and characterized.[61]
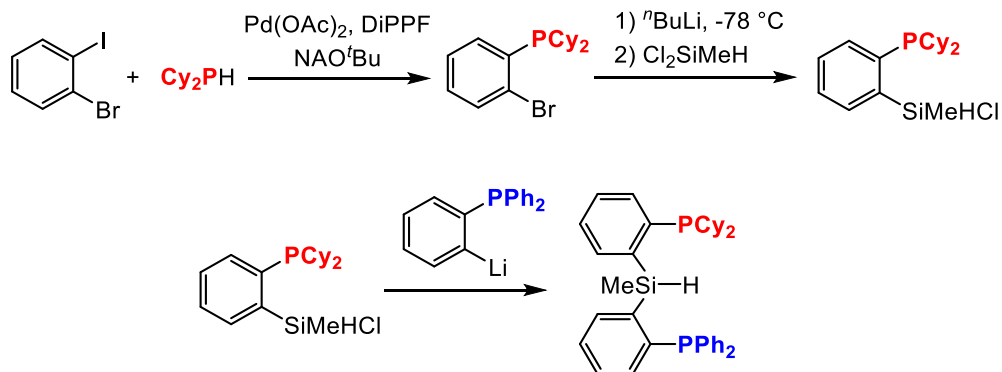
**Scheme 3.1.2** Asymmetric PSiP synthesis

To build upon this work, the hydroboration of alkenes was targeted using the previously formed potential Nickel precatalysts (Cy-PSiP-Ph)NiCl, (Cy-PSiP-Ph)NiMe, and (Cy-PSiP-Ph)NiBn.; however, due to synthetic challenges, only (Cy-PSi-Ph)NiBn and (Cy-PSiP-Ph)NiCl were used in preliminary hydroboration studies. In these preliminary studies, based on $^{11}$B NMR, (Cy-PSiP-Ph)NiCl *in-situ* with NaEt$_3$BH was catalytically active at mild conditions, (5 mol%, 15 mol% NaEt$_3$BH, 1 h, room temperature) and (Cy-PSiP-Ph)NiBn was catalytically active at mild conditions, (5 mol%, 2 h, room temperature). However, due to irreproducibility of the (Cy-PSiP-Ph)H ligand, this project was left as it was difficult to determine what was happening catalytically, and the starting material could not be reproduced to make these complexes. However, work could be expanded upon in the future of this project by further optimization of the ligand synthesis leading to a more straight forward way to form these Ni complexes. A precatalyst scan can also be performed to determine the most catalytically active complex for the hydroboration of alkenes.

Along this theme, in preliminary studies performed by Natalie Wright, an undergraduate student in the Turculet group, a buried volume analysis was performed for four different PSiP ligands of the type (Cy-PSiP)H and ($^i$Pr-PSiP$^{Ind}$)H where the substituents on phosphorus for the ($^i$Pr-PSiP$^{Ind}$)H ligand were varied from both phosphines substituted by two *iso*propyl substituents,

one phosphine substituted by two *iso*propyl substituents and the other phosphine substituted by two ethyl substituents, and both phosphines substituted by two ethyl groups. From these studies, the buried volume calculations showed that the (Et-PSiP$^{Ind}$)H ligand, where both of the phosphorus substituents were substituted by ethyl groups was the smallest ligand; therefore the synthesis of this ligand was targeted (Scheme 3.1.3) as it was of interest to form a (Et-PSiP$^{Ind}$)H ligated Ni complex to compare to the reported ($^i$Pr-PSiP$^{Ind}$)H ligated Ni complex.[48d] The crude ligand could be formed at a 75 % yield as a yellow oil, with left over unreacted of the 2-diethylphosphine-3-methylindole.
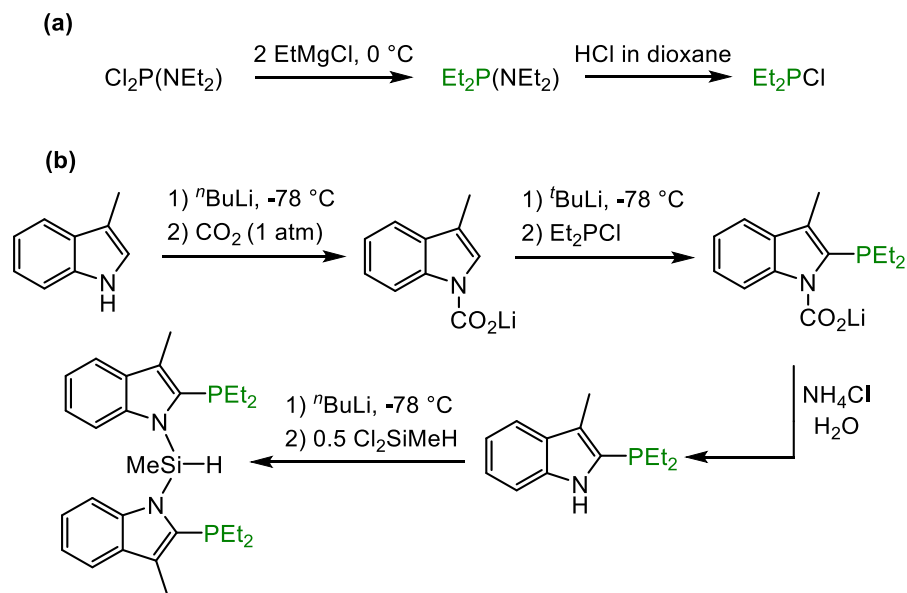


**Scheme 3.1.3** Synthetic route for the preparation of (Et-PSiP$^{Ind}$)H

The first target complexes for this work were simple Ni and Co halide complexes of the type (Et-PSiP$^{Ind}$)NiX and (Et-PSiP$^{Ind}$)CoX respectively. Treatment of (Et-PSiP$^{Ind}$)H with one equiv. of NiCl$_2$(DME) (DME = dimethoxyethane) and excess triethylamine led to the formation of the diamagnetic complex (Et-PSiP$^{Ind}$)NiCl (Scheme 3.1.4 **3-NiCl**). However, upon formation of the **3-NiCl** based on the $^{31}$P{$^1$H}, there were impurities carried over from the ligand synthesis not going to total completion. Unfortunately, the ligand synthesis proved challenging to purify, and

while there was hope that upon forming **3-NiCl**, the excess starting material could be removed upon purification, the 2-diethylphosphine-3-methylindole, remaining reacted with **3-NiCl** acting as an L-donor, therefore making it impossible to purify. While further attempts to synthesize a Ni hydride species to directly compare to the previously reported ($^i$Pr-PSiP$^{Ind}$)NiH, this unforeseen side product complicated subsequent reactions involving the (Et-PSiP$^{Ind}$)NiCl.
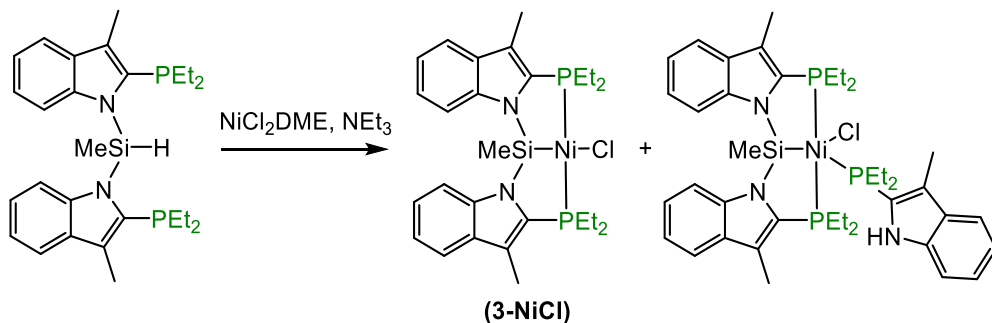


**Scheme 3.1.4** Synthesis of (Et-PSiP$^{Ind}$)NiCl (**3-NiCl**) with 2-diethylphosphine-3-methylindole impurity side product.

A Co halide complex of the type (Et-PSiP$^{Ind}$)CoBr (**3-CoBr**) was formed by treatment of (Et-PSiP$^{Ind}$)H with one equiv. of CoBr$_2$ and excess triethylamine, where a paramagnetic green solid was isolated with a 70% yield (Scheme 3.1.5). Attempted formation of Co halides of the type (Et-PSiP$^{Ind}$)CoCl and (Et-PSiP$^{Ind}$)CoI were attempted, however the use of CoBr$_2$ lead to the only clean, isolable product. The (Et-PSiP$^{Ind}$)CoBr was used to form a Co alkyne complex, where the paramagnetic (Et-PSiP$^{Ind}$)CoBr was treated with excess Zn(0) and one equiv. of diphenylacetylene where a pink diamagnetic solid was isolated in a 55% yield and determined to be a (Et-PSiP$^{Ind}$)Coalkyne (**3-CoA**) complex via single crystal X-ray diffraction (Scheme 3.1.5). The use of **3-CoA** was demonstrated in hydrogenation reactions at mild conditions based on previous Co alkene hydrogenation catalysis performed in the Tuculet group with a (Cy-PSiP) ligated Co complex (1 mol%, 1 atm H$_2$, room temperature, 4 h), using 1-octene, *trans*-4-octene, *cis*-stilbene, and $\alpha$-methyl-styrene as substrates, and observed via $^1$H NMR where integrations

were determined by use of internal standard 1,3,5-trimethoxybenzene relative to remaining alkene, no turnover from alkene to alkane occurred. This sparked further investigation into **3-CoA** and it was determined that there were salts coming through the purification steps for the work-up of **3-CoA** . Unfortunately, at this point in time this work had been put on pause due lack of excess to the chlorodiethylphosphine starting material, and the materials required to synthesize chlorodiethylphosphine. Further work in the future of this project would involve optimization of the ligand synthesis to improve the synthesis of any transition metal complexes involving this ligand, then further investigation into the catalytic ability of viable Ni and Co precursors for hydrogenation and hydroboration can also be explored and expanded upon.
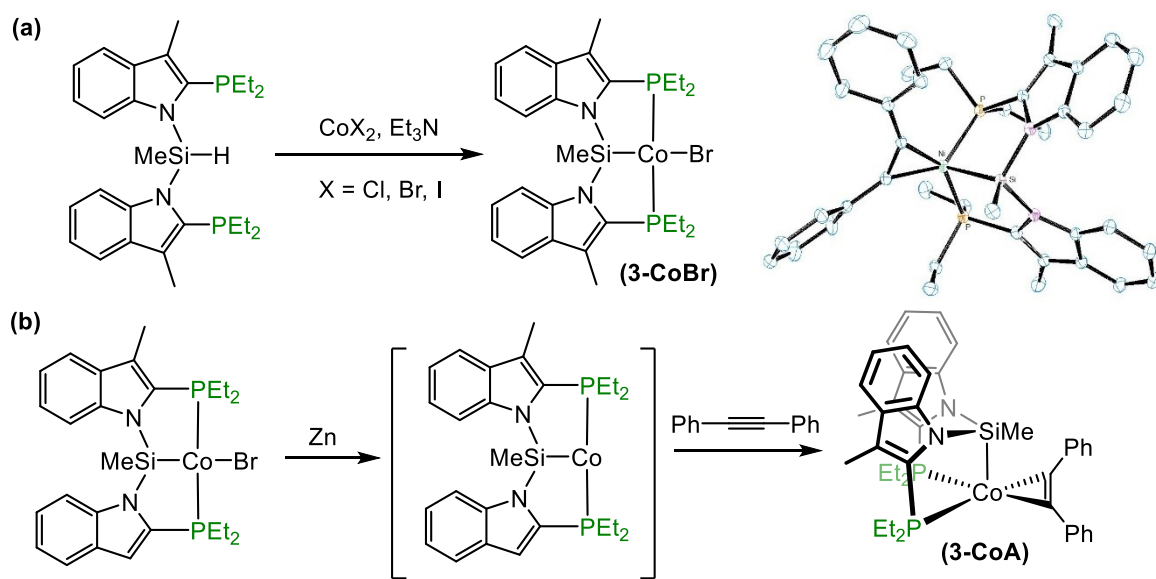


**Scheme 3.1.5** (a) Synthesis of (Et-PSiP$^{Ind}$)CoBr (**3-CoBr**). (b) Left synthesis of (Et-PSiP$^{Ind}$)Coalkyne (**3-CoA**), top right and crystallographically determined structure of **3-CoA** with thermal ellipsoids shown at the 30% probability level. Hydrogen atoms have been omitted for clarity. Selected interatomic distances (Å) and angles (°): Co(1)-C(29) 1.852(3), Co(1)-C(28) 1.885(3), Co(1)-P(1) 2.1546(8), Co(1)-Si(1) 2.1722(8), Si(1)-N(2) 1.789(2), Si(1)-N(1) 1.793(2), C(29)-Co(1)-C(28) 41.03(11), C(29)-Co(1)-P(1) 102.52(9), C(28)-Co(1)-P(1) 137.72(9), C(29)-Co(1)-Si(1) 103.60(8), C(28)-Co(1)-Si(1) 119.41(9), P(1)-Co(1)-Si(1) 83.75(3), C(29)-Co(1)-P(2) 149.74(9), C(28)-Co(1)-P(2) 108.92(9), P(1)-Co(1)-P(2) 106.36(3), Si(1)-Co(1)-P(2) 88.46(3), N(2)-Si(1)-N(1) 108.23(10), N(2)-Si(1)-C(27) 106.42(13), N(1)-Si(1)-C(27) 106.94(12), N(2)-Si(1)-Co(1) 107.19(8), N(1)-Si(1)-Co(1) 109.13(8), C(27)-Si(1)-Co(1) 118.55(10), C(12)-N(1)-C(5) 106.8(2), C(12)-N(1)-Si(1) 137.27(19), C(5)-N(1)-Si(1) 115.73(17), C(25)-N(2)-C(18) 106.8(2), C(25)-N(2)-Si(1) 133.56(19), C(18)-N(2)-Si(1)

118.88(18)

# References

1. (a) Knowles, W. S., *Angew. Chem. Int. Ed.* **2002**, *41*, 1998; (b) Noyori, R., *Angew. Chem. Int. Ed.* **2002**, *41*, 2008; (c) Sharpless, K. B., *Angew. Chem. Int. Ed.* **2002**, *41*, 2024.

2. (a) Schrock, R. R., *Angew. Chem. Int. Ed.* **2006**, *45*, 3748; (b) Grubbs, R. H., *Angew. Chem. Int. Ed.* **2006**, *45*, 3760; (c) Chauvin, Y., *Angew. Chem. Int. Ed.* **2006**, *45*, 3740.

3. Wu, X.-F.; Anbarasan, P.; Neumann, H.; Beller, M., *Angew. Chem. Int. Ed.* **2010**, *49*, 9047.

4. (a) Chirik, P.; R. Morris., *Acc. Chem. Res.* **2015**, *48*, 2495 (b) Beller, M., *Chem. Rev.* **2019**, *119*, 2089.

5. Bauer, I.; Knolker, H. J., *Chem. Rev.* **2015**, *115*, 3170.

6. (a) Tasker, Z. S.; Standley, A. E.; Jamison, F. T., *Nature.* **2014**, *509*, 299; (b) Shang, R.; Ilies,L.; Nakamura, E., *Chem. Rev.* **2017**, *117*, 9086; (c) Moselage, M.; Li, J.; Ackermann, L., *ACS Catal.* **2016**, *6*, 498.

7. Ananikov, V. P., *ACS Catal.* **2015**, *5*, 1964.

8. Yamaguchi, J.; Muto, K.; Itami, K., *Eur. J. Org. Chem.* **2013**, *1*, 19.

9. Harris, M. R.; Hanna, L. E.; Green, M. A.; Moore, C. E; Jarvo, E. R., *J. Am. Chem. Soc.* **2013**, *135*, 3303.

10. (a) Everson, D. A.; Shrestha, R.; Weix, D. J., *J. Am. Chem. Soc.* **2010**, *132*, 920; (b) Biswas, S.; Weix, D. J., *J. Am. Chem. Soc.* **2013**, *135*, 16192.

11. (a) Zaidlewicz, M.; Wolan, A.; Budny, M. Hydrometallation of C=C and C≡C Bonds. Group 3. In *Comprehensive Organic Synthesis (Second Edition)*; Knochel, P., Ed.; Elsevier: Amsterdam, **2014**; Vol. *8*, p 877-963; (b) Ager, D. Homogeneous Catalytic Hydrogenation of C=C and C≡C. In *Comprehensive Organic Synthesis (Second Edition)*; Knochel, P., Ed.; Elsevier: Amsterdam, **2014**, p 605-631. (c) Dobbs, A. P.; Chio, F. K. I. Hydrometallation Group 4 (Si, Sn, Ge, and Pb). In *Comprehensive Organic Synthesis (Second Edition)*; Knochel, P., Ed.; Elsevier: Amsterdam, **2014**; Vol. *8*, p 964-998

12. Bullock, R. M., *Science.* **2013**, *342*, 1054.

13. Chirik, P. J., *Acc Chem Res* **2015**, *48*, 1687

14. (a) Darmon, J. M.; Yu, R. P.; Semproni, S. P.; Turner, Z. R.; Stieber,S. C. E.; DeBeer, S.; Chirik, P. J., *Organometallics* **2014**, *33*, 5423; (b) Yu, R. P.; Darmon, J. M.; Hoyt, J. M.; Margulieux, G. W.; Turner, Z. R.; Chirik, P. J., *ACS Catal.* **2012**, *2*, 1760.

15. Yu, R. P.; Darmon, J. M.; Milsmann, C.; Margulieux, G. W.; Stieber, S. C. E.; DeBeer, S.; Chirik, P. J., *J. Am. Chem.Soc*. **2013**, *135*, 13168.

16. (a) Chakraborty, S.; Bhattacharya, P.; Dai, H.; Guan, H., *Acc. Chem. Res*. **2015**, *48*, 1995; (b) Bailly, B.; Thomas, P. S., *RSC Adv.,* **2011**, *1*, 1435; (c) Morris, H. R., *Acc. Chem. Res*. **2015**, *48*, 1494; (d) Friedfeld, R. M.; Shevlin, M.; Hoyt, M. J.; Krska, W. S.; Tudge, T. M.; Chirik. J. P., *Science*. **2013**, *342*, 1076; (e) Zuo, W.; Lough, J. A.; Li, F. Y.; Morris, H. R., *Science*, **2013**, *342*, 1080.

17. Lagaditis, O. P.; Sues, E. P.; Sonnenberg, F. J.; Wan, Y. K.; Lough, J. A.; Morris, H. R., *J. Am. Chem. Soc*. **2014**, *136*, 1367.

18. Monfette, S.; Turner, R. Z.; Semproni, P. S.; Chirik, J. P., *J. Am. Chem. Soc*. **2012**, *134*, 4561.

19. (a) Obligacion, V. J.; Chirik, J. P., *Nat Rev*. **2018**, *2*, 15; (b) Pappas, I.; Treacy, S.; Chirik, J. P., *ACS Catal*. **2016**, *6*, *7*, 4105 (c) Corey, J. Y., *Chem. Rev*. **2016**, *116*, 11291.

20. (a) Beletskaya, I.; Pelter, A., *Tetrahedron*. **1997**, *53*, 4957; (b) Crudden, C. M.; Edwards, D., *Eur. J. Org. Chem*. **2003**, *2003*, 4695; (c) Vogels, C. M.; Westcott, S. A., *Curr.Org. Chem*. **2005**, *9*, 687; (d) Burgess, K.; Ohlmeyer, M. J., *Chem. Rev*. **1991**, *19*, 1179; (e) Carroll, A.-M.; O'Sullivan, T. P.; Guiry, P. J., *Adv. Synth. Catal.* **2005**, *347*, 609.

21. (a) Obligacion, V. J.; Chirik, J. P., *J. Am. Chem. Soc*. **2013**, *135*, 19107; (b) Ruddy, J. A.; Sydora, L. O.; Small, L. B.; Stradiotto, M.; Turculet, L., *Chem. Eur. J*. **2014**, *20*, 13918; (c) Ogawa, T.; Ruddy, J. A.; Stradiotto, M.; Turculet, L., *Organometallics*. **2017**, *36*, 417; (d) Macaulay, M. C.; Gustafson, J. S.; Fuller, III, T. J.; Kwon, D.; Ogawa, T.; Ferguson, J. M.; McDonald, R.; Lumsden, D. M.; Bischof, M. S.; Sydor, L. O.; Ess, H. D.; Stradiotto, M.; Turculet, L., *ACS Catal*. **2018**, *8*, 9907; (e) Bose, S. K.; Mao, L.; Kuehn, L.; Radius, U.; Nekvinda, J.; Santos, W. L.; Westcott, S. A.; Steel, P. G.; Marder, T. B., *Chem. Rev*. **2021***, 121*, 13238; (f) Singh, A.; Shafiei-Haghighi, S.; Smith, C. R.; Unruh, D. K.; Findlater, M., *Asian J. Org. Chem*. **2020***, 9*, 416; (g) Obligacion, J. V.; Chirik, P. J., *Nat. Rev. Chem*. **2018**, *2*, 15.

22. Hu, M.; Ge, S., *Nature Commun*. **2020**, *11*, 765.

23. (a) Murphy, J. L.; Hollenhorst, H.; McDonald, R.; Ferguson, M.; Lumsden, D. M.; Turculet, L., *Organometallics*. **2017**, *36*, 3709; (b) Chakraborty, S.; Bhattacharya, P.; Dai, H.; Guan, H., *Acc. Chem. Res*. **2015**, *48*, 1995.

24. (a) Fan, W.; Li, L.; Zhang, G., *J. Org. Chem*. **2019**, *84*, 5987; (b) Touney, E. E.; Van Hoveln, R.; Buttke, C. T.; Freidberg, M. D.; Guzei, I. A.; Schomaker, M. J., *Organometallics*. **2016**, *35*, 3436; (c) Ulm, F.; Cornaton, Y.; Djukic, J.; Chetcuti, J. M.; Ritleng, V., *Chem. Eur. J.* **2020**, *26*, 8916; (d) Pereira, S.; Srebnik, M., *Tetrahedron Lett.* **1996**, *37*, 3283; (e) Hashimoto, T.; Ishimaru, T.; Shiota, K.; Yamaguchi, Y.; *Chem Commun*, **2020**, *56*, 11701.

25. Khusnutdinova, J. R.; Milstein, D., *Angew. Chem. Int. Ed.* **2015**, *54*, 12236.

26. Tokmic, K.; Markus, C. R.; Zhu, L.; Fout, A. R., *J. Am. Chem. Soc.* **2016**, *138*, 11907.

27. Lyaskovskyy, V.; de Bruin, B., *ACS Catal.* **2012**, *2*, 270.

28. Alig, L.; Fritz, M.; Schneider, S., *Chem. Rev.* **2019**, *119*, 2681.

29. Zell, T.; Milstein, D., *Acc. Chem. Res.* **2015**, *48*, 1979.

30. Russell, S. K.; Lobkovsky, E.; Chirik, P. J., *J. Am. Chem. Soc.* **2011**, *133*, 8858.

31. Obligacion, J. V.; Chirik, P. J., *J. Am. Chem. Soc.* **2013**, *135*, 19107.

32. (a) Monfette, S.; Turner, Z. R.; Semproni, S. P.; Chirik, P. J., *J. Am. Chem. Soc.* **2012**, *134*, 4561; (b) Friedfeld, M. R.; Shevlin, M.; Margulieux, G. W.; Campeau, L. C.; Chirik, P. J., *J. Am. Chem. Soc.* **2016**, *138*, 3314; (c) Bart, S. C.; Lobkovsky, E.; Chirik, P. J., *J. Am. Chem. Soc.* **2004**, *126*, 13794; (d) Trovitch, R. J.; Lobkovsky, E.; Bill, E.; Chirik, P. J., *Organometallics* **2008**, *27*, 1470.

33. Bowman, A. C.; Milsmann, C.; Atienza, C. C.; Lobkovsky, E.; Wieghardt, K.; Chirik, P. J., *J. Am. Chem. Soc.* **2010**, *132*, 1676.

34. Gunanathan, C.; Milstein, D., *Acc. Chem. Res.* **2011**, *44*, 588. 60

35. Langer, R.; Leitus, G.; Ben-David, Y.; Milstein, D., *Angew. Chem. Int. Ed.* **2011**, *50*, 2120.

36. Langer, R.; Diskin-Posner, Y.; Leitus, G.; Shimon, L. J. W.; Ben-David, Y.; Milstein, D., *Angew. Chem. Int. Ed.* **2011**, *50*, 9948.

37. Zhang, Y.; MacIntosh, A. D.; Wong, J. L.; Bielinski, E. A.; Williard, P. G.; Mercado, B. Q.; Hazari, N.; Bernskoetter, W. H., *Chem. Sci.* **2015**, *6*, 4291.

38. Morris, R. H., *Acc. Chem. Res.* **2015**, *48*, 1494−1502.

39. (a) Tzu-Pin, L.; Peters, C. J., *J. Am. Chem. Soc.* **2014**, *136*, 39, 13672; (a) Lin, T. P.; Peters, J. C., *J. Am. Chem. Soc.* **2013**, *135*, 15310; (b) Lin, T. P.; Peters, J. C., *J. Am. Chem. Soc.* **2014**, *136*, 13672.

40. Sunada, Y.; Ogushi, H.; Yamamoto, T.; Shoko, U.; Sawano, M.; Tahara, A.; Tanka, H.; Shiota, Y.; Yoshizawa, K.; Nagashima, H., *J. Am. Chem. Soc.* **2018**, *140*, 4119.

41. Nikonov, G. I., *Adv. Organomet. Chem.* **2005**, *53*, 217.

42.  (a) Joslin, F. L.; Stobart, S. R., *Chem. Commun.* **1989**, 504; (b) Joslin, F. L.; Stobart, S. R., *Inorg. Chem.* **1993**, *32*, 2221; (c) Gossage, R. A.; McLennan, G. D.; Stobart, S. R., *Inorg. Chem.* **1996**, *35*, 1729; (d) Brost, R. D.; Bruce, G. C.; Joslin, F. L.; Stobart, S. R., *Organometallics* **1997**, *16*, 5669; (e) Bushnell, G. W.; Casado, M. A.; Stobart, S. R., *Organometallics* **2001**, *20*, 601; (f) Stobart, S. R.; Zhou, X. B.; Cea-Olivares, R.; Toscano, A., *Organometallics* **2001**, *20*, 4766; (g) Zhou, X. B.; Stobart, S. R., *Organometallics* **2001**, *20*, 1898.

43.  MacInnis, M. C.; MacLean, D. F.; Lundgren, R. J.; McDonald, R.; Turculet, L., *Organometallics* **2007**, *26*, 6522.

44.  (a) Morgan, E.; MacLean, D. F.; McDonald, R.; Turculet, L., *J. Am. Chem. Soc.* **2009**, *131*, 14234; (b) MacLean, D. F.; McDonald, R.; Ferguson, M. J.; Caddell, A. J.; Turculet, L., *Chem. Commun.* **2008**, 5146.

45.  MacInnis, M. C.; McDonald, R.; Ferguson, M. J.; Tobisch, S.; Turculet, L., *J. Am. Chem. Soc.* **2011**, *133*, 13622.

46.  (a) Mankad, N. P.; Whited, M. T.; Peters, J. C., *Angew. Chem. Int. Ed.* **2007**, *46*, 5768; (b) Whited, M. T.; Mankad, N. P.; Lee, Y.; Oblad, P. F.; Peters, J. C., *Inorg. Chem.* **2009**, *48*, 2507; (c) Lee, Y.; Mankad, N. P.; Peters, J. C., *Nat. Chem.* **2010**, *2*, 558.

47.  (a) Murphy, L. J.; Ferguson, M. J.; McDonald, R.; Lumsden, M. D.; Turculet, L., *Organometallics* **2018,** *37*, 4814; (b) Murphy, L. J.; Ruddy, A. J.; McDonald, R.; Ferguson, M. J.; Turculet, L., *Eur. J. Inorg. Chem.* **2018,** *2018*, 4481; (c) Mitton, S. J.; McDonald, R.; Turculet, L., *Angew. Chem. Int. Ed.* **2009,** *48*, 8568; (d) Hale, D. J.; Ferguson, M. J.; Turculet, L. *ACS Catal.* **2022**, *12*, 146.

48.  (a) Charboneau, D. J.; Balcells, D.; Hazari, N.; Lant, H. M. C.; Mayer, J. M.; Melvin, P. R.; Mercado, B. Q.; Morris, W. D.; Repisky, M.; Suh, H.-W., *Organometallics* **2016,** *35*, 3154; (b) Suh, H. W.; Guard, L. M.; Hazari, N., *Chem. Sci.* **2014,** *5*, 3859; (c) Nova, A.; Suh, H.-W.; Schmeier, T. J.; Guard, L. M.; Eisenstein, O.; Hazari, N.; Maseras, F., *Angew. Chem. Int. Ed.* **2014,** *53*, 1103; (d) Suh, H. W.; Guard, L. M.; Hazari, N., *Polyhedron* **2014**, *84*, 37; (e) Suh, H. W.; Schmeier, T. J.; Hazari, N.; Kemp, R. A.; Takase, M. K., *Organometallics* **2012,** *31*, 8225; (f) Takaya, J.; Iwasawa, N., *Dalton Trans.* **2011,** *40*, 8814; (g) Wu, S.; Li, X.; Xiong, Z.; Xu, W.; Lu, Y.; Sun, H., *Organometallics* **2013,** *32*, 3227; (h) Kim, J.; Kim, Y.; Sinha, I.; Park, K.; Kim, S. H.; Lee, Y., *Chem. Commun.* **2016,** *52*, 9367; (i) Xiong, Z.; Li, X.; Zhang, S.; Shi, Y.; Sun, H., *Organometallics* **2016,** *35*, 357; (j) Imayoshi, R.; Nakajima, K.; Takaya, J.; Iwasawa, N.; Nishibayashi, Y., *Eur. J. Inorg. Chem.* **2017**, 3769.

49.  (a) Holmes-Smith, R. D.; Stobart, S. R.; Cameron, T. S.; Jochem, K. *J. Chem. Soc., Chem. Commun.* **1981**, 937; (b) Grundy, S. L.; Holmes-Smith, R. D.; Stobart, S. R.;Williams, M. A., *Inorg. Chem.* **1991**, *30*, 3333; (c) Cameron, T. S.; Holmes-Smith, R. D.; Jochem, K.; Stobart, S. R.; Vefghi, R.; Zaworotko, M. J., *J. Chem. Soc. Dalton Trans.* **1987**, 969.

50.     Clevenger, L. A.; Stolley, M. R.; Aderibigbe, J.; Louis, J., *Chem. Rev.* **2020**, *120*, 6124.

51.     (a) Ruddy, A. J.; Kelly, C.; Crawford, S. M.; Wheaton, C. A.; Sydora, O. L.; Small, B. L.; Stradiotto, M.; Turculet, L., *Organometallics* **2013**, *32*, 5581; (b) Hale, D. J.; Murphy, L. J.; McDonald, R.; Ferguson, M. J.; Turculet, L., *ChemCatChem* **2019**, *11*, 3818.

52.     (a) Bourget-Merle, L.; Lappert, F. M.; Severn, R. J., *Chem. Rev.* **2002**, *102*, 3031; (b) Zhu, Di.; Budzelaar, H. M. P., *Dalton Trans*. **2013**, *42*, 11343. (c) Tsai, Y., *Coordination Chemistry Reviews.* **2012**, *256*, 722.

53.     Turculet, L. "PSiP Transition Metal Pincer Complexes: Synthesis Bond Activation, and Catalysis." In Pincer and Pincer-Type Complexes: Applications in Organic Synthesis and Catalysis; Wiley-VCH, **2014**

54.     Nova, A.; Suh, H.-W.; Schmeier, T. J.; Guard, L.M.; Eisenstein, O.; Hazari, N.; Maseras, F., *Angew. Chem. Int*. Ed. **2014**, *53*: 1103.

55.     The synthesis of PSiP variants featuring ethyl substitution at phosphorus is currently under investigation in the Turculet group: Tremblay, D. Dalhousie University, Halifax, NS, Canada. Unpublished work, **2022.**

56.     Murata, M.; Buchwalk, S. L., *Tetrahedron* **2004**, *60*, 7367.

57.     (a) Duncan Lyngdoh, R. H.; Schaefer III, H. F.; King, R. B., *Chem. Rev.* **2018**, *118*, 11626; (b) Lu, E.; Liddle, S. T. Group 10 Metal-Metal Bonds. In *Molecular Metal-Metal Bonds;* Liddle, S. T., Ed.; Wiley-VCH: Weinheim, **2015**; pp 325–395.

58.     (a) Laskowski, C. A.; Hillhouse, G. L., *Organometallics* **2009***, 28*, 6114; (b) Ashley, A. E.; Cooper, R. T.; Wildgoose, G. G.; Green, J. C.; O'Hare, D., *J. Am. Chem. Soc.* **2008**, *130*, 15662.

59.     Zaidlewicz, M.; Wolan, A.; Budny, M. Hydrometallation of C=C and C≡C Bonds. Group 3. In *Comprehensive Organic Synthesis*, 2nd ed.; Knochel, P., Ed,; Elsevier, **2014**; Vol. 8, pp 877-963.

60.     (a) Denk, M.; Hayashi, K. R.; West, R., *J. Chem. Soc., Chem. Commun.*, **1994**, *24*, 2473; (b) Schmedake, A. T.; Haaf, M.; Paradise, J. B.; Douglas Powell, D.; West, R., *Organometallics*. **2000**, *19*, *17*, 3263; (c) Kong, L.; Zhang, J.; Song, H.; Cui, C., *Dalton Trans*. **2009**, 5444; (d) Handford, C. R.; Smith, W. P.; Tily, T. D., *Organometallics* **2018**, *37*, *21*, 4077; (e) Strauss, A. D.; Grumbine, D. S.; Tily, T. D., *J. Am. Chem. Soc.* **1990**, *112*, *21*, 7801.

61.     Hoey, M. R. Synthesis of Transition Metal Complexes Supported by Mixed Donor PSiP' Bis-Phosphino Silyl Pincer Ligands. MSc Thesis, Dalhousie University, **2016**

# Appendix A: Crystallographic Experimental Details

**Table A1.** Crystallographic experimental details for **2-NiCl**

| | |
|---|---|
| Empirical formula | $C_{48}H_{80}Cl_2Ni_2P_2Si_2$ |
| Formula weight | 963.56 |
| Temperature | 125(2) K |
| Wavelength | 0.71073 Å |
| Crystal system | Monoclinic |
| Space group | $P2_1/c$ |
| Unit cell dimensions | $a = 17.1787(6)$ Å $\quad \alpha = 90°$ |
| | $b = 14.8756(4)$ Å $\quad \beta = 94.7836(14)°$ |
| | $c = 19.8491(7)$ Å $\quad \gamma = 90°$ |
| Volume | 5054.6(3) Å$^3$ |
| $Z$ | 4 |
| Density (calculated) | 1.266 Mg/m$^3$ |
| Absorption coefficient | 0.992 mm$^{-1}$ |
| F(000) | 2064 |
| Crystal size | 0.125 x 0.060 x 0.052 mm$^3$ |
| Theta range for data collection | 2.059 to 30.508° |
| Index ranges | -24<=h<=24, -21<=k<=21, -28<=l<=28 |
| Reflections collected | 249646 |
| Independent reflections | 15449 [R(int) = 0.0349] |
| Completeness to theta = 25.242° | 100.0 % |
| Absorption correction | Semi-empirical from equivalents |
| Max. and min. transmission | 0.0401 and 0.0110 |
| Refinement method | Full-matrix least-squares on F$^2$ |
| Data / restraints / parameters | 15449 / 0 / 513 |
| Goodness-of-fit on F$^2$ | 1.108 |
| Final R indices [I>2sigma(I)] | R1 = 0.0437, wR2 = 0.1043 |
| R indices (all data) | R1 = 0.0579, wR2 = 0.1186 |
| Extinction coefficient | n/a |
| Largest diff. peak and hole | 0.607 and -0.501 e.Å$^{-3}$ |

A clear gold, diamond-shaped plate specimen of $C_{48}H_{80}Cl_2Ni_2P_2Si_2$, approximate dimensions 0.052 mm x 0.060 mm x 0.125 mm, was used for the X-ray crystallographic analysis. The X-ray

intensity data were measured using Mo Kα radiation ($\lambda$ = 0.71073 Å). A total of 3046 frames were collected. The total exposure time was 15.97 hours. The frames were integrated with the Bruker SAINT software package using a narrow-frame algorithm. The integration of the data using a monoclinic unit cell yielded a total of 439603 reflections to a maximum θ angle of 36.40° (0.60 Å resolution). The final cell constants of $a$ = 17.1787(6) Å, $b$ = 14.8756(4) Å, $c$ = 19.8491(7) Å, $\beta$ = 94.7836(14)°, volume = 5054.6(3) Å$^3$, are based upon the refinement of the XYZ-centroids of 9807 reflections above 20 σ(I) with 4.925° < 2θ < 72.20°. Data were corrected for absorption effects using the Multi-Scan method (SADABS). The ratio of minimum to maximum apparent transmission was 0.274.

**Table A2.** Crystallographic experimental details for **2-NiBn**

| | |
|---|---|
| Empirical formula | $C_{31}H_{47}NiPSi$ |
| Formula weight | 537.45 |
| Temperature | 125(2) K |
| Wavelength | 0.71073 Å |
| Crystal system | Monoclinic |
| Space group | $P2_1/c$ |
| Unit cell dimensions | $a$ = 10.0774(4) Å        $\alpha$ = 90° |
| | $b$ = 15.2169(6) Å        $\beta$ = 103.7213(14)° |
| | $c$ = 19.5314(7) Å        $\gamma$ = 90° |
| Volume | 2909.60(19) Å$^3$ |
| $Z$ | 4 |
| Density (calculated) | 1.227 Mg/m$^3$ |
| Absorption coefficient | 0.780 mm$^{-1}$ |
| F(000) | 1160 |
| Crystal size | 0.180 x 0.097 x 0.058 mm$^3$ |
| Theta range for data collection | 2.147 to 33.141° |
| Index ranges | -15<=h<=15, -23<=k<=23, -24<=l<=30 |
| Reflections collected | 151968 |
| Independent reflections | 11095 [R(int) = 0.0383] |
| Completeness to theta = 25.242° | 99.9 % |
| Absorption correction | Semi-empirical from equivalents |
| Max. and min. transmission | 0.2740 and 0.2247 |
| Refinement method | Full-matrix least-squares on F$^2$ |
| Data / restraints / parameters | 11095 / 234 / 392 |
| Goodness-of-fit on F$^2$ | 1.079 |
| Final R indices [I>2sigma(I)] | R1 = 0.0451, wR2 = 0.1038 |

| R indices (all data) | R1 = 0.0591, wR2 = 0.1186 |
| Extinction coefficient | n/a |
| Largest diff. peak and hole | 0.874 and -0.469 e.Å$^{-3}$ |

A clear yellow, irregular specimen of $C_{31}H_{47}NiPSi$, approximate dimensions 0.058 mm x 0.097 mm x 0.180 mm, was used for the X-ray crystallographic analysis. The X-ray intensity data were measured using Mo Kα radiation (λ = 0.71073 Å). A total of 2799 frames were collected. The total exposure time was 14.60 hours. The frames were integrated with the Bruker SAINT software package using a narrow-frame algorithm. The integration of the data using a monoclinic unit cell yielded a total of 237367 reflections to a maximum θ angle of 36.47° (0.60 Å resolution). The final cell constants of $a$ = 10.0774(4) Å, $b$ = 15.2169(6) Å, $c$ = 19.5314(7) Å, β = 103.7213(14)°, volume = 2909.60(19) Å$^3$, are based upon the refinement of the XYZ-centroids of 9891 reflections above 20 σ(I) with 4.947° < 2θ < 71.68°. Data were corrected for absorption effects using the Multi-Scan method (SADABS). The ratio of minimum to maximum apparent transmission was 0.820.

**Table A3.** Crystallographic experimental details for **2-NiHPPh₃**

*A. Crystal Data*

| formula | $C_{44}H_{61}Ni_{0.50}P_2Si$ |
| formula weight | 746.66 |
| crystal dimensions (mm) | 0.20 × 0.19 × 0.03 |
| crystal system | monoclinic |
| space group | $P2_1/c$ (No. 14) |
| unit cell parameters$^a$ | |
| $a$ (Å) | 11.0038(3) |
| $b$ (Å) | 20.2120(5) |
| $c$ (Å) | 19.4067(6) |
| $β$(deg) | 104.9420(14) |
| $V$ (Å$^3$) | 4170.3(2) |
| $Z$ | 4 |
| $\rho_{calcd}$ (g cm$^{-3}$) | 1.189 |
| $\mu$ (mm$^{-1}$) | 1.884 |

*B. Data Collection and Refinement Conditions*

| diffractometer | Bruker D8/APEX II CCD$^b$ |
| radiation ($\lambda$ [Å]) | Cu Kα (1.54178) (microfocus source) |
| temperature (°C) | −100 |
| scan type | ω and Ø scans (1.0°) (5 s exposures) |
| data collection 2Ø limit (deg) | 140.57 |
| total data collected | 159050 (-13 ≤ h ≤ 13, -24 ≤ k ≤ 24, -22 ≤ l ≤ 23) |
| independent reflections | 7943 ($R_{int}$ = 0.0655) |

| number of observed reflections ($NO$) | 7132 [$F_o^2 \geq 2\sigma(F_o^2)$] |
|---|---|
| structure solution method | intrinsic phasing (*SHELXT-2014*[c]) |
| refinement method | full-matrix least-squares on $F^2$ (*SHELXL–2018*[d,e]) |
| absorption correction method | Gaussian integration (face-indexed) |
| range of transmission factors | 0.9738–0.7019 |
| data/restraints/parameters | 7943 / 0 / 419 |
| goodness-of-fit ($S$)[f] [all data] | 1.084 |
| final $R$ indices[g] | |
| $R_1$ [$F_o^2 \geq 2\sigma(F_o^2)$] | 0.0311 |
| $wR_2$ [all data] | 0.0844 |
| largest difference peak and hole | 0.341 and –0.211 e Å$^{-3}$ |

[a]Obtained from least-squares refinement of 9813 reflections with 6.42° < 2∅ < 140.36°.

[b]Programs for diffractometer operation, data collection, data reduction and absorption correction were those supplied by Bruker.

[c]Sheldrick, G. M. *Acta Crystallogr.* **2015**, *A71*, 3–8. (*SHELXT-2014*)

[d]Sheldrick, G. M. *Acta Crystallogr.* **2015**, *C71*, 3–8. (*SHELXL-2018/3*)

[e]Attempts to refine peaks of residual electron density as disordered or partial-occupancy solvent dithylether oxygen or carbon atoms were unsuccessful. The data were corrected for disordered electron density through use of the SQUEEZE procedure as implemented in *PLATON* (Spek, A. L. *Acta Crystallogr.* **2015**, *C71*, 9–18. *PLATON* - a multipurpose crystallographic tool. Utrecht University, Utrecht, The Netherlands). A total solvent-accessible void volume of 480 Å$^3$ with a total electron count of 82 (consistent with 2 molecules of solvent diethylether, or 0.5 molecules per formula unit of the nickel complex) was found in the unit cell.

[f]$S = [\Sigma w(F_o^2 - F_c^2)^2/(n - p)]^{1/2}$ ($n$ = number of data; $p$ = number of parameters varied; $w = [\sigma^2(F_o^2) + (0.0371P)^2 + 1.7181P]^{-1}$ where $P = [\text{Max}(F_o^2, 0) + 2F_c^2]/3$).

[g]$R_1 = \Sigma||F_o| - |F_c||/\Sigma|F_o|$; $wR_2 = [\Sigma w(F_o^2 - F_c^2)^2/\Sigma w(F_o^4)]^{1/2}$.

**Table A4.** Crystallographic experimental details for **2-NiH**

| Empirical formula | $C_{24}H_{40}NiPSi$ |
|---|---|
| Formula weight | 446.33 |
| Temperature | 150(2) K |
| Wavelength | 0.71073 Å |
| Crystal system | Triclinic |
| Space group | *P*-1 |

| | | |
|---|---|---|
| Unit cell dimensions | $a = 14.0807(12)$ Å | $\alpha = 91.770(3)°$ |
| | $b = 16.6960(14)$ Å | $\beta = 90.736(3)°$ |
| | $c = 20.3924(17)$ Å | $\gamma = 90.150(4)°$ |
| Volume | 4791.4(7) Å$^3$ | |
| $Z$ | 8 | |
| Density (calculated) | 1.237 Mg/m$^3$ | |
| Absorption coefficient | 0.934 mm$^{-1}$ | |
| F(000) | 1928 | |
| Crystal size | 0.323 x 0.213 x 0.067 mm$^3$ | |
| Theta range for data collection | 1.998 to 26.372° | |
| Index ranges | -17<=h<=17, -20<=k<=20, -25<=l<=25 | |
| Reflections collected | 268834 | |
| Independent reflections | 19592 [R(int) = 0.0509] | |
| Completeness to theta = 25.242° | 99.9 % | |
| Absorption correction | Semi-empirical from equivalents | |
| Max. and min. transmission | 0.0998 and 0.0635 | |
| Refinement method | Full-matrix least-squares on F$^2$ | |
| Data / restraints / parameters | 19592 / 1012 / 1049 | |
| Goodness-of-fit on F$^2$ | 1.119 | |
| Final R indices [I>2sigma(I)] | R1 = 0.0718, wR2 = 0.1671 | |
| R indices (all data) | R1 = 0.0777, wR2 = 0.1710 | |
| Extinction coefficient | n/a | |
| Largest diff. peak and hole | 2.031 and -1.224 e.Å$^{-3}$ | |

A red, plate (cut) specimen of $C_{24}H_{40}NiPSi$, approximate dimensions 0.067 mm x 0.213 mm x 0.323 mm, was used for the X-ray crystallographic analysis. The X-ray intensity data were measured using Mo Kα radiation ($\lambda = 0.71073$ Å). A total of 5092 frames were collected. The total exposure time was 27.34 hours. The frames were integrated with the Bruker SAINT software package using a narrow-frame algorithm. The integration of the data using a triclinic unit cell yielded a total of 417413 reflections to a maximum θ angle of 30.63° (0.70 Å resolution). The final cell constants of $a = 14.0807(12)$ Å, $b = 16.6960(14)$ Å, $c = 20.3924(17)$ Å, $\alpha = 91.770(3)°$, $\beta = 90.736(3)°$, $\gamma = 90.150(4)°$, volume = 4791.4(7) Å$^3$, are based upon the refinement of the XYZ-centroids of 9548 reflections above 20 σ(I) with 5.426° < 2θ < 61.17°. Data were corrected for absorption effects using the Multi-Scan method (SADABS). The ratio of minimum to maximum apparent transmission was 0.636.

**Table A5.** Crystallographic experimental details for **2-NiCOD**

| | |
|---|---|
| Empirical formula | $C_{32}H_{53}NiPSi$ |
| Formula weight | 555.51 |
| Temperature | 125(2) K |
| Wavelength | 0.71073 Å |
| Crystal system | Monoclinic |
| Space group | *P2/n* |
| Unit cell dimensions | $a$ = 9.8926(5) Å $\quad$ $\alpha$ = 90° |
| | $b$ = 9.0445(5) Å $\quad$ $\beta$ = 97.3700(19)° |
| | $c$ = 34.7375(16) Å $\quad$ $\gamma$ = 90° |
| Volume | 3082.4(3) Å$^3$ |
| *Z* | 4 |
| Density (calculated) | 1.197 Mg/m$^3$ |
| Absorption coefficient | 0.739 mm$^{-1}$ |
| F(000) | 1208 |
| Crystal size | 0.170 x 0.075 x 0.057 mm$^3$ |
| Theta range for data collection | 1.773 to 28.345° |
| Index ranges | -13<=h<=13, -12<=k<=12, -46<=l<=46 |
| Reflections collected | 106621 |
| Independent reflections | 7760 [R(int) = 0.0590] |
| Completeness to theta = 25.242° | 99.9 % |
| Absorption correction | Semi-empirical from equivalents |
| Max. and min. transmission | 0.7457 and 0.6935 |
| Refinement method | Full-matrix least-squares on F$^2$ |
| Data / restraints / parameters | 7760 / 1652 / 749 |
| Goodness-of-fit on F$^2$ | 1.100 |
| Final R indices [I>2sigma(I)] | R1 = 0.0592, wR2 = 0.1541 |
| R indices (all data) | R1 = 0.0723, wR2 = 0.1662 |
| Extinction coefficient | n/a |
| Largest diff. peak and hole | 0.433 and -0.365 e.Å$^{-3}$ |

A yellow, rectangular prism (cut) specimen of $C_{32}H_{53}NiPSi$, approximate dimensions 0.057 mm x 0.075 mm x 0.170 mm, was used for the X-ray crystallographic analysis. The X-ray intensity data were measured using Mo Kα radiation (λ = 0.71073 Å). A total of 3240 frames were collected. The total exposure time was 12.80 hours. The frames were integrated with the Bruker SAINT software package using a narrow-frame algorithm. The integration of the data using a

monoclinic unit cell yielded a total of 134708 reflections to a maximum $\theta$ angle of 28.46° (0.75 Å resolution). The final cell constants of $a$ = 9.8926(5) Å, $b$ = 9.0445(5) Å, $c$ = 34.7375(16) Å, $\beta$ = 97.3700(19)°, volume = 3082.4(3) Å$^3$, are based upon the refinement of the XYZ-centroids of 9990 reflections above 20 $\sigma$(I) with 4.460° < 2$\theta$ < 56.30°. Data were corrected for absorption effects using the Multi-Scan method (SADABS). The ratio of minimum to maximum apparent transmission was 0.927.

**Figure B1.** ^{1}H NMR (500 MHz, $C_6D_6$) spectrum for the bidentate (phosphino)silyl ligand **(Cy-PSi)H**
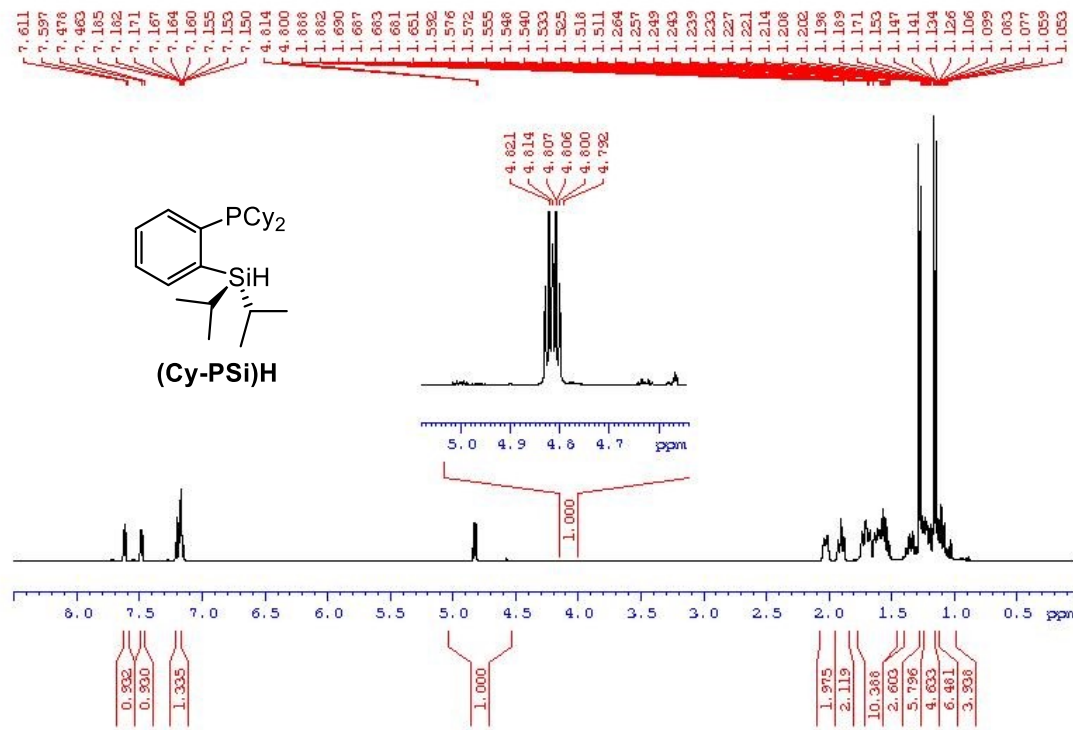
**Figure B2.** $^{13}C\{^{1}H\}$ NMR (125.7 MHz, C$_6$D$_6$) spectrum for the bidentate (phosphino)silyl ligand **(Cy-PSi)H**
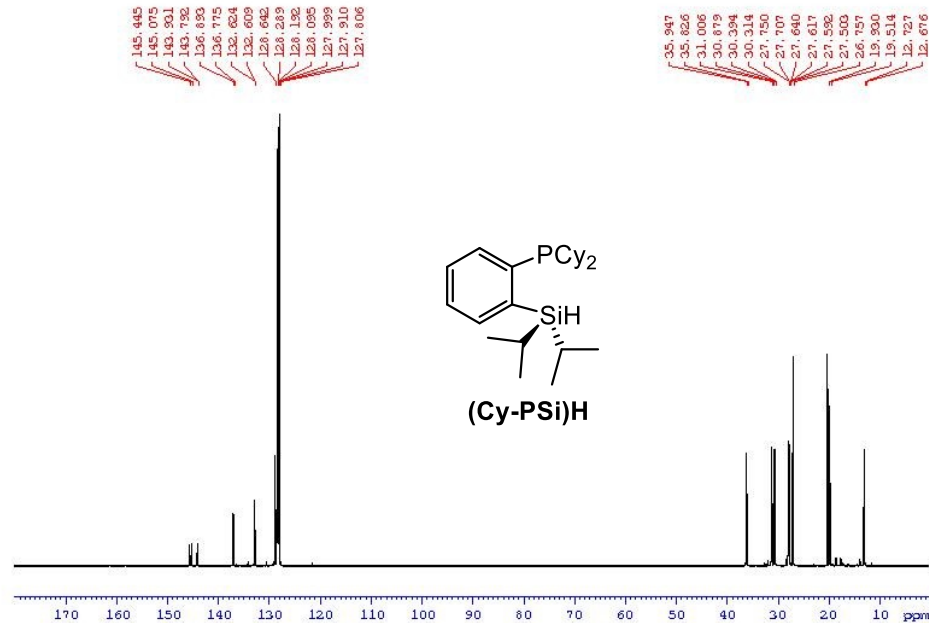
**Figure B3.** $^{31}P\{^{1}H\}$ NMR (202.1 MHz, C$_6$D$_6$) spectrum for the bidentate (phosphino)silyl ligand **(Cy-PSi)H**
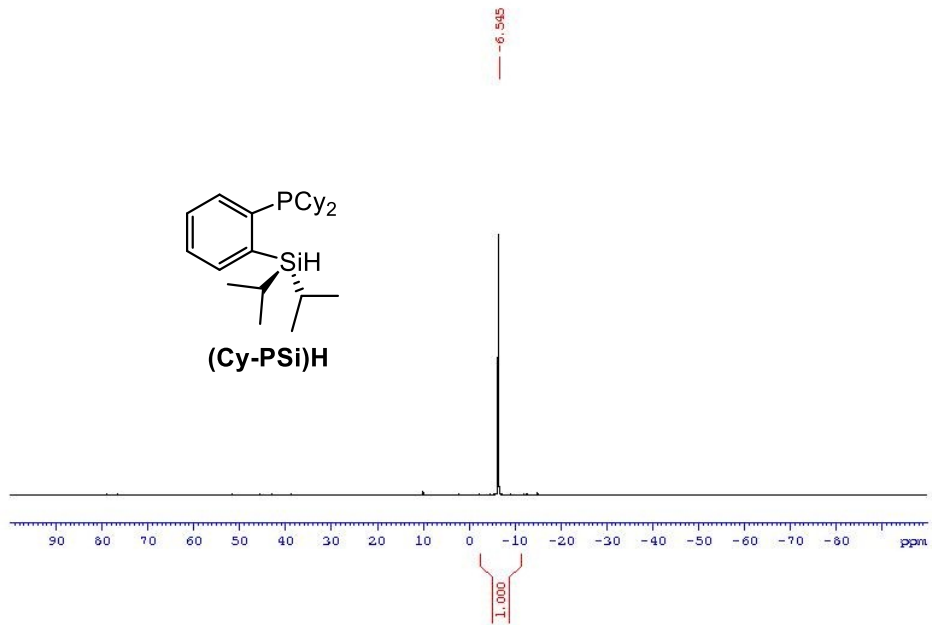
**Figure B4.** $^1$H NMR (500 MHz, C$_6$D$_6$) spectrum of [(Cy-PSi)NiCl]$_2$ dimer **(2-NiCl)**
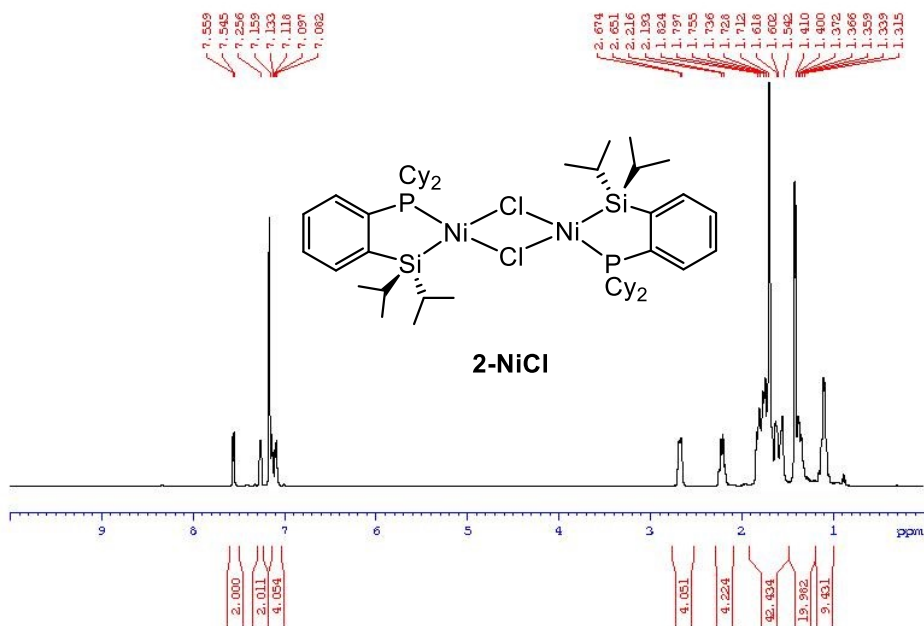
**Figure B5.** $^{13}C\{^1H\}$ NMR (125.7 MHz, $C_6D_6$) spectrum of $[(Cy-PSi)NiCl]_2$ dimer **(2-NiCl)**
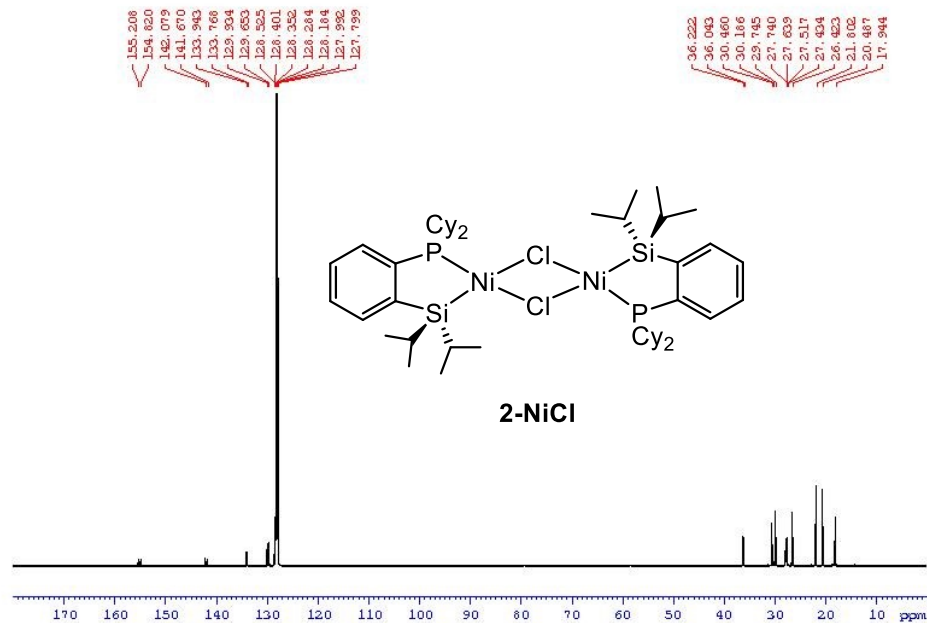


2-NiCl

**Figure B6.** $^{31}$P{$^1$H} NMR (202.1 MHz, C$_6$D$_6$) spectrum of [(Cy-PSi)NiCl]$_2$ dimer **(2-NiCl)**
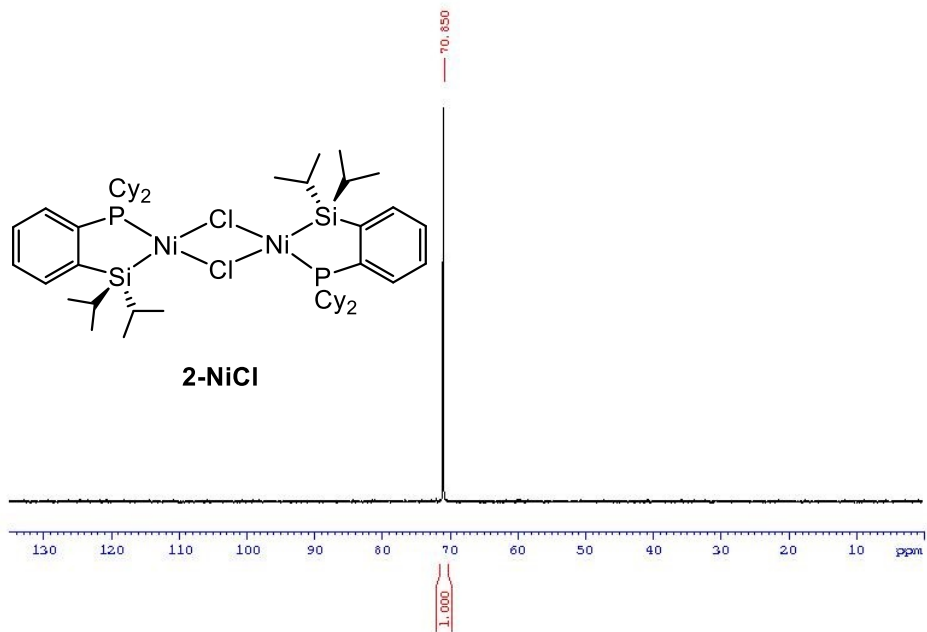
**Figure B7.** ^{1}H NMR (300 MHz, C$_6$D$_6$) spectrum of (Cy-PSi)NiBn complex **(2-NiBn)**
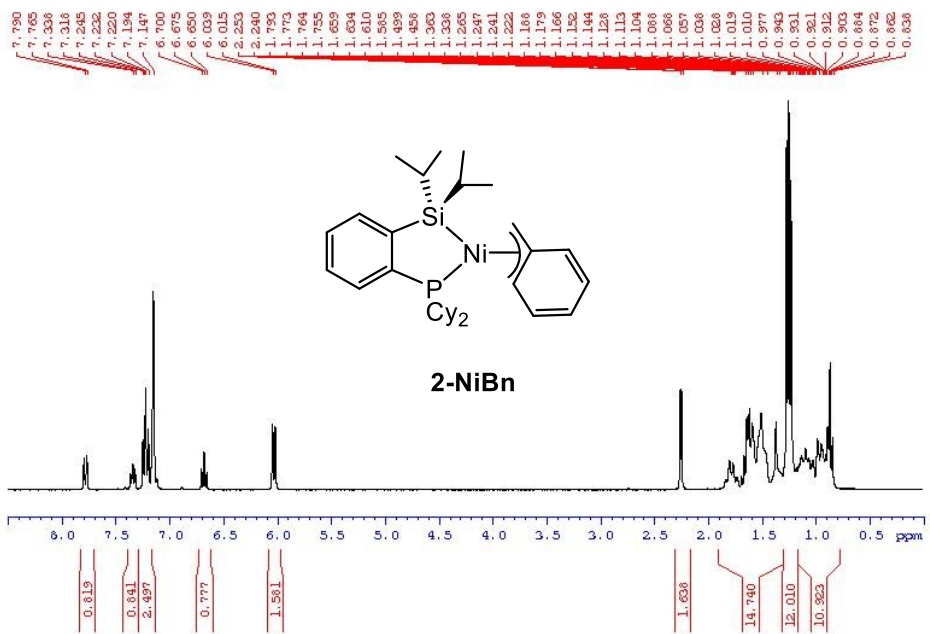
**Figure B8.** $^{13}C\{^1H\}$ NMR (125.7 MHz, $C_6D_6$) spectrum of (Cy-PSi)NiBn complex **(2-NiBn)**



2-NiBn

**Figure B9.** $^{31}P\{^1H\}$ NMR (202.1 MHz, $C_6D_6$) spectrum of (Cy-PSi)NiBn complex **(2-NiBn)**



2-NiBn
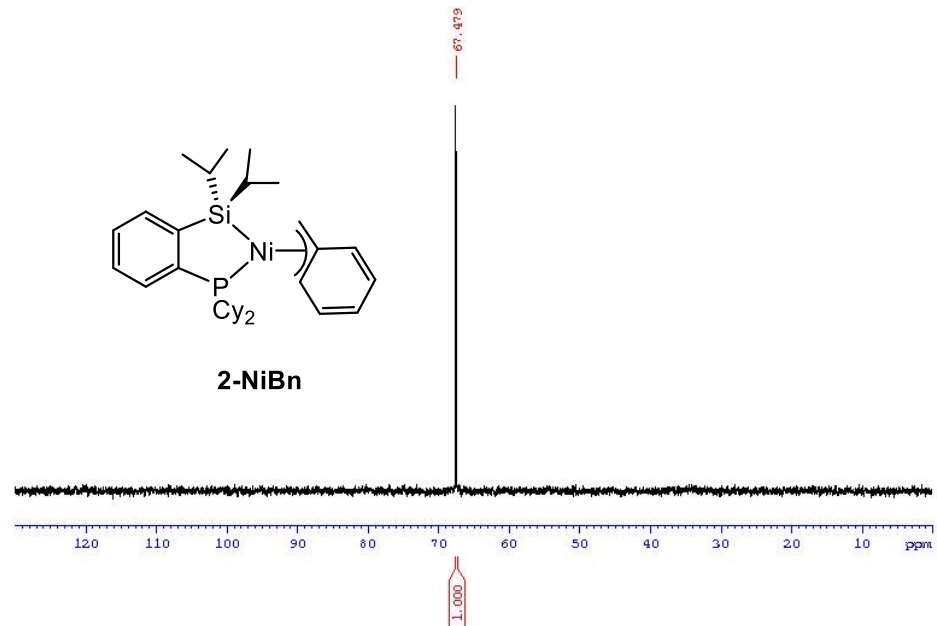
**Figure B10.** $^1$H NMR (500 MHz, C$_6$D$_6$) spectrum of (Cy-PSi)Ni($\eta^3$-C$_8$H$_{13}$) complex **(2-NiCOD)**
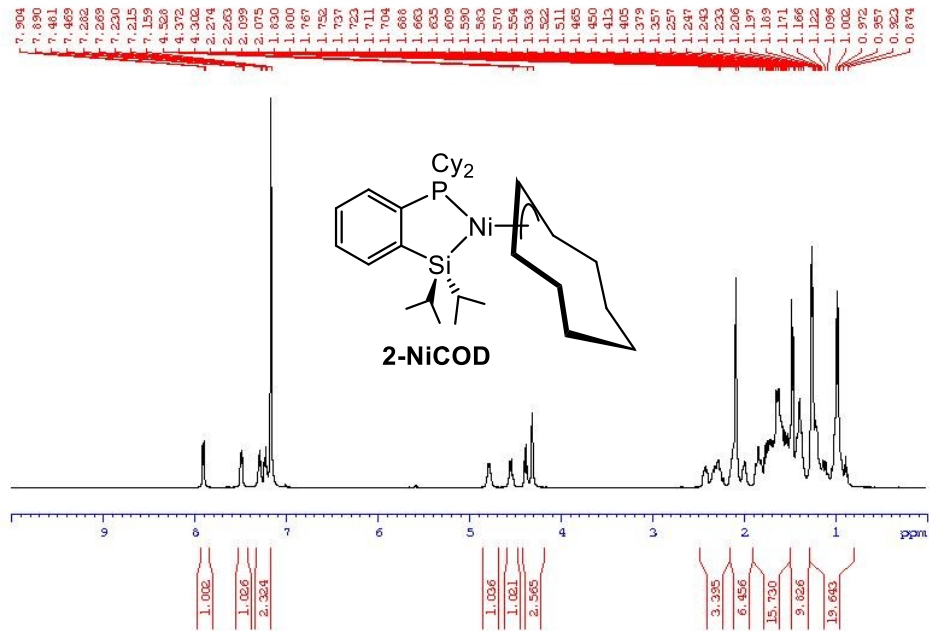
**Figure B11.** $^{13}C\{^1H\}$ NMR (125.7 MHz, $C_6D_6$) spectrum of (Cy-PSi)Ni($\eta^3$-$C_8H_{13}$) complex **(2-NiCOD)**
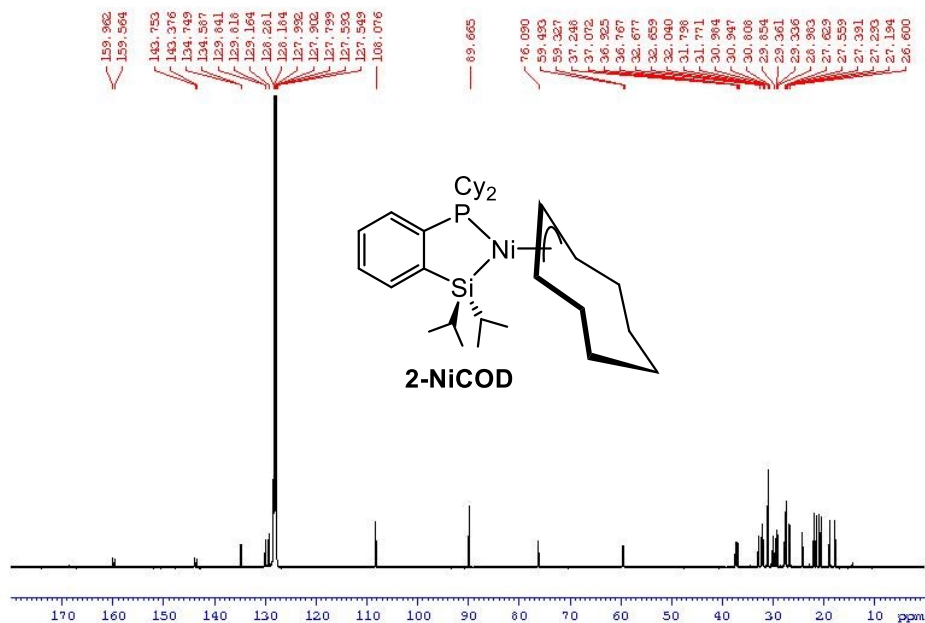
**Figure B12.** $^{31}P\{^1H\}$ NMR (202.1 MHz, $C_6D_6$) spectrum of (Cy-PSi)Ni($\eta^3$-$C_8H_{13}$) complex **(2-NiCOD)**
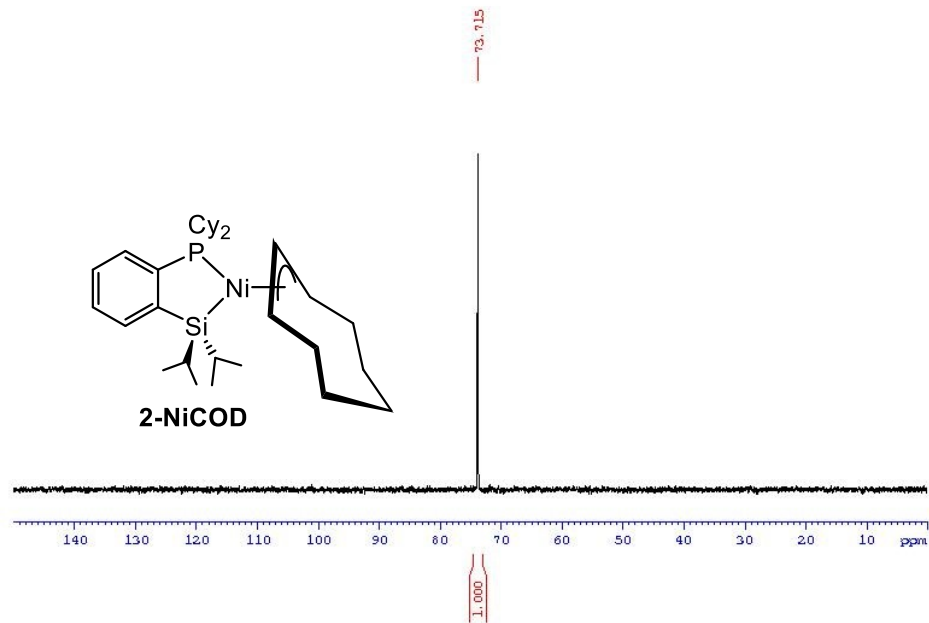
**Figure B13.** $^1$H NMR (500 MHz, C$_6$D$_6$) spectrum of [(Cy-PSi)NiH]$_2$ dimer **(2-NiH)**
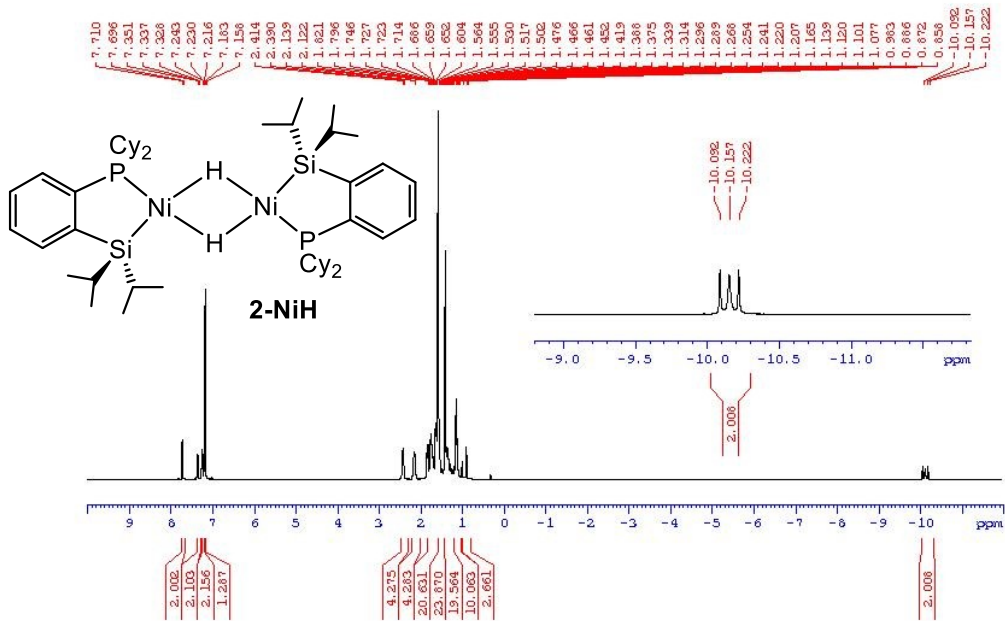
**Figure B14.** $^{13}C\{^1H\}$ NMR (125.7 MHz, $C_6D_6$) spectrum of [(Cy-PSi)NiH]$_2$ dimer **(2-NiH)**
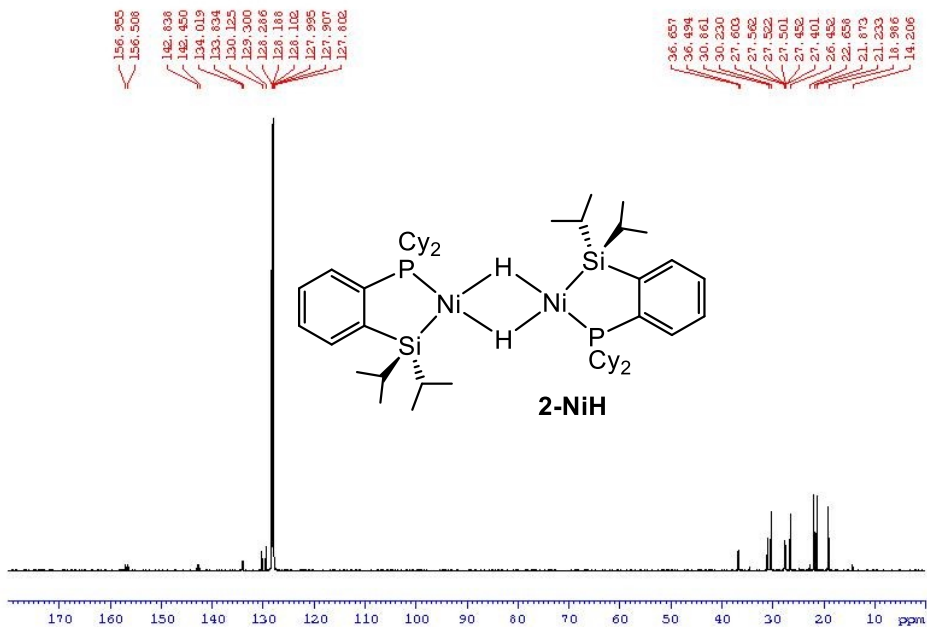
**Figure B15.** $^{31}P\{^1H\}$ NMR (202.1 MHz, C$_6$D$_6$) spectrum of [(Cy-PSi)NiH]$_2$ dimer **(2-NiH)**
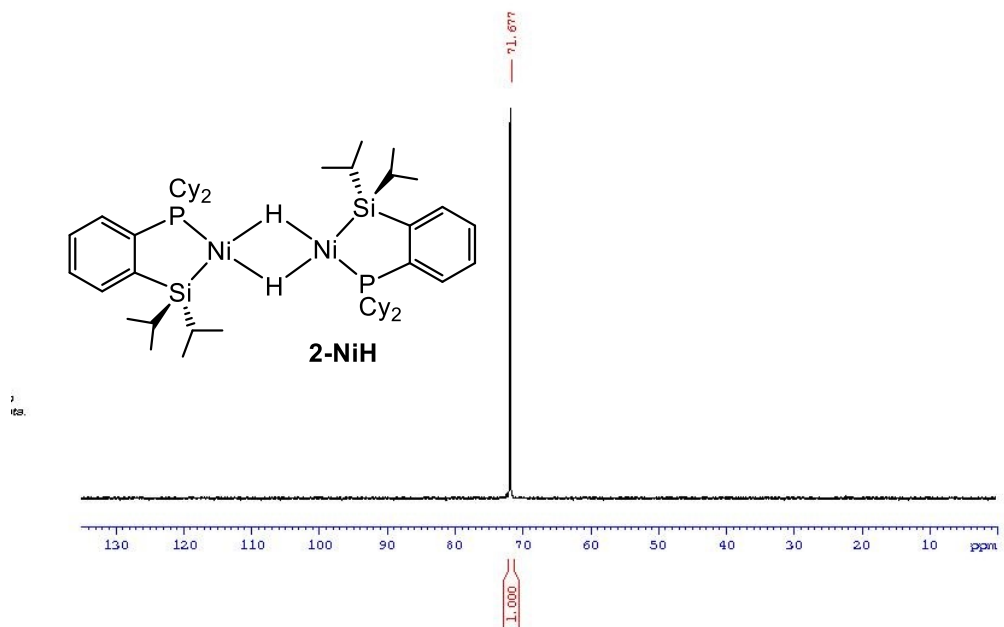
**Figure B16.** IR spectrum of [(Cy-PSi)NiH]₂ dimer **(2-NiH)**
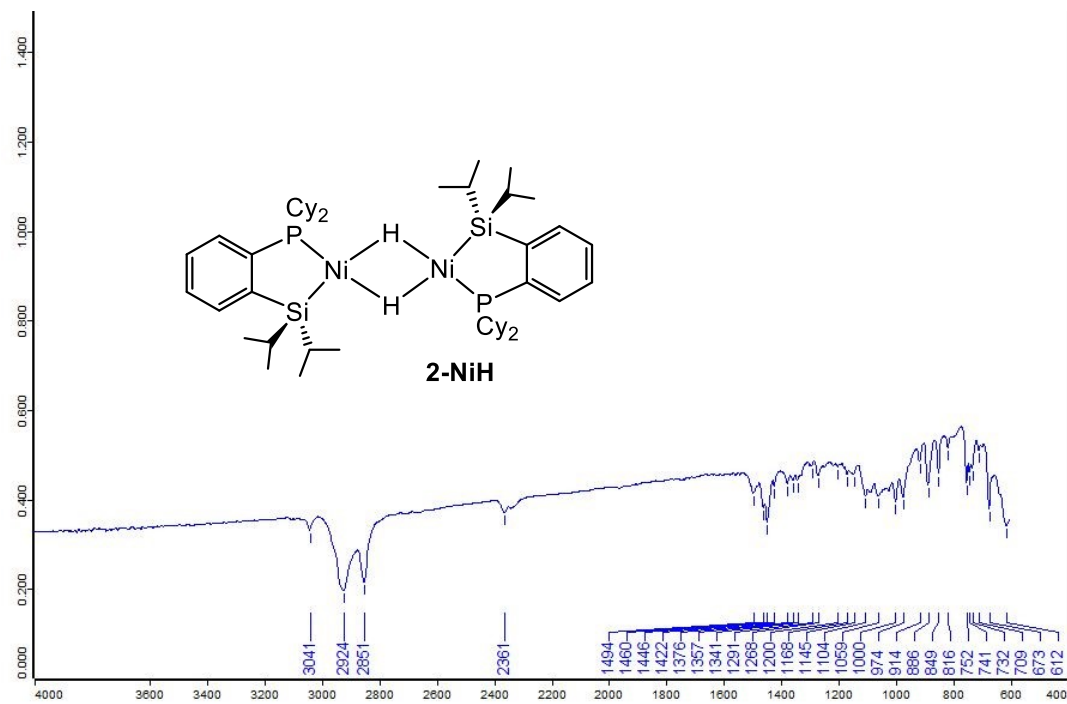
**Figure B17.** $^1$H NMR (300.1 MHz, C$_6$D$_6$) spectrum of (Cy-PSi$^H$)Ni(PPh$_3$) **(2-NiHPPh$_3$)**
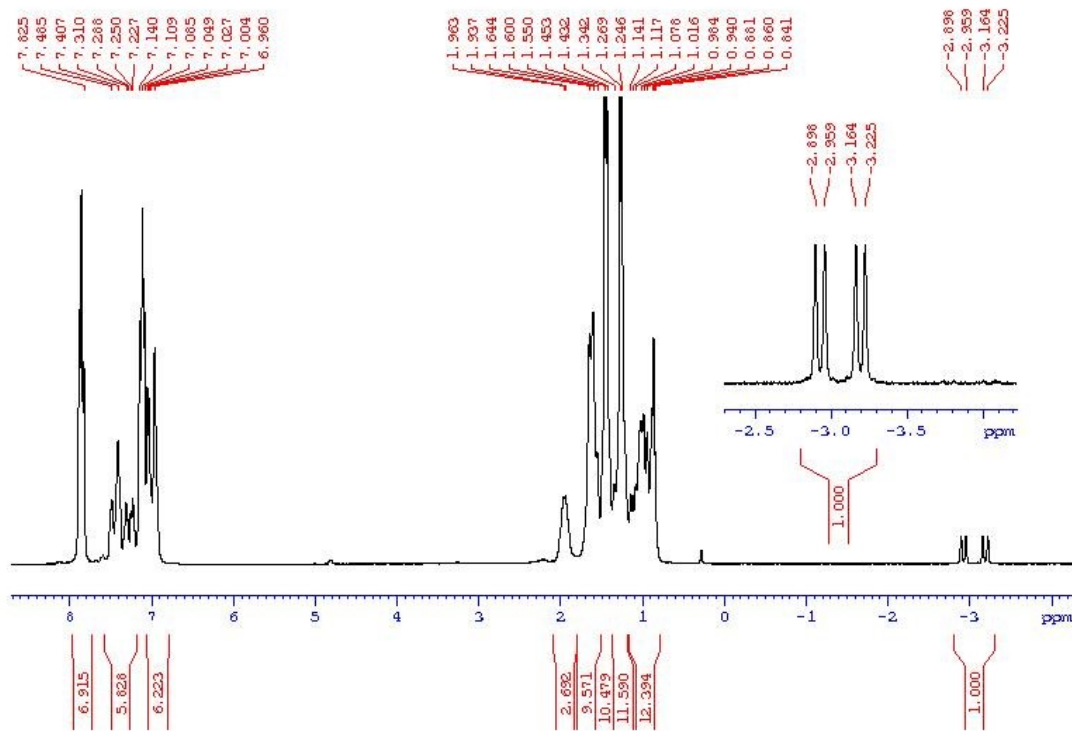
**Figure B18.** $^{31}P\{^1H\}$ NMR (121.5 MHz, C$_6$D$_6$) spectrum of (Cy-PSi$^H$)Ni(PPh$_3$) **(2-NiHPPh₃)**
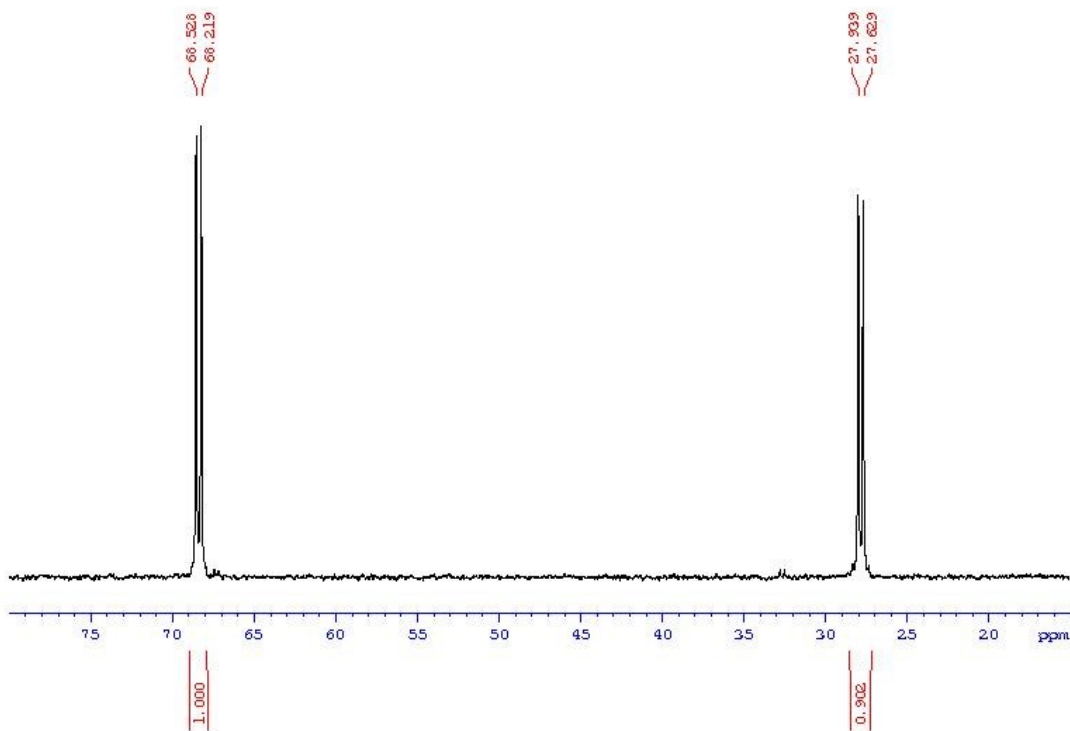
**Figure B19.** Hydroboration of 1-octene with 5 mol% **2-NiBn** ^{1}H NMR (300.1 MHz, CDCl$_3$) 2-octyl-4,4,5,5-tetramethyl-1,3,2-dioxaborolane
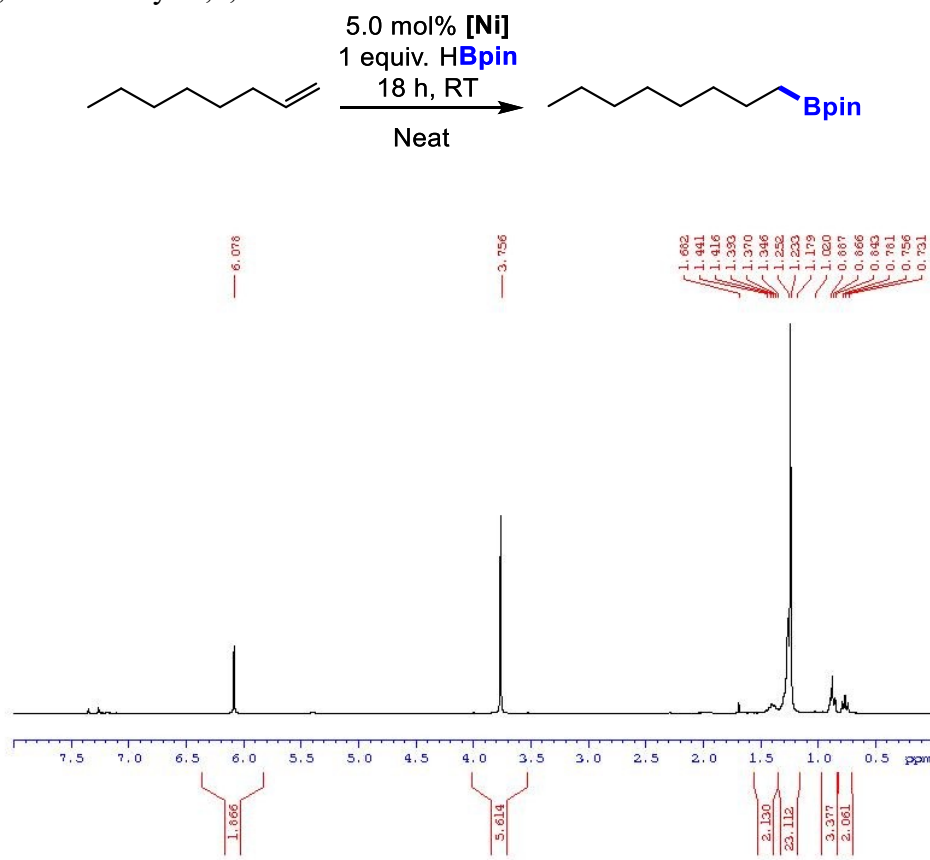
**Figure B20.** Hydroboration of 1-octene with 5 mol% **2-NiBn** $^{13}$C{$^1$H} DEPT-135 NMR (75.47 MHz, CDCl$_3$) 2-octyl-4,4,5,5-tetramethyl-1,3,2-dioxaborolane
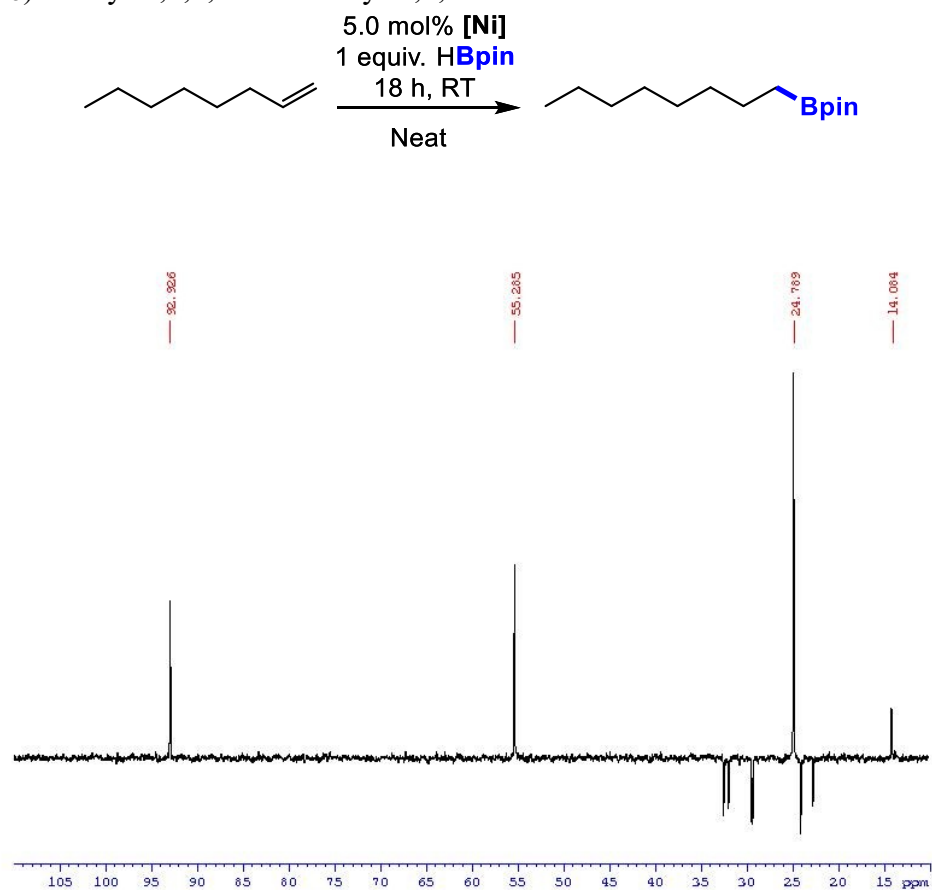
**Figure B21.** Hydroboration of *trans*-4-octene with 5 mol% **2-NiBn** $^1$H NMR (300.1 MHz, CDCl$_3$) 2-octyl-4,4,5,5-tetramethyl-1,3,2-dioxaborolane
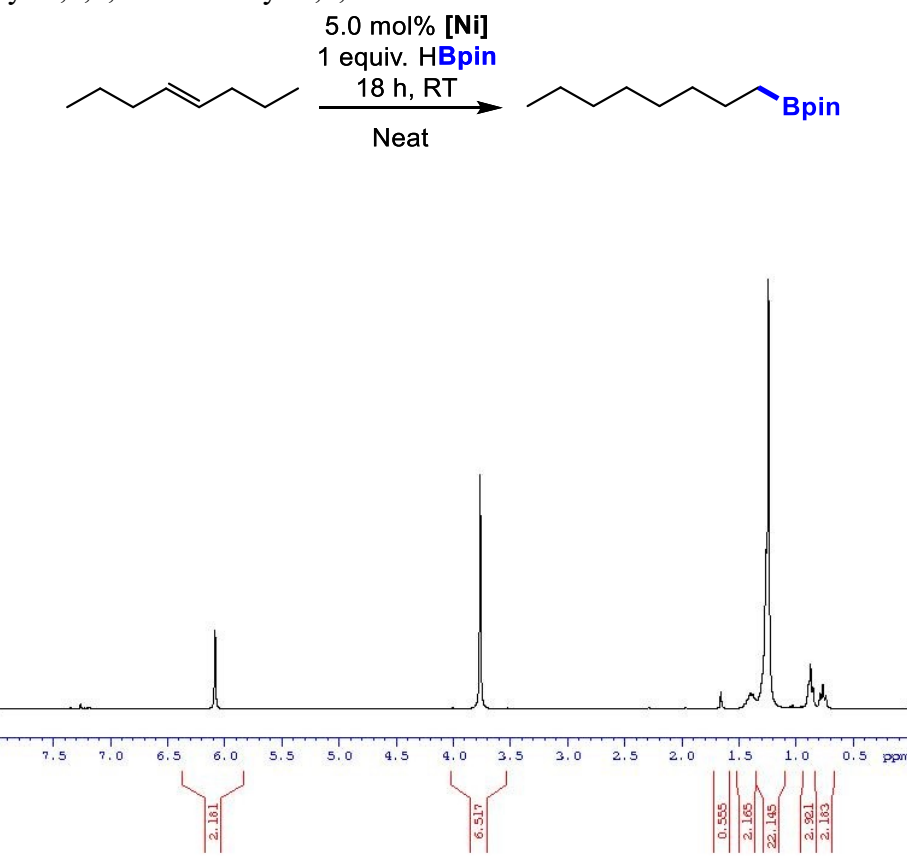
**Figure B22.** Hydroboration of *trans*-4-octene with 5 mol% **2-NiBn** $^{13}C\{^1H\}$ DEPT-135 NMR (75.47 MHz, CDCl$_3$) 2-octyl-4,4,5,5-tetramethyl-1,3,2-dioxaborolane
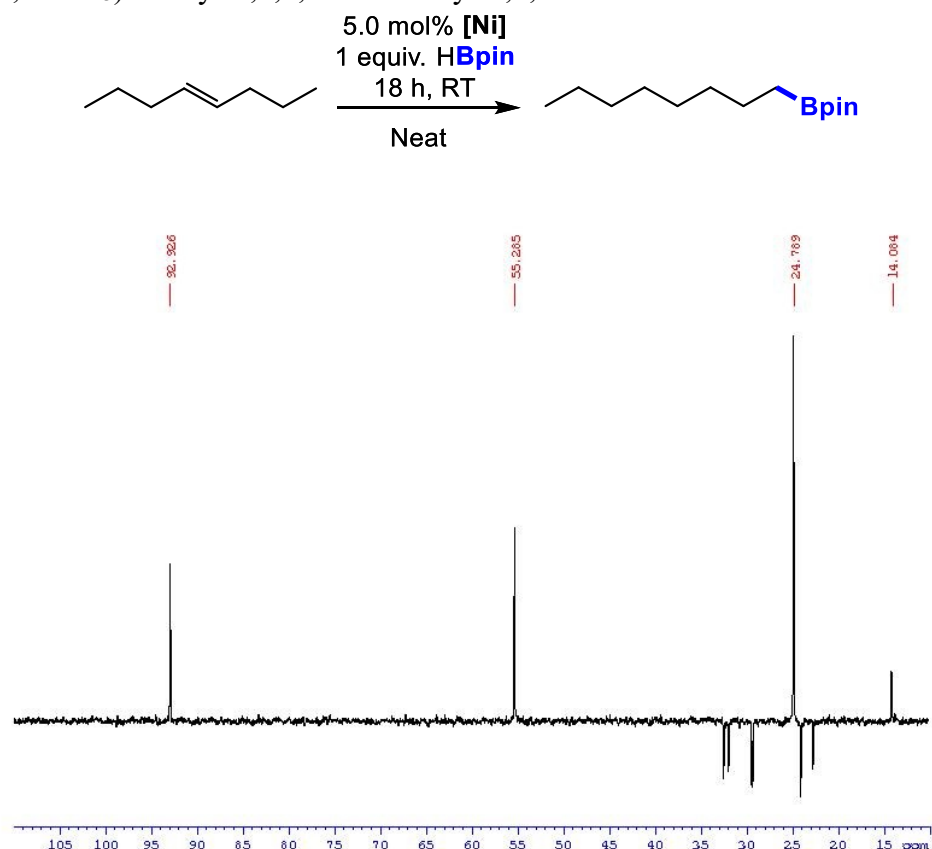
**Figure B23.** Hydroboration of *cis*-4-octene with 5 mol% **2-NiBn** $^1$H NMR (300.1 MHz, CDCl$_3$) 2-octyl-4,4,5,5-tetramethyl-1,3,2-dioxaborolane
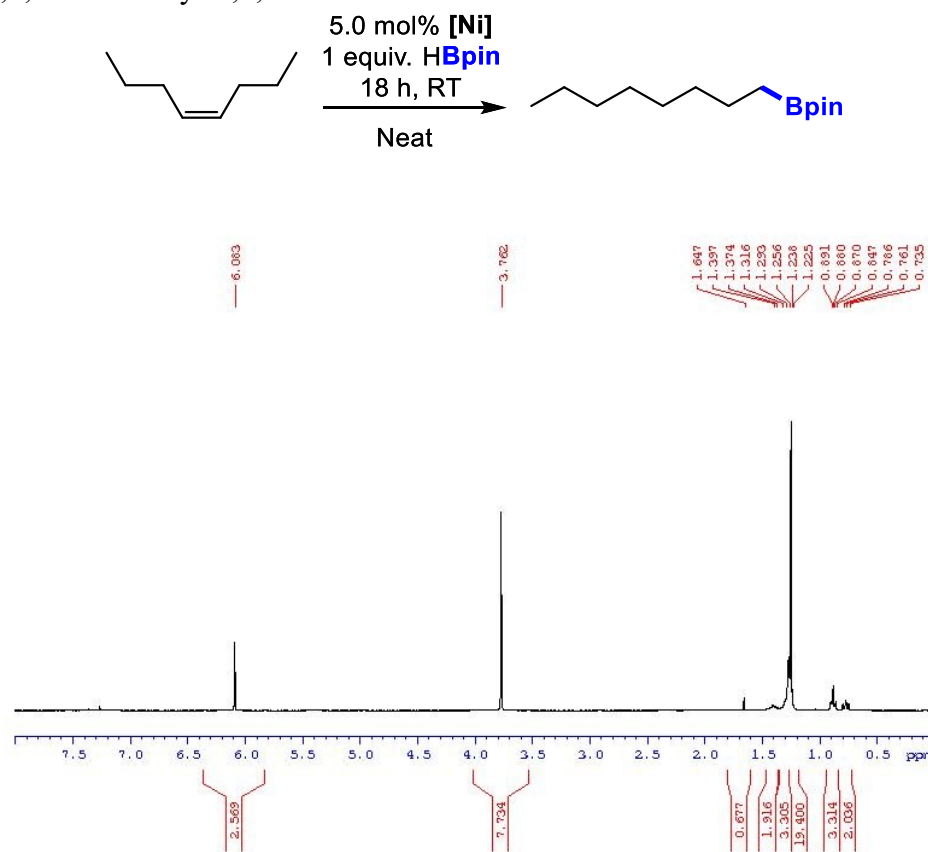
**Figure B24.** Hydroboration of *cis*-4-octene with 5 mol% **2-NiBn** $^{13}C\{^1H\}$ DEPT-135 NMR (75.47 MHz, CDCl$_3$) 2-octyl-4,4,5,5-tetramethyl-1,3,2-dioxaborolane
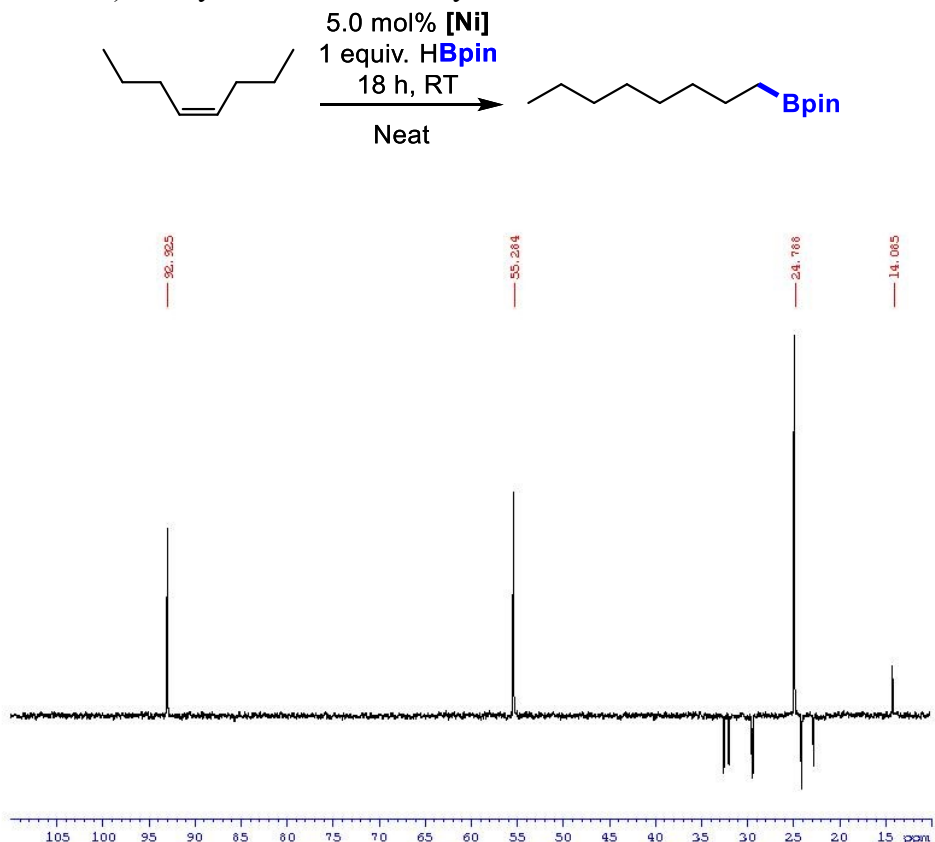
**Figure B25.** Hydroboration of *trans*-4-methyl-2-pentene with 5 mol% **2-NiBn** ^{1}H NMR (300.1 MHz, CDCl$_3$) 2-(4-methylpentyl)-4,4,5,5-tetramethyl-1,3,2-dioxaborolane
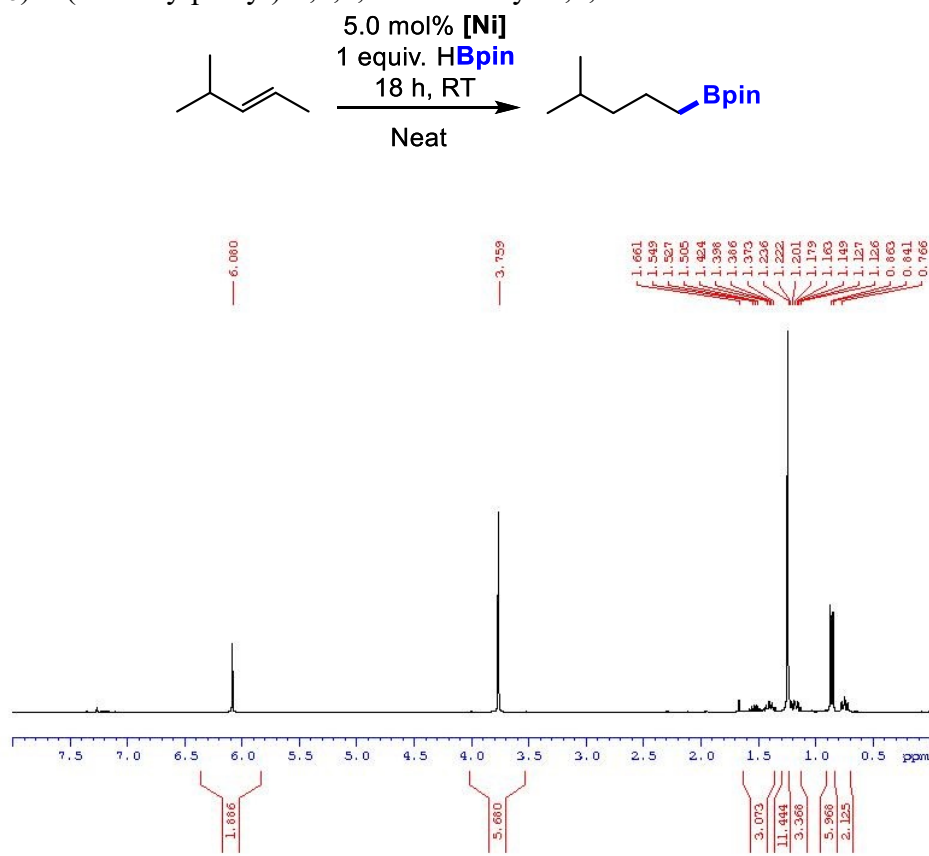
**Figure B26.** Hydroboration of *trans*-4-methyl-2-pentene with 5 mol% **2-NiBn** $^{13}C\{^1H\}$ DEPT-135 NMR (75.47 MHz, CDCl₃) 2-(4-methylpentyl)-4,4,5,5-tetramethyl-1,3,2-dioxaborolane
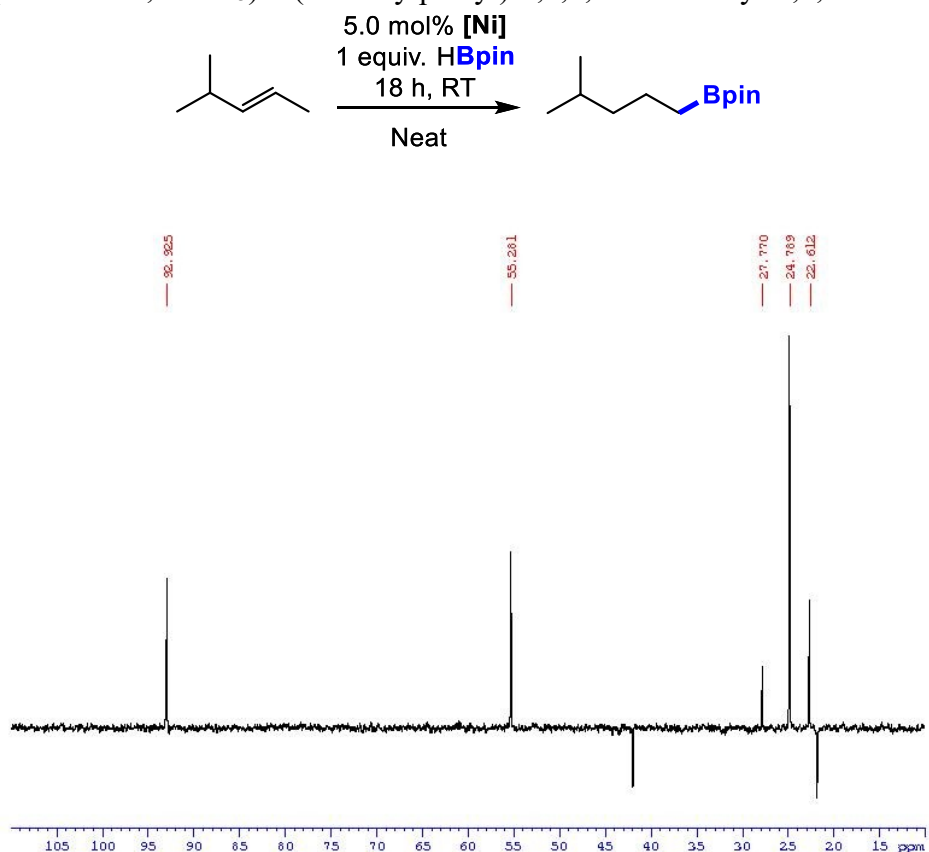
**Figure B27.** Hydroboration of *trans*-4-methyl-1-pentene with 5 mol% **2-NiBn** ^{1}H NMR (500.1 MHz, CDCl₃) 2-(4-methylpentyl)-4,4,5,5-tetramethyl-1,3,2-dioxaborolane
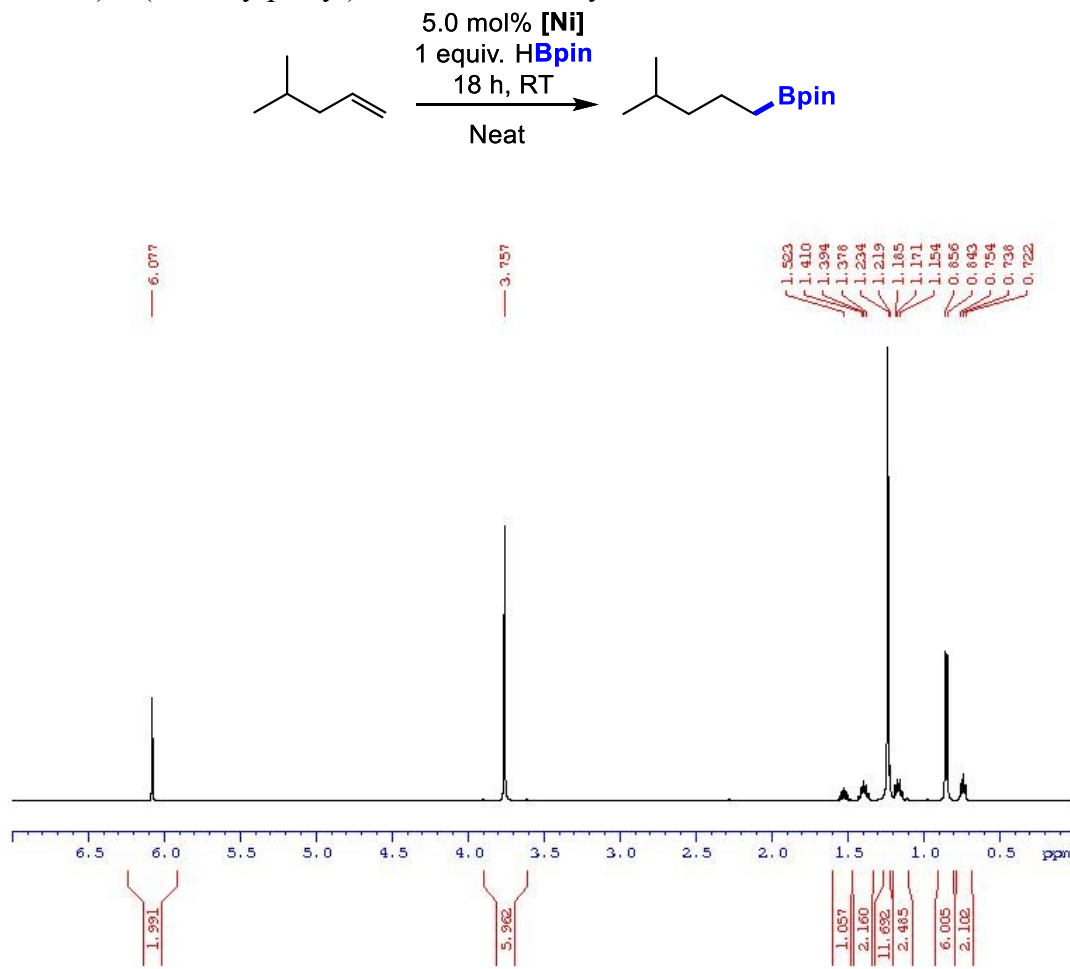
**Figure B28.** Hydroboration of *trans*-4-methyl-1-pentene with 5 mol% **2-NiBn** $^{13}$C{$^1$H} DEPT-135 NMR (125.7 MHz, CDCl₃) 2-(4-methylpentyl)-4,4,5,5-tetramethyl-1,3,2-dioxaborolane
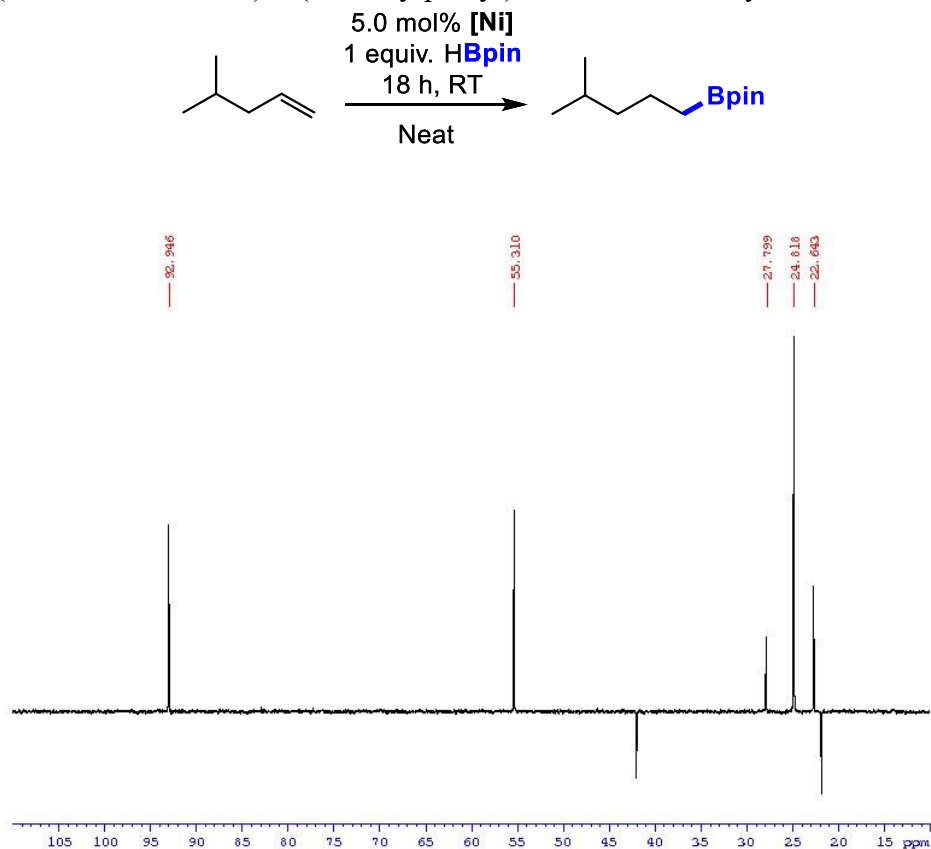
**Figure B29.** Hydroboration of 4-vinylcyclohexane with 5 mol% **2-NiBn** ^{1}H NMR (500.1 MHz, CDCl₃) 2-(2-cyclohexylethyl)-4,4,5,5-tetramethyl-1,3,2-dioxaborolane
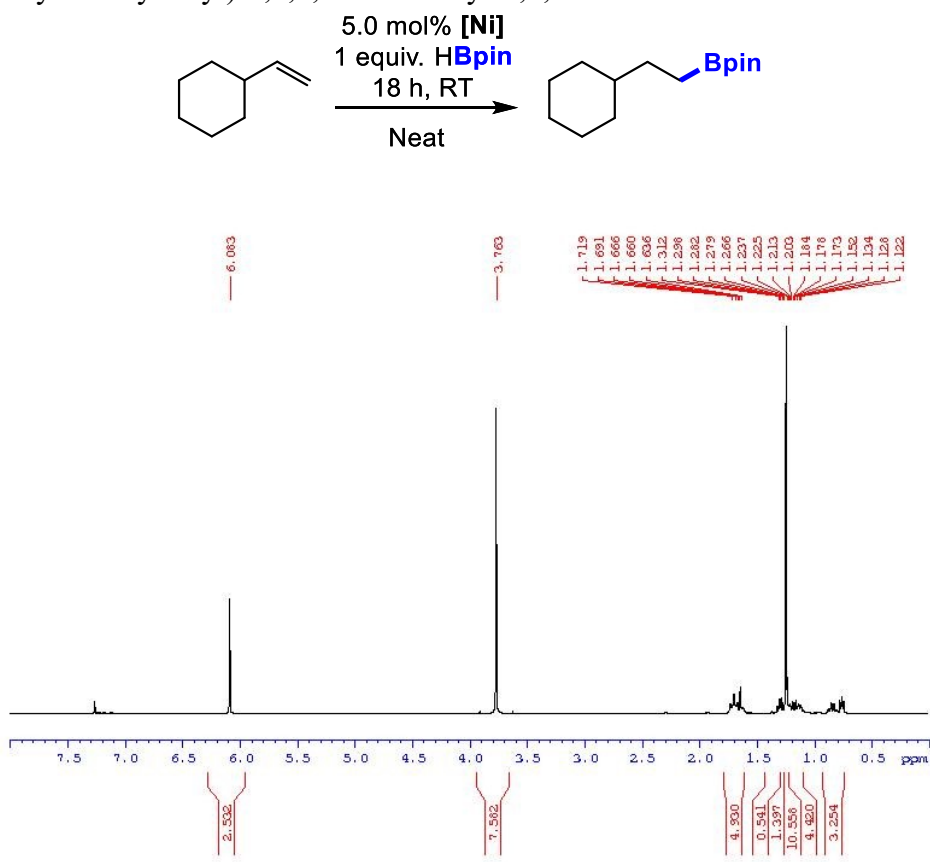
**Figure B30.** Hydroboration of 4-vinylcyclohexane with 5 mol% **2-NiBn** $^{13}C\{^1H\}$ DEPT-135 NMR (125.7 MHz, CDCl$_3$) 2-(2-cyclohexylethyl)-4,4,5,5-tetramethyl-1,3,2-dioxaborolane
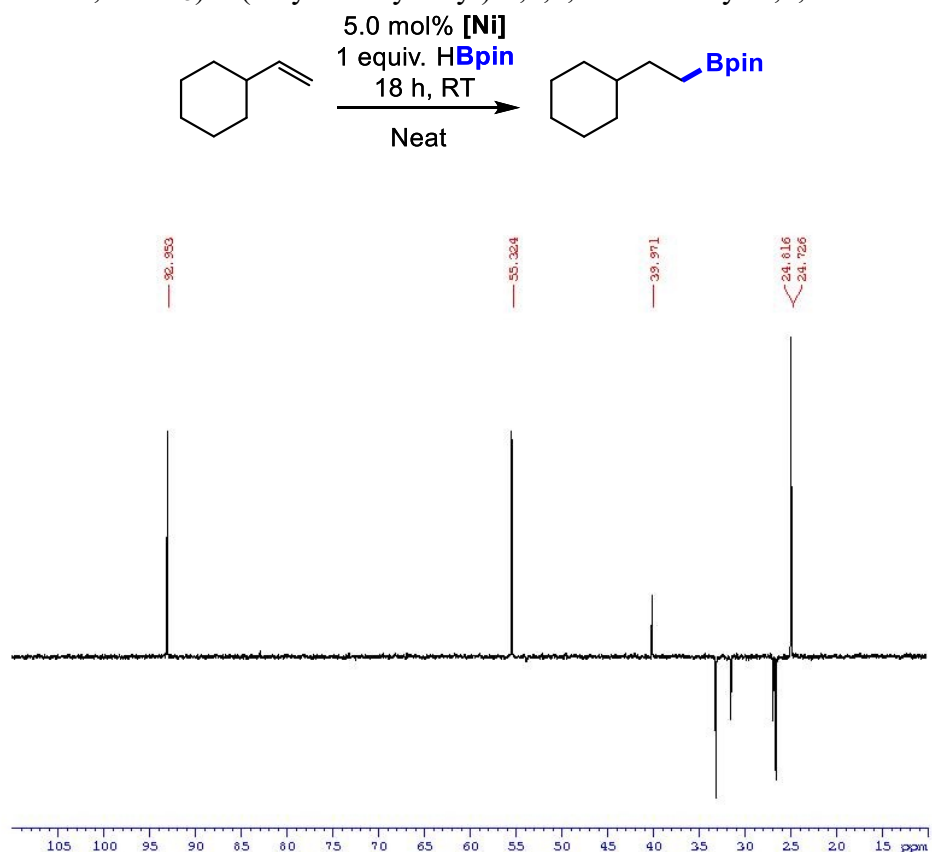
**Figure B31.** Hydroboration of ethylidenecyclohexane with 5 mol% **2-NiBn** ^{1}H NMR (500.1 MHz, CDCl$_3$) 2-(2-cyclohexylethyl)-4,4,5,5-tetramethyl-1,3,2-dioxaborolane
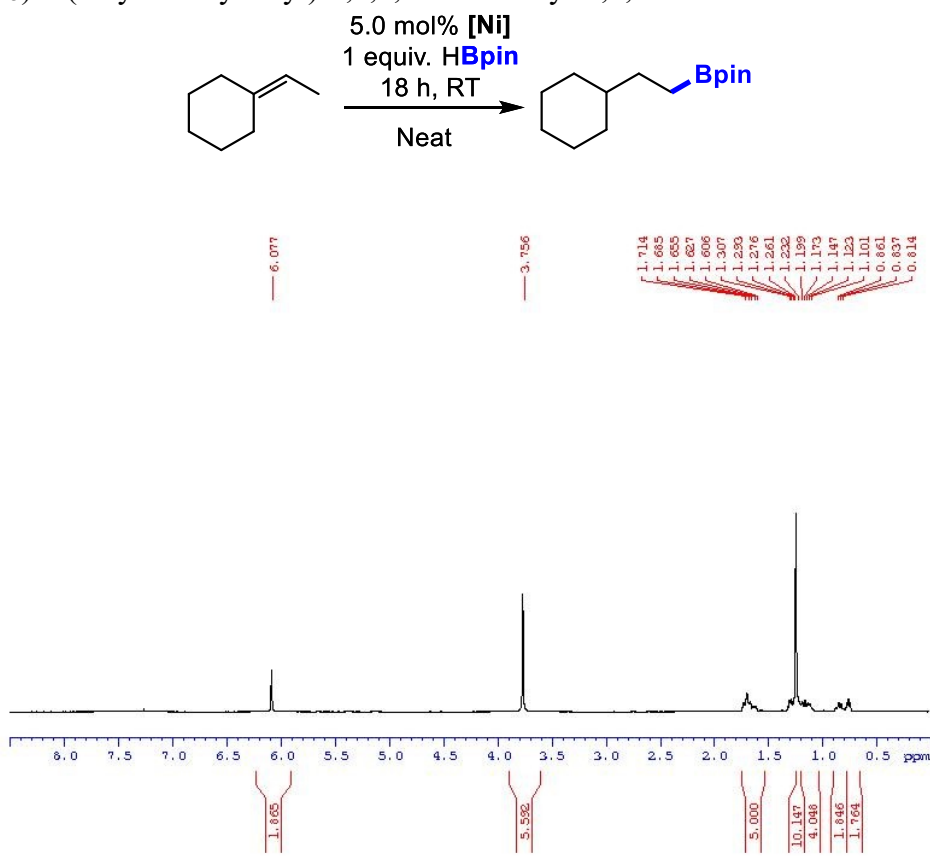
**Figure B32.** Hydroboration of ethylidenecyclohexane with 5 mol% **2-NiBn** $^{13}C\{^1H\}$ DEPT-135 NMR (125.7 MHz, CDCl$_3$) 2-(2-cyclohexylethyl)-4,4,5,5-tetramethyl-1,3,2-dioxaborolane
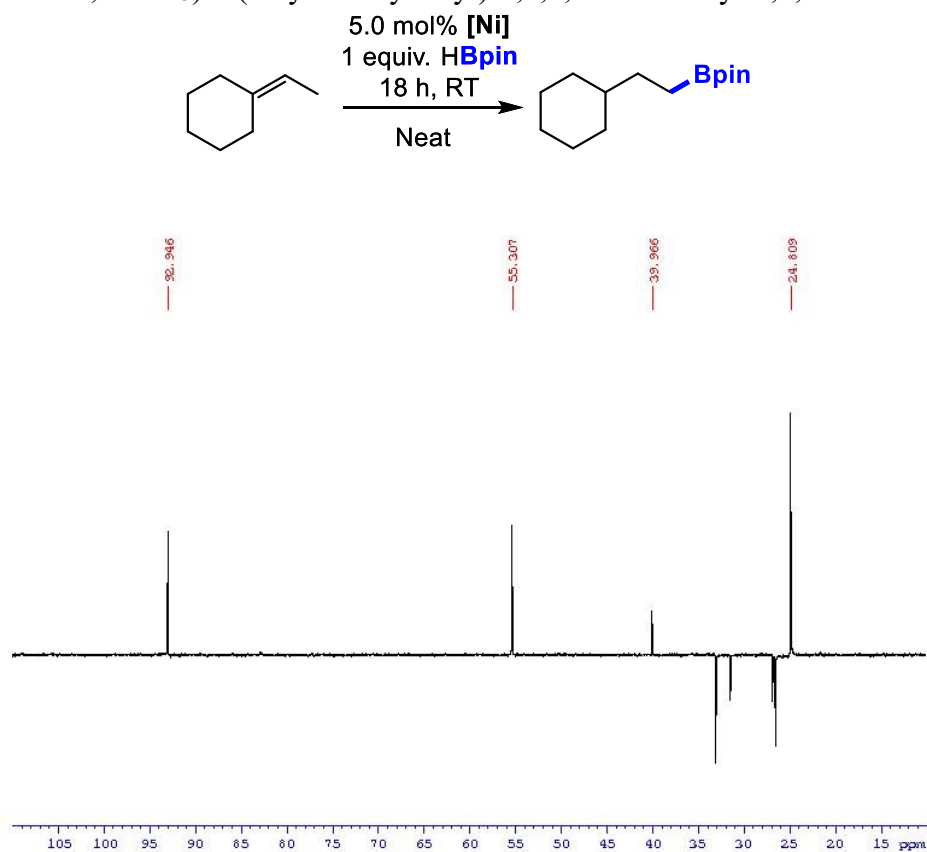
**Figure B33.** Hydroboration of 1-methylcyclohexene with 5 mol% **2-NiBn** ^{1}H NMR (500.1 MHz, CDCl3)
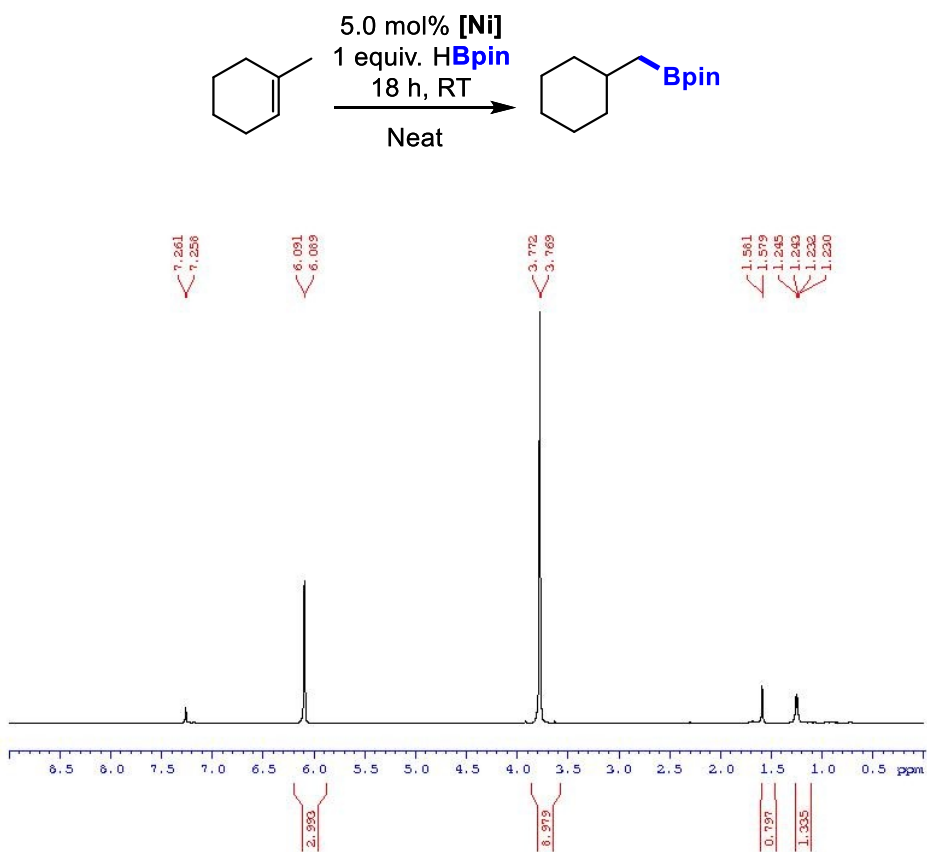
**Figure B34.** Hydroboration of 1-methylcyclohexene with 5 mol% **2-NiBn** $^{13}C\{^1H\}$ DEPT-135 NMR (125.7 MHz, CDCl$_3$)
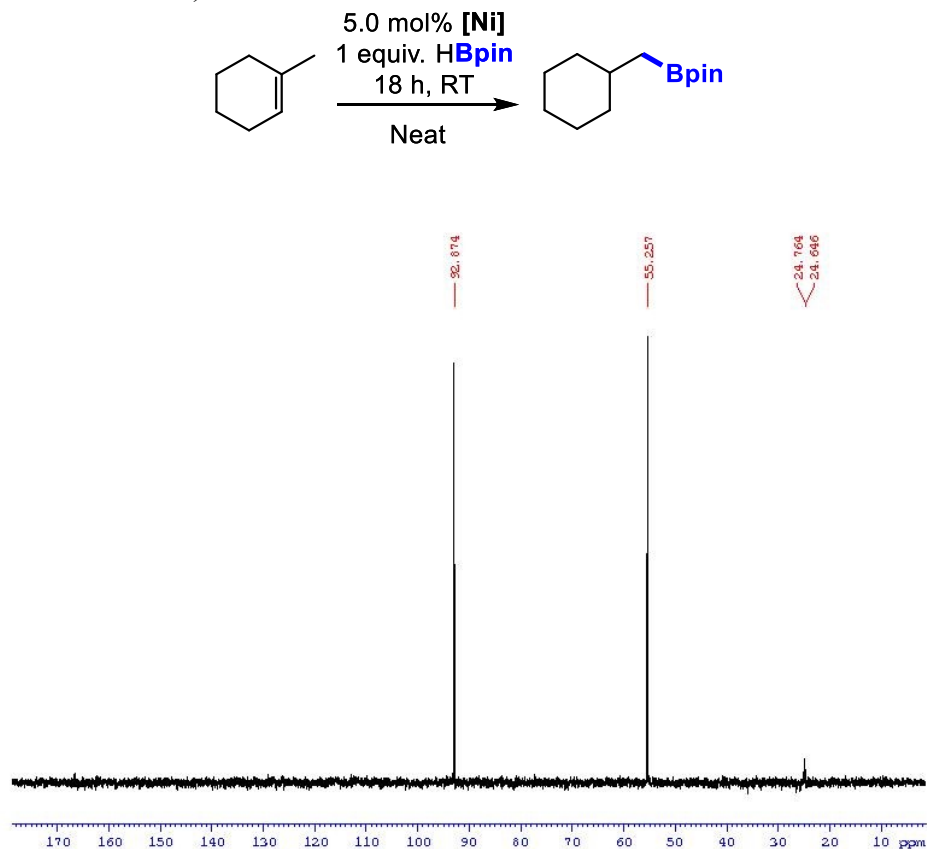
**Figure B35.** Hydroboration of 1-bromobutene with 5 mol% **2-NiBn** $^1$H NMR (500.1 MHz, CDCl$_3$) 2-(4-bromobutyl)-4,4,5,5-tetramethyl-1,3,2-dioxaborolane
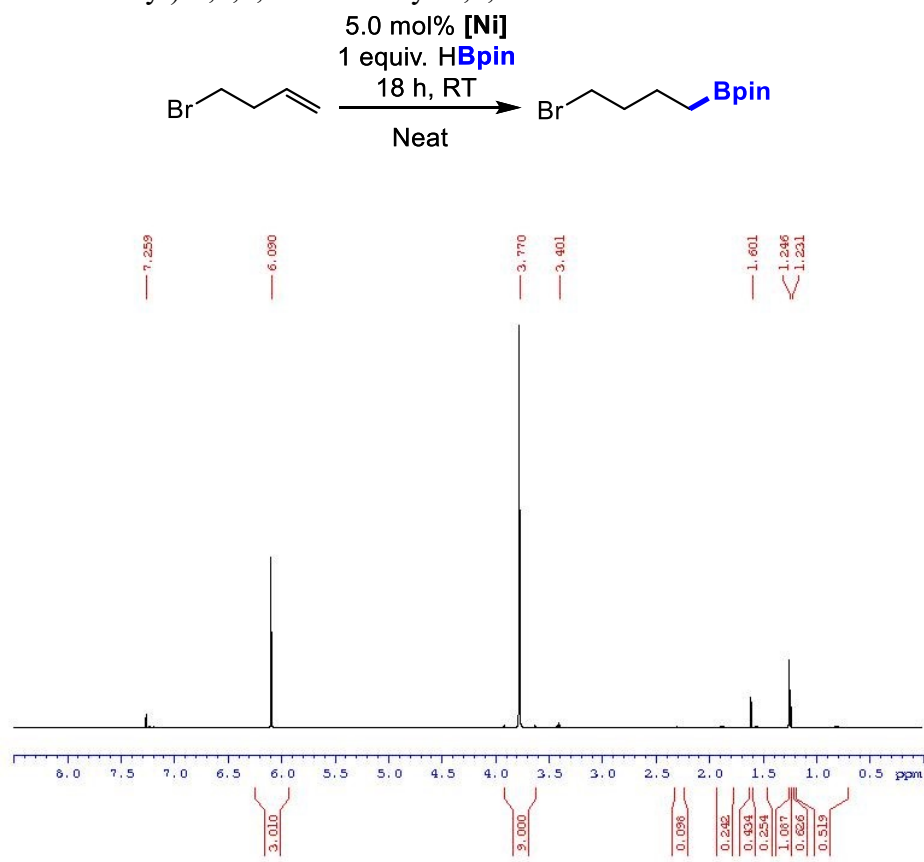
**Figure B36.** Hydroboration of 1-bromobutene with 5 mol% **2-NiBn** $^{13}$C{$^1$H} DEPT-135 NMR (125.7 MHz, CDCl$_3$) 2-(4-bromobutyl)-4,4,5,5-tetramethyl-1,3,2-dioxaborolane
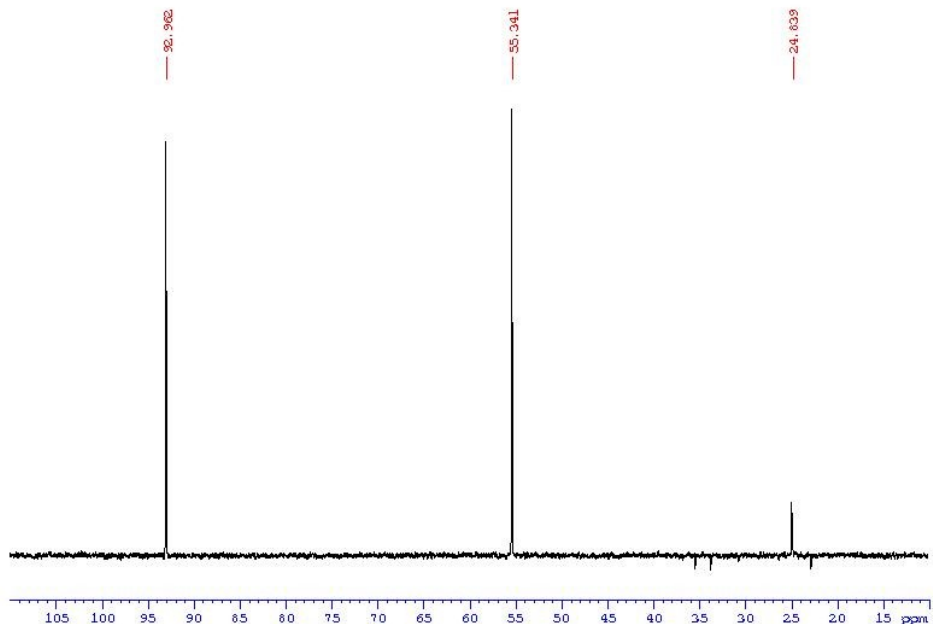
**Figure B37.** Hydroboration of styrene with 5 mol% **2-NiBn** ^{1}H NMR (500.1 MHz, CDCl$_3$) 4,4,5,5-tetramethyl-2-phenethyl-1,3,2-dioxaborolane, and 4,4,5,5-tetramethyl-2-(1-pheynlethyl)-1,3,2-dioxaborolane
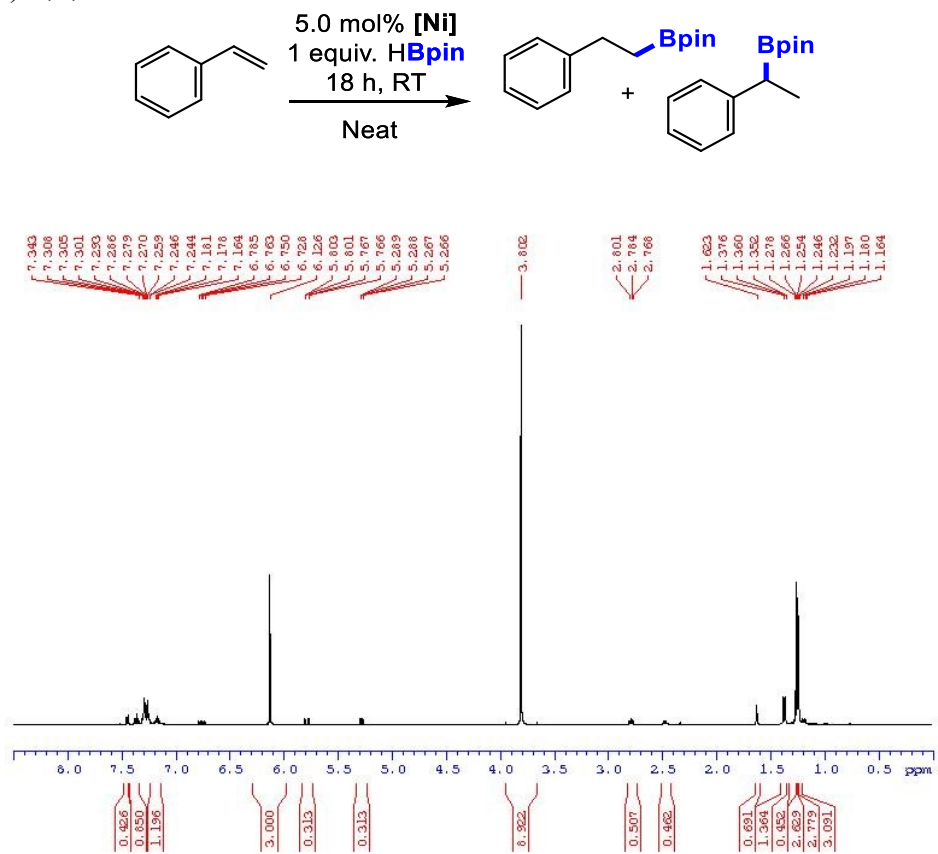
**Figure B38.** Hydroboration of styrene with 5 mol% **2-NiBn** $^{13}C\{^1H\}$ DEPT-135 NMR (125.7 MHz, CDCl$_3$) 4,4,5,5-tetramethyl-2-phenethyl-1,3,2-dioxaborolane, and 4,4,5,5-tetramethyl-2-(1-pheynlethyl)-1,3,2-dioxaborolane
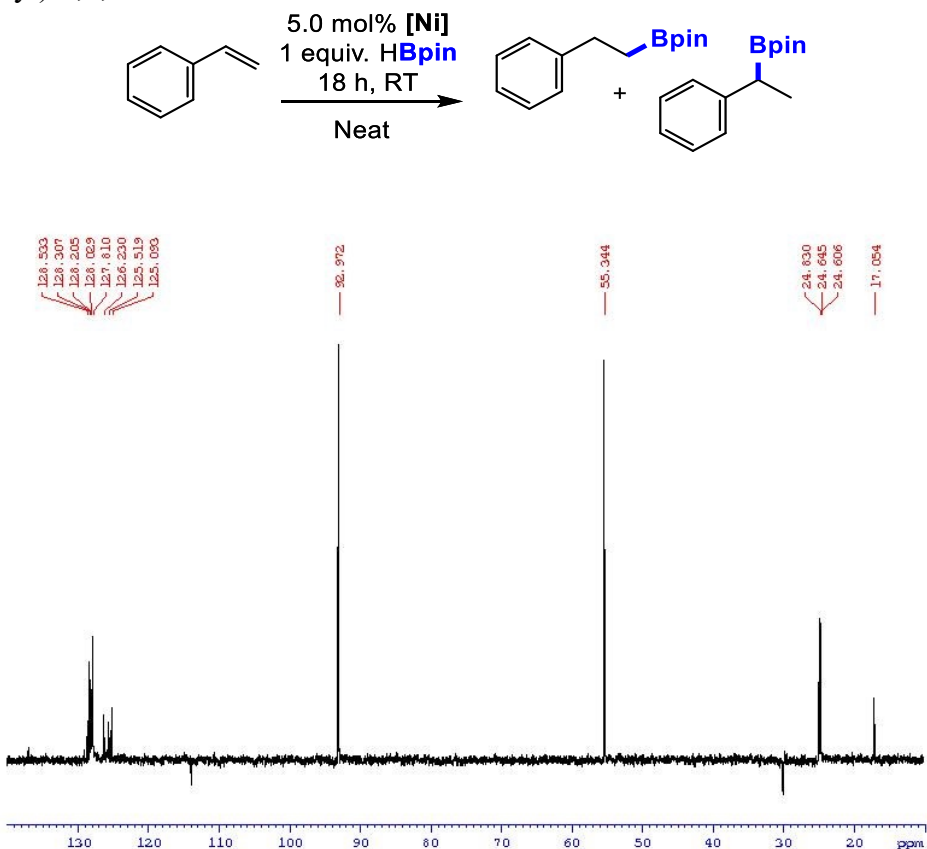
**Figure B39.** Hydroboration of phenylpropylene with 5 mol% **2-NiBn** ^{1}H NMR (300.1 MHz, CDCl$_3$) 4,4,5,5-tetramethyl-2-(3-phenylpropyl)-1,3,2-dioxaborolane
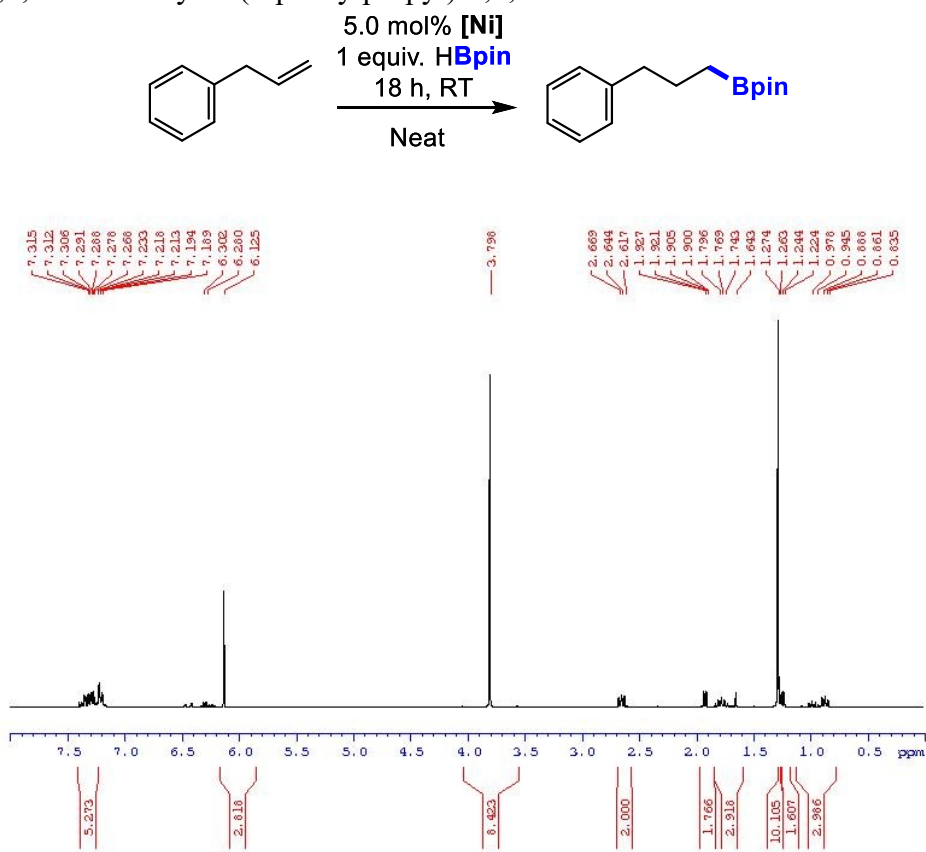
**Figure B40.** Hydroboration of phenylpropylene with 5 mol% **2-NiBn** $^{13}$C{$^1$H} DEPT-135 NMR (75.47 MHz, CDCl$_3$) 4,4,5,5-tetramethyl-2-(3-phenylpropyl)-1,3,2-dioxaborolane
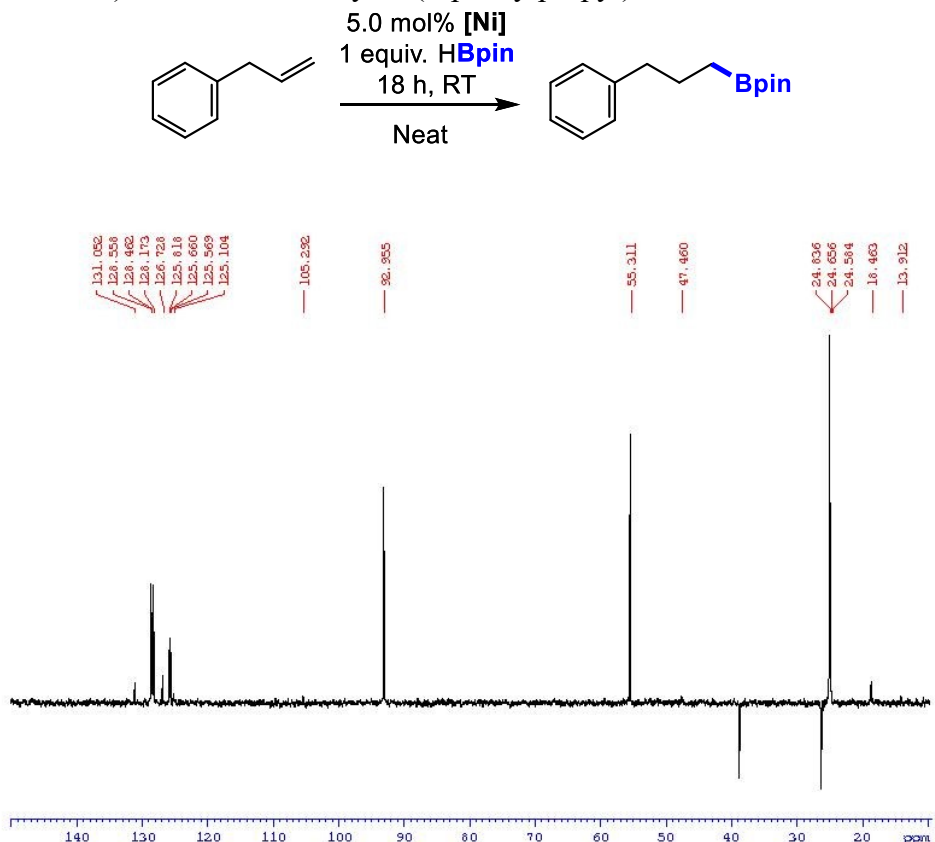
**Figure B41.** Hydroboration of 3-(dimethylamino)-1-propene with 5 mol% **2-NiBn** ^{1}H NMR (500.1 MHz, CDCl3) *N,N*,4,4,5,5-hexamethyl-1,3,2-dioxaborolane-2-propanamine
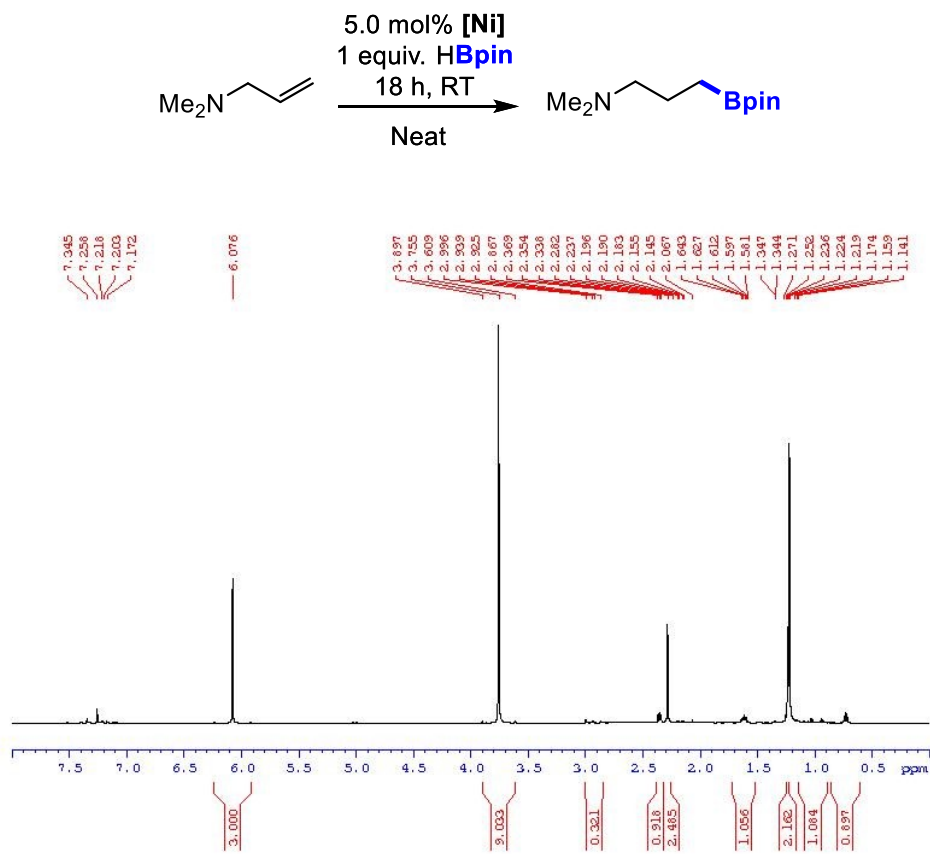
**Figure B42.** Hydroboration of 3-(dimethylamino)-1-propene with 5 mol% **2-NiBn** $^{13}C\{^1H\}$ DEPT-135 NMR (125.7 MHz, CDCl₃) *N,N*,4,4,5,5-hexamethyl-1,3,2-dioxaborolane-2-propanamine